

## **INFORMATION TO USERS**

This manuscript has been reproduced from the microfilm master. UMI films the text directly from the original or copy submitted. Thus, some thesis and dissertation copies are in typewriter face, while others may be from any type of computer printer.

**The quality of this reproduction is dependent upon the quality of the copy submitted.** Broken or indistinct print, colored or poor quality illustrations and photographs, print bleedthrough, substandard margins, and improper alignment can adversely affect reproduction.

In the unlikely event that the author did not send UMI a complete manuscript and there are missing pages, these will be noted. Also, if unauthorized copyright material had to be removed, a note will indicate the deletion.

Oversize materials (e.g., maps, drawings, charts) are reproduced by sectioning the original, beginning at the upper left-hand corner and continuing from left to right in equal sections with small overlaps.

Photographs included in the original manuscript have been reproduced xerographically in this copy. Higher quality 6" x 9" black and white photographic prints are available for any photographs or illustrations appearing in this copy for an additional charge. Contact UMI directly to order.

Bell & Howell Information and Learning  
300 North Zeeb Road, Ann Arbor, MI 48106-1346 USA

**UMI**<sup>®</sup>  
800-521-0600



**University of Alberta**

**Cyclic Behavior of Stiffened Gusset Plate-Brace Member Assemblies**

by

**Trina Elizabeth Nast**



**A thesis submitted to the Faculty of Graduate Studies and Research in partial fulfillment  
of the requirements for the degree of Master of Science**

in

**Structural Engineering**

**Department of Civil and Environmental Engineering**

**Edmonton, Alberta**

**Fall 1999**



National Library  
of Canada

Acquisitions and  
Bibliographic Services

395 Wellington Street  
Ottawa ON K1A 0N4  
Canada

Bibliothèque nationale  
du Canada

Acquisitions et  
services bibliographiques

395, rue Wellington  
Ottawa ON K1A 0N4  
Canada

*Your file Votre référence*

*Our file Notre référence*

The author has granted a non-exclusive licence allowing the National Library of Canada to reproduce, loan, distribute or sell copies of this thesis in microform, paper or electronic formats.

The author retains ownership of the copyright in this thesis. Neither the thesis nor substantial extracts from it may be printed or otherwise reproduced without the author's permission.

L'auteur a accordé une licence non exclusive permettant à la Bibliothèque nationale du Canada de reproduire, prêter, distribuer ou vendre des copies de cette thèse sous la forme de microfiche/film, de reproduction sur papier ou sur format électronique.

L'auteur conserve la propriété du droit d'auteur qui protège cette thèse. Ni la thèse ni des extraits substantiels de celle-ci ne doivent être imprimés ou autrement reproduits sans son autorisation.

0-612-47076-8

**University of Alberta**

**Library Release Form**

**Name of Author:** Trina Elizabeth Nast

**Title of Thesis:** Cyclic Behavior of Stiffened Gusset Plate-Brace Member Assemblies

**Degree:** Master of Science

**Year This Degree Granted:** 1999

Permission is hereby granted to the University of Alberta Library to reproduce single copies of this thesis and to lend or sell such copies for private, scholarly, or scientific research purposes only.

The author reserves all other publication and other rights in association with the copyright in the thesis, and except as hereinbefore provided, neither the thesis nor any substantial portion thereof may be printed or otherwise reproduced in any material form whatever without the author's prior written permission.

  
\_\_\_\_\_

7211 - 139 Avenue

Edmonton, Alberta

CANADA

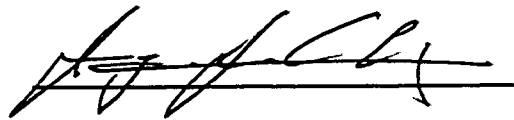
T5C 2M3

Date: SEP 24, 1999

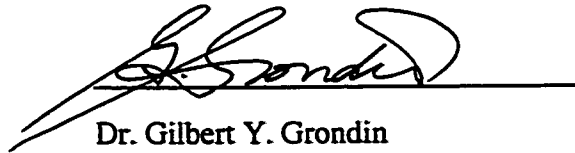
**University of Alberta**

**Faculty of Graduate Studies and Research**

The undersigned certify that they have read, and recommended to the Faculty of Graduate Studies and Research for acceptance, a thesis entitled Cyclic Behavior of Stiffened Gusset Plate-Brace Member Assemblies submitted by Trina Elizabeth Nast in partial fulfillment of the requirements for the degree of Master of Science in Structural Engineering.



Dr. J.J. Roger Cheng



Dr. Gilbert Y. Grondin

---

Dr. Chongqing Ru



Date: Sept. 24, 1999

## ABSTRACT

This report summarizes the experimental and numerical investigation on the effects of gusset plate free edge stiffeners and brace member – gusset plate interaction on the behavior of corner gusset plates subjected to cyclic loading.

The experimental program included four full-scale gusset plate-brace member assemblies. All four specimens included the same connection details and gusset plate geometry, except that two specimens included gusset plate free edge stiffeners. The other variable in the specimens was the slenderness of the brace member which was adjusted by altering the brace member length. By doing so, two specimens were designed with the gusset plate to buckle under the compressive loads, and two were designed with the brace member as the weak compressive element. These tests were then modeled using the finite element models proposed by Walbridge *et al.* (1998).

Based on the results of this investigation it was found that free edge stiffeners significantly increase the post buckling strength and energy absorption capabilities of weak gusset – strong brace assemblies, and less effect for strong gusset – weak brace assemblies. It was also found that the finite element models proposed in earlier research by Walbridge *et al.* (1998) adequately predict the strength properties and energy absorption characteristics of the tested assemblies.

## **ACKNOWLEDGEMENTS**

The author wishes to acknowledge the financial support in the form of scholarships from the C.W. Carry Chair at the University of Alberta as well as the Faculty of Graduate Studies and Research.

The technicians of the Department of Civil Engineering of the University of Alberta are thanked for their many contributions during the testing program.

I would also like to thank my family and friends who have continuously provided encouragement and support.



# TABLE OF CONTENTS

1. INTRODUCTION	
1.1. General	1
1.2. Objectives	3
1.3. Scope	3
2. LITERATURE REVIEW	
2.1. Introduction	5
2.2. General Gusset Plate Behavior	5
2.3. Monotonic Tension Behavior	6
2.4. Monotonic Compression Behavior	9
2.5. Cyclic Behavior	12
2.6. Summary	17
3. EXPERIMENTAL PROGRAM	
3.1. Introduction	22
3.2. Preliminary Considerations	22
3.3. Description of Test Specimens	23
3.4. Material Properties	25
3.5. Initial Imperfections	26
3.6. Test Set-Up	27
3.7. Instrumentation	29
3.8. Test Procedure	31
4. EXPERIMENTAL RESULTS	
4.1. Introduction	47
4.2. Load-Deformation Behavior	48
4.3. Energy Absorption	51
4.4. Out-of-Plane Deformation	52
4.5. Strain Gauge Data	54
4.5.1. <i>Strains in Gusset Plate and Brace Member</i>	55
4.5.2. <i>Strains in Free Edge Stiffeners</i>	57
5. FINITE ELEMENT ANALYSIS	
5.1. Introduction	81
5.2. Preliminary Finite Element Analysis for Stiffener Selection	82
5.2.1. <i>Model Description</i>	83
5.2.2. <i>Results of the Preliminary Analysis</i>	84
5.3. Description of the Finite Element Models	86
5.3.1. <i>Elements and Mesh</i>	86
5.3.2. <i>Initial Imperfections</i>	88
5.3.3. <i>Material Models</i>	88
5.4. Analysis	89

6. DISCUSSION	
6.1. Introduction	101
6.2. Experimental Results	101
6.2.1. <i>Load versus Displacement Response</i>	101
6.2.2. <i>Energy Absorption</i>	105
6.2.3. <i>Out-of-Plane Displacement</i>	108
6.3. Comparison of Finite Element Analysis Results with Test Results	109
6.3.1. <i>Load versus Displacement Behavior</i>	109
6.3.2. <i>Energy Absorption</i>	112
6.3.3. <i>Out-of-Plane Displacements</i>	113
6.3.4. <i>Principal Strain Directions</i>	114
7. CONCLUSION	
7.1. Summary	129
7.2. Conclusions	130
7.3. Recommendations for Future Research	132
REFERENCES	134
APPENDIX A: Preliminary Finite Element Analysis Results	137
APPENDIX B: Initial Imperfection Measurements	145

## LIST OF TABLES

Table	Page
3-1 Specimen Description .....	33
3-2 Bolted Connection Slip Resistance .....	33
3-3 Welding Processes and Specifications .....	34
3-4 Material Properties .....	35
4-1 Maximum Test Loads Obtained (kN) .....	58
4-2 Load Levels used for Comparison (kN) .....	58
4-3 Brace Member Rotations for Tests T-1 and T-2 .....	58
4-4 Maximum Strains Measured in Gusset Plate ( $\mu\epsilon$ ) .....	59
4-5 Loads and Axial Assembly Displacement at Which First Yield was Detected .....	59
4-6 Principal Strain Magnitudes and Directions at Whitmore Yield Load (Tension) .....	60
4-7 Principal Strain Magnitudes and Directions at Whitmore Yield Load (Compression) .....	61
4-8 Principal Strain Magnitudes and Directions at Brace Yield Load (Compression) .....	61
4-9 Average of Strains in Free Edge Stiffeners ( $\mu\epsilon$ ) .....	62
5-1 Description of Preliminary Finite Element Models .....	91
6-1 Comparison of Experimental Results with Predicted Strengths - Tension .....	115
6-2 Comparison of Experimental Results with Predicted Strengths - Compression .....	115
6-3 Comparison of Finite Element Results with Experimental Results	116
A-1 Gusset Plate Initial Imperfection Measurements: Specimen T-1 ...	140
A-2 Gusset Plate Initial Imperfection Measurements: Specimen T-2 ...	141
A-3 Gusset Plate Initial Imperfection Measurements: Specimen T-3 ...	142
A-4 Gusset Plate Initial Imperfection Measurements: Specimen T-4 ...	143
A-5 Brace Member Initial Imperfection Measurements (mm) .....	144
B-1 Results of Preliminary Finite Element Analysis - Series I .....	147
B-2 Results of Preliminary Finite Element Analysis - Series II .....	147
B-3 Results of Preliminary Finite Element Analysis - Series III .....	147

## LIST OF FIGURES

Figure	Page
2-1 Whitmore Effective Width Method .....	19
2-2 Block Shear Model Proposed by Hardash and Bjorhovde, 1985 .....	19
2-3 Compressive Capacity Calculation - Thornton's Method (1984) .....	20
2-4 Typical Test Specimen by Jain, Goel, and Hanson (1978) .....	20
2-5 Typical Test Specimen by Astaneh-Asl and Goel (1985) .....	21
2-6 Test Set-up used by Rabinovitch and Cheng (1993) .....	21
3-1 Subassembly Details .....	36
3-2 Gusset Plate Geometry .....	36
3-3 Initial Imperfection Measurement .....	37
3-4 Location of Initial Imperfection Measurements on Brace Member .....	38
3-5 Test Set-Up for Specimen T-1 .....	39
3-6 Test Set-Up for Specimens T-2, T-3, and T-4 .....	40
3-7 Cable Transducer Location .....	41
3-8 Cable Transducer Frame - Gusset Plate .....	41
3-9 Cable Transducer Frame - Brace Member .....	42
3-10 Strain Gauge Location on Gusset Plate .....	43
3-11 Strain Gauge Position on Brace Members for Specimens T-2, T-3, and T-4 .....	44
3-12 Deformation Spectrum Applied to Specimen T-1 .....	45
3-13 Deformation Spectrum Applied to Specimen T-2 .....	45
3-14 Deformation Spectrum Applied to Specimen T-3 .....	46
3-15 Deformation Spectrum Applied to Specimen T-4 .....	46
4-1 Load versus Deformation Relationship for Gusset Plate: Specimen T-1 ..	63
4-2 Load versus Deformation Relationship for Gusset Plate: Specimen T-2 ..	63
4-3 Load versus Deformation Relationship for Gusset Plate: Specimen T-3 ..	64
4-4 Load versus Deformation Relationship for Gusset Plate: Specimen T-4 ..	64
4-5 Load versus Deformation Relationship for Assembly: Specimen T-1 ...	65
4-6 Load versus Deformation Relationship for Assembly: Specimen T-2 ...	65
4-7 Load versus Deformation Relationship for Assembly: Specimen T-3 ...	66
4-8 Load versus Deformation Relationship for Assembly: Specimen T-4 ...	66
4-9 Deterioration of Buckling Load Due to Applied Cycles .....	67
4-10 Failed Gusset Plate Specimens .....	68
4-11 Cycle at Which Bolt Slip First Occurs in Specimens T-1 and T-2 .....	69
4-12 Determination of Energy Absorbed .....	70
4-13 Cumulative Energy Dissipated by Test Specimens .....	70
4-14 Effect of Bolt Slip on the Cumulative Energy Absorption Capacity of the Assembly .....	71
4-15 Out-of-Plane Deformation of Gusset Plate Free Edges - Specimen T-1 ..	72

4-16	Out-of-Plane Deformation of Gusset Plate Free Edges - Specimen T-2	72
4-17	Deformed Shape of Gusset Plate Long Free Edge	73
4-18	Out-of-Plane Deformation of Gusset Plate Free Edges - Specimen T-3	74
4-19	Out-of-Plane Deformation of Gusset Plate Free Edges - Specimen T-4	74
4-20	Out-of-Plane Deformation of Gusset Plate Free Edges	75
4-21	Out-of-Plane Deformation of Brace Member - Specimen T-3	76
4-22	Out-of-Plane Deformation of Brace Member - Specimen T-4	76
4-23	Out-of-Plane Deformation of Brace Member at Specific Displacement Levels - Specimen T-4	77
4-24	Out-of-Plane Deformation of Assembly - Specimen T-3 at Peak Compression - Cycle 21	78
4-25	Principal Strain Magnitudes and Directions at Whitmore Compressive Yield Level - Specimen T-1	79
4-26	Principal Strain Magnitudes and Directions at Compressive Brace Yield Load Level - Specimen T-2	79
4-27	Principal Strain Magnitudes and Directions at Compressive Brace Yield Load Level - Specimen T-3	80
4-28	Principal Strain Magnitudes and Directions at Compressive Brace Yield Load Level - Specimen T-4	80
5-1	Typical Finite Element Models	92
5-2	Effect of Gusset Plate Thickness and Stiffener Dimensions on Gusset Plate Behavior	93
5-3	Deformation Spectrum Applied to Series III	93
5-4	Load versus Gusset Plate In-Plane Axial Displacement Relationship for Series II (With Brace Member) Under Monotonic Compressive Loading	94
5-5	Load versus Gusset Plate Axial Displacement Relationship for Series III (With Brace Member) Under Cyclic Loading	94
5-6	Finite Element Model for Specimens T-1 and T-2	95
5-7	Finite Element Model for Specimens T-3 and T-4	95
5-8	Location of "Bolts" as Rigid Links in the Finite Element Models	96
5-9	Location of "Contact Points" in the Finite Element Models	96
5-10	Boundary Conditions and Point of Load Application	97
5-11	Gusset Plate Out-of-Plane Initial Imperfection for Test Specimen T-1	98
5-12	Gusset Plate Out-of-Plane Initial Imperfection for Test Specimen T-2	98
5-13	Gusset Plate Out-of-Plane Initial Imperfection for Test Specimen T-3	99
5-14	Gusset Plate Out-of-Plane Initial Imperfection for Test Specimen T-4	99
5-15	Stress versus Strain Curves used in Finite Element Analysis	100
6-1	Load versus Deformation Relationship for Assembly: Specimen T-1 and T-2	117
6-2	Load versus Deformation Relationship for Assembly: Specimen T-3 and T-4	117
6-3	Experimental Gusset Plate Free Edge Displacements at the	

	Peak Compressive Load: Specimens T-1 and T-2 .....	118
6-4	Experimental Gusset Plate Free Edge Displacements at the Peak Compressive Load: Specimens T-3 and T-4 .....	118
6-5	Out-of-Plane Deformation of Brace Member at the Peak Compressive Load of the Last Load Cycle: Specimens T-3 and T-4 .....	119
6-6	Load versus Displacement Relationship for Assembly: Specimen T-1 ...	120
6-7	Load versus Displacement Relationship for Assembly: Specimen T-2 ...	120
6-8	Load versus Displacement Relationship for Assembly: Specimen T-3 ...	121
6-9	Load versus Displacement Relationship for Assembly: Specimen T-4 ...	121
6-10	Energy Dissipated by Specimen T-1 and T-2: Test versus Predicted ....	122
6-11	Energy Dissipated by Specimen T-3 and T-4: Test versus Predicted ....	122
6-12	Energy Dissipated at Each Displacement Cycle by Specimen T-1: Test Result versus Predicted .....	123
6-13	Energy Dissipated at Each Displacement Cycle by Specimen T-2: Test Result versus Predicted .....	123
6-14	Energy Dissipated at Each Displacement Cycle by Specimen T-3: Test Result versus Predicted .....	124
6-15	Energy Dissipated at Each Displacement Cycle by Specimen T-4: Test Result versus Predicted .....	124
6-16	Buckled Shape of Gusset Plate at Maximum Displacement of Final Compression Cycle: Specimen T-1 .....	125
6-17	Buckled Shape of Gusset Plate at Maximum Displacement of Final Compression Cycle: Specimen T-2 .....	125
6-18	Buckled Shape of Brace Member at Maximum Displacement of Final Compression Cycle: Specimen T-3 .....	126
6-19	Buckled Shape of Brace Member at Maximum Displacement of Final Compression Cycle: Specimen T-4 .....	126
6-20	Major Principal Stress Distribution just before First Yield in the Gusset Plate: Specimen T-1 .....	127
6-21	Major Principal Stress Distribution just before First Yield in the Gusset Plate: Specimen T-2 .....	127
6-22	Major Principal Stress Distribution just before First Yield in the Gusset Plate: Specimen T-3 .....	128
6-23	Major Principal Stress Distribution just before First Yield in the Gusset Plate: Specimen T-4 .....	128
A-1	Nodes at Which Gusset Plate Out-of-Plane Initial Imperfections are Measured .....	139

## LIST OF SYMBOLS

### Symbols

$A_1$	area under the load deflection curve for positive loads
$A_2$	area under the load deflection curve for negative loads
$A_n$	net section area
$A_{nc}$	net section area
$A_t$	net tension area
$A_v$	net shear area
$b$	half width of free edge stiffener
$C_L$	connection length factor
$E$	modulus of elasticity
$F_y$	tensile yield strength
$F_u$	ultimate yield strength
$F_{eff}$	effective tensile stress
$K$	effective length factor
$l_1$	maximum unsupported length of gusset plate strip
$L$	gusset plate connection length
$L_b$	length of brace member
$L_n$	net gusset plate connection length
$P$	brace force
$P_A^+$	predicted peak tensile load
$P_A^-$	predicted peak compressive load
$P_b$	compressive brace strength
$P_{HB}$	horizontal component of brace force
$P_{PA}$	predicted post-buckling strength
$P_{PE}$	experimental post-buckling strength
$P_t$	Thornton compressive strength
$P_u^+$	ultimate tensile resistance of test specimen

$P_u^-$	ultimate compressive resistance of test specimen
$P_{VC}$	vertical component of brace force
$P_w^+$	Whitmore tensile strength
$P_w^-$	Whitmore compressive strength
$r$	radius of gyration
$R_n$	block shear strength as per Hardash and Bjorhovde (1985)
$S_{net}$	net distance between outside bolt lines
$t$	gusset plate thickness
$T_r$	block shear resistance as per CAN/CSA-S16.1, 1997, Clause 13.2
$t_{st}$	free edge stiffener plate thickness
$u_1$	translation along axis-1
$u_2$	translation along axis-2
$u_3$	translation along axis-3
$\epsilon$	strain
$\epsilon_{ln}$	logarithmic strain
$\epsilon_{nom}$	engineering strain
$\phi$	resistance factor
$+\delta$	maximum displacement reached in tension in a loading cycle
$-\delta$	maximum displacement reached in compression in a loading cycle
$\theta_1$	rotation about axis-1
$\theta_2$	rotation about axis-2
$\theta_3$	rotation about axis-3
$\sigma_{nom}$	engineering stress
$\sigma_{true}$	true stress



# CHAPTER 1

## INTRODUCTION

### 1.1 General

Gusset plate connections are typically found in concentrically braced frames to connect bracing members to beams and columns. Their primary function is to transfer the compressive or tensile loads from the bracing member to a beam and column joint, which results in bending, shear, and normal forces in the gusset plate.

Traditionally, energy dissipation in concentrically braced frames has been performed by the brace members yielding or buckling and the gusset plates are designed to accommodate these forces without failing in tension or buckling in compression. Recently, research conducted at the University of Alberta indicated that concentrically braced frames could dissipate more energy if the gusset plate was allowed to buckle rather than the brace member; this was referred to as the strong brace – weak gusset plate concept (Rabinovitch and Cheng, 1993). The effect of gusset plate free edge stiffeners on the energy absorption characteristics of a gusset plate assembly was also briefly investigated.

Previous research has shown that the strength and energy dissipation characteristics of gusset plates are dependent on many variables. These variables include: the slenderness and geometry of the plate, the stiffness and details of the connection (Jain, Goel, and Hanson, 1978), length of the splice members used to connect the brace member to the gusset plate, and the presence of free edge stiffeners (Whitmore, 1952; Bjorhovde and Chakrabarti, 1985; Williams and Richard, 1986; Rabinovitch and Cheng, 1993;

Walbridge *et al.*, 1998). Brace member strength and ductility has also been studied and found to depend on brace member slenderness, and has been linked to the flexural stiffness of the connection between the brace member and gusset plate (Jain, Goel, and Hanson, 1978; Astaneh-Asl, Goel, and Hanson, 1985).

Many failure modes of a subassembly involving a bracing member and gusset plate subjected to cyclic loading are possible and, until recently, the interaction between the gusset plate and the bracing member had not been studied. The brace member can fail by yielding of the gross section or rupture at the net section under tension or by flexural buckling under compression. A tensile block-shear failure can occur in the gusset plate connection, or the gusset plate can buckle in compression as suggested by the strong brace – weak gusset concept presented by Rabinovitch and Cheng (1993). In this case the gusset plate free edges buckle locally and crippling of the gusset plate occurs near the connected edge of the splice member. These failure modes were studied analytically by Walbridge *et al.* (1998) to predict the behavior of steel gusset plate connections, and to study various factors that influence the behavior and energy dissipation characteristics of gusset plate connections subjected to cyclic loading.

The research presented in the following chapters is intended to test the finite element models presented by Walbridge *et al.* (1993) and add to the experimental research conducted by Rabinovitch and Cheng (1993) on the effect of free edge stiffeners on assemblies designed with either the brace member or the gusset plate as the weak element in compression.

## **1.2 Objectives**

The investigation described in the following includes an experimental and analytical program. The objectives of this investigation are as follows:

- Observe the behavior of the gusset plate – brace member interaction;
- Compare experimental results with the finite element model presented by Walbridge, *et al.* (1998) in order to verify previous conclusions;
- Determine the effect of free edge stiffeners on the behavior of the gusset plate – brace member assembly for cases in which either the gusset plate or the brace member is designed as the weak element in compression;
- Investigate the energy dissipation characteristics of gusset plates, including the effect of the interaction with the bracing member.

## **1.3 Scope**

The scope of the investigation is limited to single gusset plate connections representing those in concentric braced frames. The brace members, connected at 45° to the framing members, consist of a wide flange section bolted with splice members to the gusset plates. The bolted connection details and the brace member cross-section are kept constant in all tests. The slenderness of the free edge stiffeners was selected so that local buckling of the stiffeners was not a governing factor. In all tests, the stiffener dimensions were held constant. The gusset plates are welded to the beam and column framing members along two plate boundaries. The forces that typically exist in the beam and

column framing members are neglected. In order to satisfy the objectives mentioned above, the presence of gusset plate free edge stiffeners and the slenderness of the brace member are the two variables considered in this study.

## CHAPTER 2

### LITERATURE REVIEW

#### 2.1 Introduction

Current design of gusset plates is based on simple beam theory, experience, general practice, and engineering judgement (Bjorhovde and Chakrabarti, 1985). The most significant research on gusset plate connections began in the 1950's with the experimental work performed by Whitmore (1952). Following the 1950's, more research on the behavior of gusset plate connections was performed to gain a better understanding of the behavior of gusset plate connections and to develop simple guidelines for the design of gusset plates for monotonic and cyclic loading. A summary of this earlier work is presented in the following.

#### 2.2 General Gusset Plate Behavior

In 1952, Whitmore published the results of an experimental investigation to determine the stress distribution in common gusset plates and a simple method to determine the maximum stress magnitude in gusset plates. From tests conducted on models of Warren truss connections, Whitmore observed that the maximum normal stresses in the gusset plate were located near the last row of fasteners in the gusset plate – brace member connection. Based on this observation, Whitmore proposed that the maximum stress in the plate could be calculated by taking the brace load and dividing it by an area equal to the plate thickness times what later became known as the “Whitmore effective width”. The Whitmore effective width was defined as the distance between two lines radiating outward at 30 degree angles from the first row of bolts in the gusset-to-brace connection

along a line running through the last row of bolts as illustrated in Figure 2-1. Whitmore's effective width concept assumes that the stress on the effective width will reach the yield strength in tension. Although the method was proposed for gusset plates subjected to a tension brace force, it has been used to estimate an upper bound on the capacity in compression (Hu and Cheng, 1987; Rabinovitch and Cheng, 1993; Walbridge *et al.*, 1998). For thin plates, however, the buckling strength in compression can be significantly lower than the yield strength. Whitmore also observed that the compressive stresses along the free edges of the gusset plate are lower than predicted by simple beam theory, which predicts maximum stresses at the free edges. Based on this observation, Whitmore suggested that consideration should be given to the omission of stiffener angles along the free edges of gusset plates, except in unusual cases.

Irvan (1957) and Hardin (1958) investigated gusset plates using models of a double gusset plate Pratt truss connection detail with and without chord splices at the joint. Irvan and Hardin's conclusions concurred with those made by Whitmore with respect to the location of maximum shearing and normal stresses, as well as the inaccuracy of the beam theory for stress calculations in gusset plates. Irvan's work also further reinforced Whitmore's statement regarding the omission of free edge stiffeners.

### **2.3 Monotonic Tension Behavior**

In 1984, Thornton proposed a block shear tear-out model to check the adequacy of gusset plates in tension. The proposed tensile capacity of the gusset plate was based on the net section,  $A_n$ , which is composed of the net shear area,  $A_v$ , and the net tension area,  $A_t$ , with the hole size taken as the bolt diameter plus an allowance.

Hardash and Bjorhovde (1985) and Bjorhovde and Chakrabarti (1985) investigated the behavior of gusset plate connections in the inelastic range. From the tests conducted by Hardash and Bjorhovde (1985) and those of other investigators, a refined block shear model was proposed to predict the ultimate capacity of gusset plate connections in tension. Hardash and Bjorhovde (1985) proposed that the ultimate strength of the gusset plate is the sum of the tensile strength of the net area between the bolts in the last row of bolts and the shear strength along the connection length, (Figure 2-2). Three equations were proposed.

$$R_n = (F_u S_{net} + 1.15 F_{eff} L) t \quad (2-1)$$

$$F_{eff} = (1 - C_L) F_y + C_L F_u \quad (2-2)$$

$$C_L = 0.95 - 0.047 L \quad (2-3)$$

In the above equations,  $R_n$  is the tensile resistance of the gusset plate,  $F_y$  is the tensile yield strength of the material,  $F_u$  is the ultimate tensile strength of the material, and  $S_{net}$  is the net distance between the outside bolt lines and  $L$  is the connection length. The other variables are defined as the effective tensile stress,  $F_{eff}$ , given in Equation 2-2, the plate thickness,  $t$ , and  $C_L$  is the connection length factor defined in Equation 2-3, where  $L$  is expressed in inches. In 1988, Bjorhovde recommended that the block shear approach be used with a resistance factor of 0.85 for use with limit states design.

The block shear design equation presented in CAN/CSA S16.1 (1997) is shown below;

$$T_r = 0.85 \phi A_{ne} F_u \quad (2-4)$$

where,

$$A_{ne} = (2)(0.6)L_n t + S_{net} t \quad (2-5)$$

In the above equations,  $T_r$  represents the tensile resistance of the connection,  $A_{ne}$  is the net connection area, given by  $L_n$ , the net connection length, and  $S_{net}$  the net distance between the outside bolt lines. The plate thickness is  $t$ , and  $\phi$  is a resistance factor. The strength of the connection is therefore the sum of the net tensile strength of the connection and its shear strength. The main difference between the method presented in CAN/CSA-S16.1 (1997) and that by Hardash and Bjorhovde (1985) is that CAN/CSA-S16.1 (1997) assumes that tensile failure and shear failure occur at the same time, whereas Hardash and Bjorhovde's (1985) method assumes that failure in tension and in shear do not occur simultaneously. Hardash and Bjorhovde's block shear model is more consistent with the observed failure mode in tension (Bjorhovde and Chakrabarti, 1984). The block shear model used in CAN/CSA-S16.1. Since rupture in shear is assumed, the ultimate shear strength is used on the net shear area for strength calculations. The block shear model proposed by Hardash and Bjorhovde, however, Since the shear area is not assumed to fail, the gross area is used rather than the net area. The shear stress acting on the shear area is somewhat lower than the ultimate shear stress. This latter model is consistent with the experimental observations that indicate that failure in tension occurs by rupture along the net tension area and large shear deformations along the length of the connection.



## 2.4 Monotonic Compression Behavior

In 1984, Thornton described a method to calculate the compressive strength of gusset plates. Whitmore's section was used as a basis for checking gusset plate stability. The allowable brace force was calculated by considering a unit strip of gusset plate extending from the Whitmore section to the gusset plate and framing member boundary (see Figure 2-3). The longest of strips L<sub>1</sub>, L<sub>2</sub>, or L<sub>3</sub> is used for the strength calculations. The strip can be considered to act as a fixed-fixed equivalent column with a slenderness ratio given by  $Kl_1/r$ , with  $K=0.65$ ,  $l_1$  and  $r$  being the maximum unsupported length and the radius of gyration of the unit strip, respectively. If the allowable stress determined in this fashion exceeds the stress in the Whitmore effective width, the plate will not buckle. This method is considered conservative because it ignores plate action and the post-buckling strength of the gusset plate. Alternatively, using an average of the three lengths, L<sub>1</sub>, L<sub>2</sub>, and L<sub>3</sub>, may provide a shorter length, hence a more reasonable approximation of buckling strength.

Bjorhovde and Chakrabarti (1985) proposed that plate buckling is a significant factor in the development of design criteria and that gusset plate stiffeners be considered in design specifications. This is in contradiction with the earlier conclusion proposed by Whitmore (1952), Irvan (1957), and Hardin (1958).

Part of the research presented by Williams and Richard (1986) focused on a numerical investigation of gusset plate assemblies. There were 17 finite element models generated to study the effect of brace angle, boundary conditions, and plate dimensions on the elastic buckling load of gusset plate connections. The conclusions presented in this

portion of their investigation were that the maximum deformations in the gusset plate occurred on the long free edges of the plate and that fixed boundary conditions resulted in greater buckling capacities than a simple support edge condition. Williams and Richard concluded, based on their results, that to increase the buckling strength of the plate, one could either increase the plate thickness, reduce the plate dimensions, or add stiffeners to the long unsupported plate edge. The work of Williams and Richard supported the block shear model to calculate the strength of gusset plates in tension and Thornton's column model to calculate their capacity in compression.

Hu and Cheng (1987) investigated the behavior and failure modes of single corner gusset plate connections with bolted splice plates at 45 degrees subjected to compressive loading. Fourteen tests were performed on six specimens to investigate the effects of various parameters including gusset plate thickness and size, eccentric versus concentric loading, as well as the effects of boundary conditions. The two boundary conditions investigated in the study included a free case, allowing for free out-of-plane displacement of the gusset plate relative to the bracing member, and a fixed case, which allowed no out-of-plane movement. The gusset plate size was varied by changing the plate's width and height, as well as its thickness. The effect of splice stiffeners on the flexural rigidity of the splice plate and the strength of the gusset plate was also examined. Based on the experimental results, the following conclusions were made. The tests indicated an increase in the buckling strength of the gusset plate when the width of the plate was increased. The buckling load was found to be independent of the boundary conditions for the minimum size of gusset plate tested in this program. It was also indicated that the out-of-plane rotational restraint provided by the splice and brace members to the gusset

plate had a significant influence on the buckling strength of the gusset plate. This restraint was dependent on the relative stiffness of the splice plate and gusset plate, as well as the bending stiffness of the bracing member.

In 1993, Yam and Cheng published the results of an experimental investigation to study the effects of beam-to-column moments on gusset plate behavior, gusset plate size and thickness, bracing angle, as well as eccentricity and out-of-plane restraint at the gusset plate to splice member junction. The experimental program consisted of 19 gusset plate test specimens that resembled single gusset plate connections in a steel braced frame. The study by Yam and Cheng (1993) indicated that the beam-to-column connection moment had a negligible effect on the gusset plate behavior under monotonic compressive loads. It was also found that a 45-degree bracing angle connection resulted in a lower stress concentration in the gusset plate at the end of the splice member than a 30-degree connection, thus resulting in less in-plane bending. With out-of-plane restraint applied at the junction of the splice member and gusset plate, failure occurred by local buckling of the gusset plate at higher loads. The dominating failure mode was out-of-plane buckling of the gusset plate when there was no out-of-plane restraint. It was also observed that the ultimate strength of eccentrically loaded specimens was improved when the out-of-plane flexural rigidity of the splicing member was increased.

Yam and Cheng (1994) also presented the results of a numerical investigation of the effect of splice thickness and length and the flexural stiffness of the bracing member on the strength and behavior of gusset plates. It was found that when the splice plate thickness was increased, the elastic buckling load of the gusset plate also increased. The

increase in thickness significantly increased the buckling load until a critical value of splice plate thickness was reached, approximately four times the gusset plate thickness. The numerical results also showed that, as the splice plate length was increased, the out-of-plane and rotational restraint of the connection was increased and thus so was the elastic buckling load, and a stiffer gusset plate-brace member conjunction resulted in a greater the elastic buckling load. As a result of their numerical investigation, Yam and Cheng (1994) proposed a modification to Thornton's method, using 45-degree dispersion lines rather than 30-degree lines as in Whitmore's method to better represent the results of the numerical analysis. Based on their results, Yam and Cheng concluded that the use of splice members with a high out-of-plane rigidity should be used, the splice member should extend as close as possible to the beam and column boundary, and bracing members with high out-of-plane flexural rigidity should also be used. Yam and Cheng also made the recommendations that tests be performed to study the relative stiffness of the gusset plate and splice member and stiffener requirements.

## **2.5 Cyclic Behavior**

Compared to gusset plates under monotonic loading, gusset plates under cyclic loading have received little attention. Jain *et al.* (1978) carried out an experimental investigation that included 18 specimens consisting of 25mm x 25mm cold rolled steel tubes of varying lengths welded to hot rolled gusset plates of various dimensions. A typical test specimen of Jain *et al.* (1978) is shown in Figure 2-4. Their experimental program was designed to determine the hysteresis behavior of axially loaded steel bracing members with rotational end restraint provided by gusset plate connections and to study the effect of gusset plate

bending stiffness and bracing member length on the cyclic behavior. The gusset plates used in the tests were designed to have a higher axial yield strength than that of the brace member. Although the focus of their investigation was the bracing member, observations were made regarding the gusset plate. The results of the test program by Jain *et al.* (1978) indicated that there was no benefit in having a connection with a larger flexural strength than that of the member because the hysteresis behavior of the member remains relatively unchanged. It was also indicated that the hysteresis behavior of the members was most influenced by their slenderness.

Later work was performed by Jain *et al.* (1980) on seventeen test specimens with the same details as their previous tests. The main objective of these tests was to quantify the effect of the number of applied loading cycles on the reduction of compressive strength. The test results indicated that local buckling of the tubular bracing member was shown to have no effect on the hysteresis behavior of the assembly. However, local buckling of angle section bracing members did reduce the strength of the test specimens. Jain, *et al.* (1980) also observed that the total energy dissipation of the assembly was independent of whether tension or compression loading was applied first.

Astaneh-Asl and Goel (1984) conducted an experimental investigation with the objective of increasing the ductility and energy dissipating capacity of bracing members during cyclic loading. Tests were performed on eight specimens resembling double angle bracing members in a steel frame with gusset plate end connections. The specimens were subjected to cyclic loading. The parameter investigated in this study included the brace member slenderness. Although the focus of the investigation was to improve the

behavior of bracing members, some observations were made regarding the behavior of the assembly and the gusset plate. The gusset plates were designed using beam theory because of the simplicity of the procedure. It was noted, however, that the beam theory did not give an accurate approximation of the state of stress in the plate, as noted by previous researchers. The experimental program made use of full-scale specimens. The brace member consisted of two unequal leg angles with their short legs back-to-back resulting in in-plane buckling. The specimens included both welded and bolted connections between the gusset plate and brace member (see Figure 2-5). The tests indicated that under cyclic loading the compression capacity of the bracing members deteriorated with the number of loading cycles and the strength and ductility of the bracing member were strongly linked to the details of the connection.

Work performed by Astaneh-Asl *et al.* (1985) looked at double angle bracing members with their long legs back-to-back subjected to out-of-plane buckling under cyclic loading. Nine specimens were tested in this experiment to study the effects of brace member slenderness. This series of tests indicated that the effective length factor for out-of-plane buckling of the compression member was dependent on the bending stiffness of the gusset plate connection. Jain *et al.* (1978) noted this in earlier research as well. It was also noted that the buckling load decreased significantly from the first to the second cycle with a gradual but stable decrease in compression capacity with increasing number of cycles. Astaneh-Asl *et al.* (1985) observed that early cracking of the gusset plate could be avoided by the formation of a plastic hinge in the gusset plate normal to the longitudinal axis of the bracing member. From this observation, they suggested that the gusset plate should be designed to allow the free formation of this plastic hinge in order to prevent

fracture of the gusset plate. It was suggested that by allowing a plastic hinge to form in the gusset plate, the ductility of the gusset plate would be improved. The plastic hinge was formed by providing an adequate free length of gusset plate, equal to twice the gusset plate thickness, between the end of the bracing member and the connected edge of the gusset plate.

Rabinovitch and Cheng (1993) conducted an experimental investigation of brace member and gusset plate assemblies under cyclic loading. Five specimens designed with the gusset plate as the weak element in compression were tested. The variables that were studied included gusset plate thickness, free edge stiffeners, and the free hinge formation as suggested by Astaneh-Asl *et al.* (1985). Of the five specimens tested, two specimens included free edge stiffeners, two gusset plate thicknesses were chosen, and one specimen was designed to allow for a free hinge to form in the gusset plate at the end of the bracing member. The test set-up used in the experiment is shown in Figure 2-6. Specimens were subjected to cyclic tension and compression until their failure in tension. Failure occurred due to plate fracture between the last row of bolts in the gusset plate as was observed in earlier tests (Bjorhovde and Chakrabarti, 1984). The compression and tension capacity of the gusset plate was found to be directly proportional to the gusset plate thickness. Rabinovitch and Cheng designed one of their test specimens to allow for the formation of a plastic hinge in the gusset plate as recommended by Astaneh-Asl *et al.* (1985). This change in geometry resulted in a more rapid deterioration of the gusset plate than observed with the more traditional corner gusset plates with the bracing member close to the beam-to-column corner. It was concluded that the geometry proposed by Astaneh-Asl *et al.* (1985) would result in an overly ductile system for corner gusset

plates. The addition of free edge stiffeners was found to have no effect on the tensile capacity of the plates but did increase the energy absorption capability of the assembly and resulted in a more stable post-buckling response. Although free edge stiffeners were found to be beneficial, the effect of their slenderness on the gusset plate behavior was not investigated.

In a recent numerical study on the behavior of gusset plate connections under monotonic and cyclic loading, Walbridge *et al.* (1998) developed finite element models of gusset plate connection details and validated their models using the test results presented by Yam and Cheng (1993) and Rabinovitch and Cheng (1993). The finite element models were developed using the finite element code ABAQUS. Parameters such as gusset plate geometry, beam and column framing members, non-linear material behavior, initial imperfections, bolt slip, and boundary conditions were incorporated in the finite element models. The finite element models were found to accurately model the response of the test specimens under monotonic and cyclic loading. In order to study the interaction between the brace member and gusset plate, determine the effect of load sequence, and to verify the strong brace - weak gusset concept proposed by Rabinovitch and Cheng (1993), the validated models were modified to include bracing members of various cross sections and lengths. Different combinations of possible failure modes of the brace member and gusset plate were investigated, including: yielding of the gusset plate in tension, yielding of the brace member in tension, buckling of the gusset plate in compression, and buckling of the brace member in compression. The brace member definition and gusset plate thickness were varied in each model to obtain the desired failure mode. Three load sequences were investigated; the first load application in either



tension or compression with each subsequent load step increased, and a tension load applied first and increased subsequently with each cycle repeated three times. The effect of loading sequence was found to be negligible. It was also found from the study that the monotonic compression and tension load displacement curves tended to delineate the envelope of the hysteresis curves from the cyclic loading of the same specimen. The analysis showed that the effect of the brace member was small in cases where the gusset plate was designed as the weak element and that the gusset plate was more effective at dissipating energy than the brace member. The hysteresis loops for the weak gusset – strong brace models exhibited less pinching and sustained higher post-buckling compressive loads than the conventional weak brace – strong gusset design. Recommendations were made regarding further investigation on the potential of free edge stiffeners to improve gusset plate behavior under cyclic loads. In order to test the findings of the analytical study by Walbridge *et al.* (1998), physical tests should be undertaken on gusset plate – brace member assemblies.

## 2.6 Summary

Various behavioral and strength properties of gusset plates and brace members have been studied. Although many parameters have been investigated, some require a more thorough investigation.

Research done by Bjorhovde and Chakrabarti (1985), Hu and Cheng (1987), Yam and Cheng (1994), as well as Jain, Goel and Hanson (1980) indicated that the strength and ductility of the brace member was related to the bending stiffness of the gusset plate connection. Only recently has the interaction of the brace member and gusset plate

assembly been studied. The recent research by Walbridge *et al.* (1998) demonstrated analytically that the interaction between the brace member and gusset plate was significant in the energy dissipation characteristics of the subassembly. Experimental verification of the models used to study the gusset plate – brace member interaction is required.

Many researchers also commented on the use of gusset plate free edge stiffeners. While some thought they were not necessary (Whitmore, 1952; Irvan, 1957), others (Bjorhovde and Chakrabarti, 1985; Williams and Richard, 1986; Yam and Cheng, 1994; Rabinovitch and Cheng, 1993; Walbridge *et al.*, 1998) commented on their potential benefit on the buckling strength and energy dissipation capacity of the gusset plates. In 1993, Rabinovitch and Cheng demonstrated experimentally that gusset plate free edge stiffeners do improve the post-buckling response of gusset plates subjected to cyclic loading and may also increase the compressive capacity of the plates. However, the required slenderness of the free edge stiffeners was not determined, therefore more research is required to come up with practical design recommendations for free edge stiffeners. It was also noted by various researchers (Jain, Goel, and Hanson, 1978; Astaneh-Asl *et al.* 1985) that the strength and ductility of the bracing member would benefit from a stiffer end restraint. Therefore, the influence of the addition gusset plate free edge stiffeners to the connection should therefore be investigated as well.

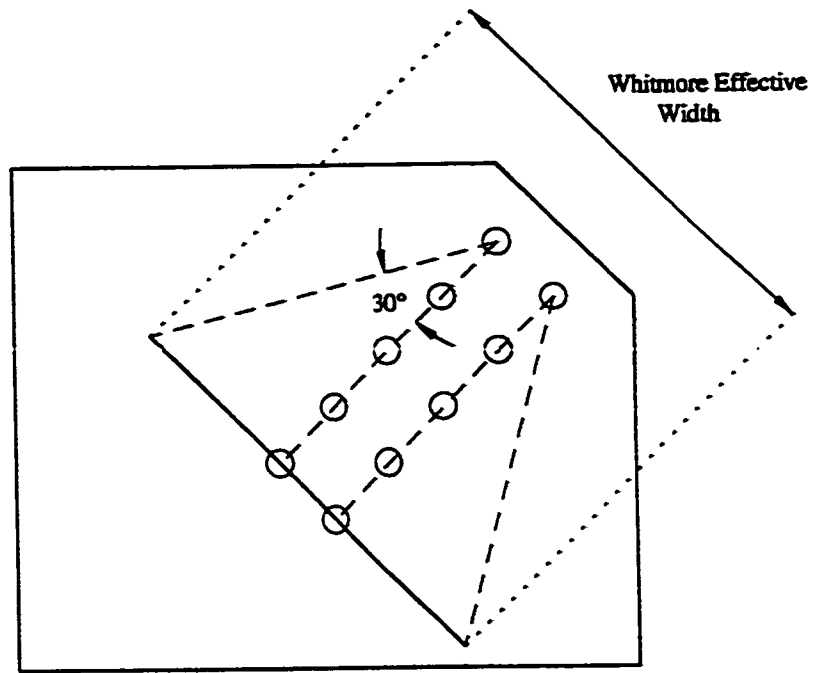


**Figure 2-1: Whitmore Effective Width Method**

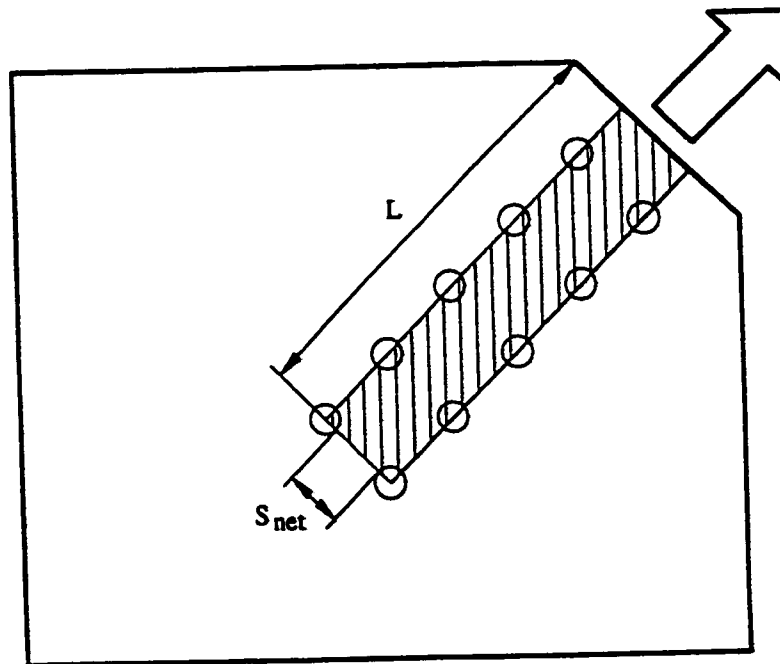


**Figure 2-2: Block Shear Model Proposed by Hardash and Bjorhovde, 1985**

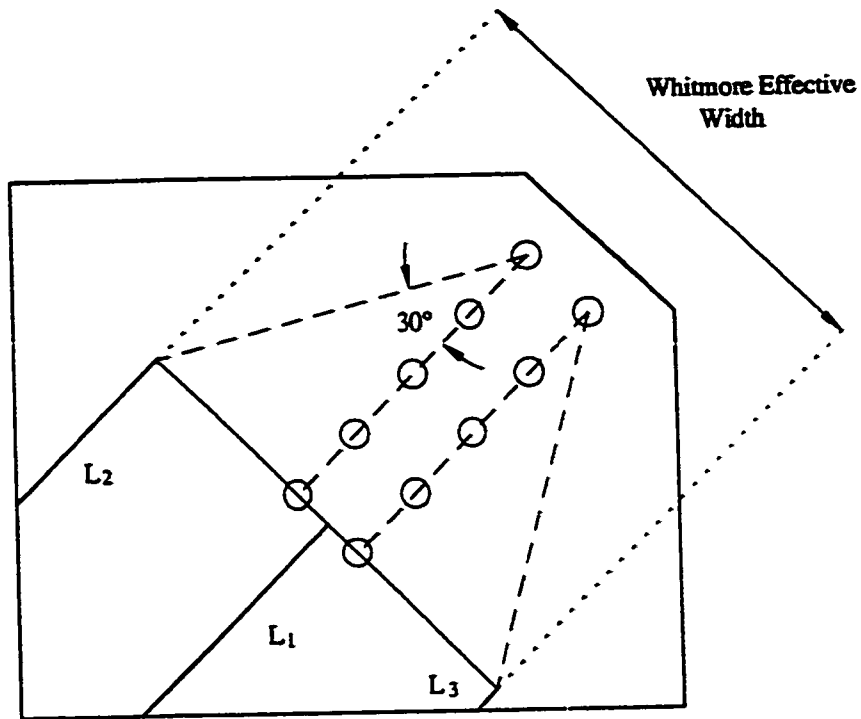


Figure 2-3: Compressive Capacity Calculation—Thornton's Method (1984)

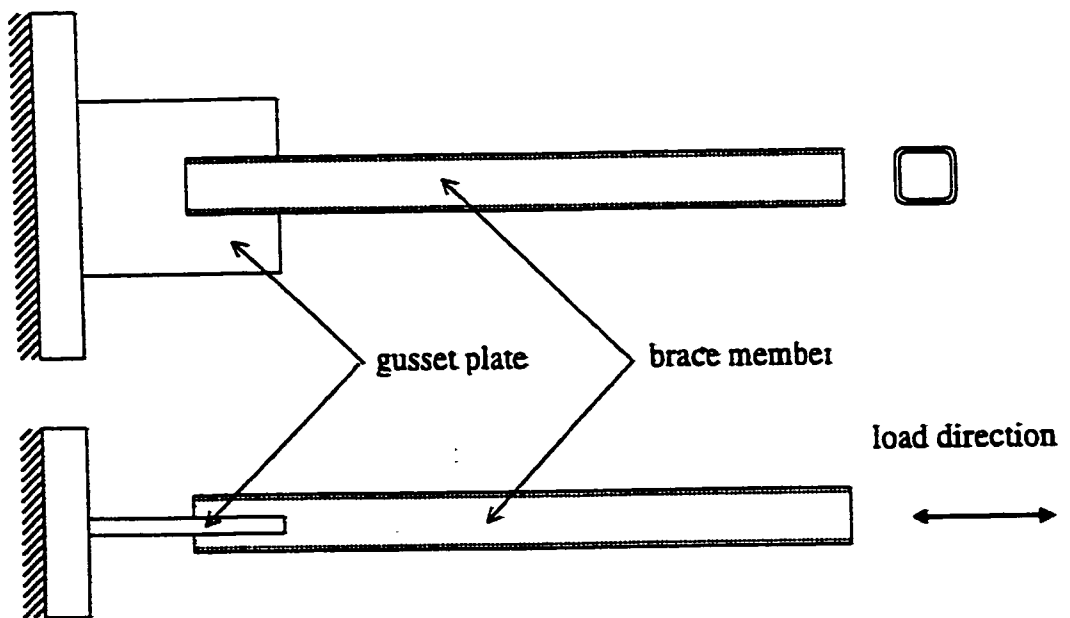


Figure 2-4: Typical Test Specimen by Jain, Goel, and Hanson (1978)

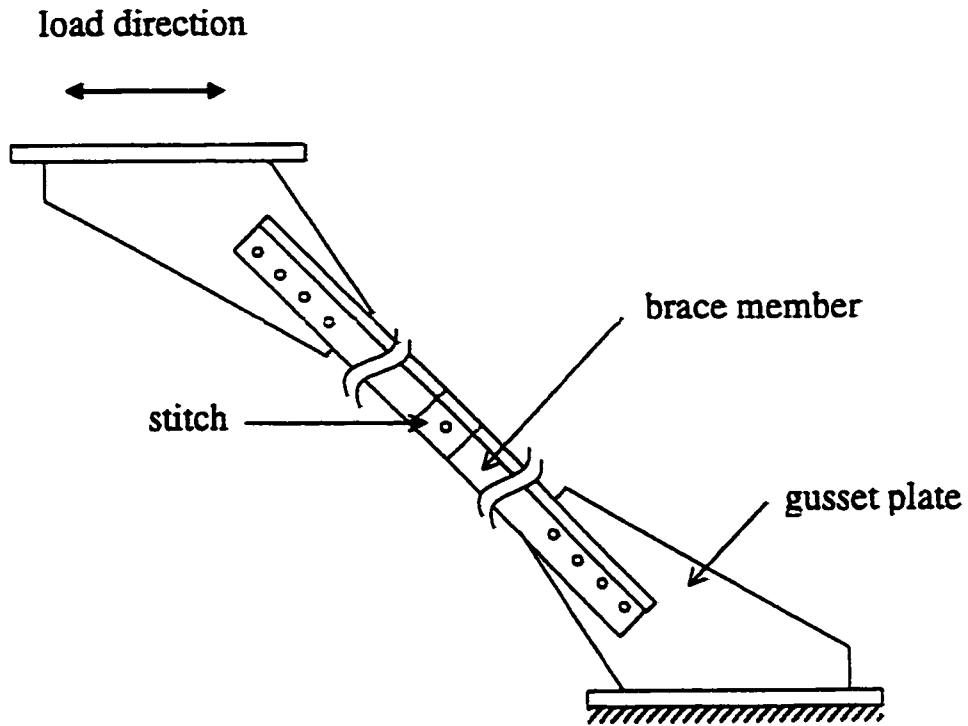


Figure 2-5: Typical Test Specimen by Astaneh-Asl and Goel (1985)

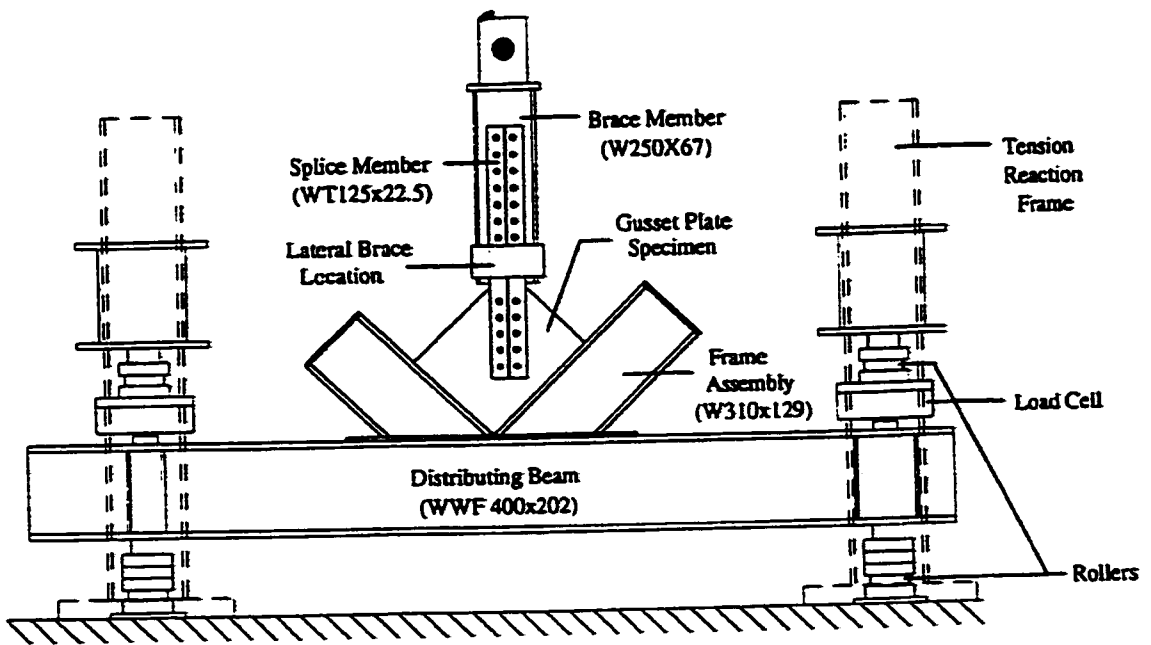


Figure 2-6: Test Set-up used by Rabinovitch and Cheng (1993)

## CHAPTER 3

### EXPERIMENTAL PROGRAM

#### 3.1 Introduction

Many parameters affecting the strength and behavior of gusset plates have been previously studied. These include the effects of gusset plate thickness, size and configuration, boundary conditions, angle of bracing, application of load, and length of splice member (Astaneh-Asl *et al.*, 1985; Hu and Cheng, 1987; Yam and Cheng, 1993; Rabinovitch and Cheng, 1993). The purpose of the experimental program described in this chapter is to test the finite element models and conclusions proposed by Walbridge *et al.* (1998) and add to the experimental data presented by Rabinovitch and Cheng (1993) on the effect of free edge stiffeners. This chapter describes the test specimens used in the experimental program as well as the test set-up, instrumentation, and testing procedure.

#### 3.2 Preliminary Considerations

The finite element models proposed by Walbridge *et al.* (1998) were based on the subassemblies tested by Yam and Cheng (1993), and Rabinovitch and Cheng (1993). The experimental program presented in this chapter uses a similar configuration of gusset plate and brace member as that used by Cheng and co-workers. To satisfy the objectives outlined in Chapter 1, the presence of gusset plate free edge stiffeners and the slenderness of the brace member are the two variables considered in this study. Each test specimen consisted of a gusset plate welded to beam and column boundary members, a splice member, and a brace member inclined at 45 degrees, as shown in Figure 3-1. The gusset plate geometry, as shown in Figure 3-2, remained constant in all tests. Since it was also

desirable to maintain the same connection details in all tests, the brace member and splice member cross-sections were kept constant. To achieve the desired compressive capacity of the brace member, its slenderness was adjusted by varying the brace member length. The gusset plate was welded to beam and column framing members and the bracing member was bolted to the gusset plate using tee shape splice members. The bolted connection was designed to exceed the compressive capacity of the assembly using the methods outlined in CAN/CSA-S16.1-M94, Clause 13.11.

### **3.3 Description of Test Specimens**

Four specimens were tested in the experimental part of the investigation. A description of the components used in each specimen is presented in Table 3-1. In all the test specimens, the splice member consisted of two tee-sections (WT205 x 42.5), and the framing member was a W310 x 129 section. The details of the connection of the gusset plate, splice member, and brace member are shown in Figure 3-1. To avoid slip in the connections under cyclic loading, all bolted connections were designed as slip critical connections. The calculated slip resistance of the connections is listed in Table 3-2. Based on the connection resistance and the anticipated loads, all connection surfaces were specified to be Class B, blast-cleaned. Bolts were pretensioned using the turn-of-nut method as specified in CAN/CSA-S16.1-M94, Clause 23.5.

A welded connection was used to join the gusset plate to the beam and column members. The required fastener strengths along the two connected edges of the gusset plate to the framing members were approximated using the equations presented by Williams and Richard (1996).

$$P_{HB} = P \cos \theta \quad (3-1)$$

$$P_{VC} = P \sin \theta \quad (3-2)$$

In the above equations,  $P_{VC}$  and  $P_{HB}$  are the vertical and horizontal components, respectively, of the brace force,  $P$  which acts at an angle  $\theta$  to the horizontal member. A single pass 8 mm fillet weld was found to provide adequate strength. A description of the welding process and specifications of the gusset plate-to-framing members and the brace member-to-tongue (used to transfer the load from the testing machine to the brace member) is given in Table 3-3. Upon completion of each test, the damaged gusset plate was flame cut from the framing members and the surface was ground smooth in preparation for the next plate to be welded into place.

An upper and lower bound axial compressive capacity of the bracing member was determined using the column design equation presented in CAN/CSA-S16.1-M94, Clause 13.3. The lower bound was obtained using an effective length factor,  $K$ , equal to 1.0, assuming that the gusset plate provided no out-of-plane rotational restraint to the bracing member. The upper bound was obtained using an effective length factor of 0.7, assuming that the gusset plate provided an infinitely stiff end restraint. From these limiting strengths, a brace member was chosen such that the desired failure mode governed.

To evaluate the effect of free edge stiffeners on the post buckling strength of gusset plate assemblies, Specimens T-1 and T-3 included free edge stiffeners. The stiffener size was determined based on preliminary results from a finite element analysis that will be described in Chapter 5. In addition to affecting the post-buckling behavior of the gusset



plate, previous research (Astaneh-Asl, Goel, and Hanson, 1985) suggested that the compressive capacity of the brace member was also dependent on the stiffness of the end condition, in this case the gusset plate. By increasing the stiffness of the gusset with the addition of edge stiffeners, this effect can be investigated further.

In order to validate the finite element models and the conclusions proposed by Walbridge *et al.* (1998), the brace member – gusset plate interaction was examined. Specimens T-3 and T-4 were designed to have the brace member fail in flexural buckling before the gusset plate and Specimens T-1 and T-2 were designed to have the gusset plate buckle before the bracing member. The specimens were designed so that the load limitation mechanism in compression was either inelastic buckling of the gusset plate or elastic buckling of the bracing member. The tensile strength of all four specimens was governed by yielding of the gusset plate followed by block shear failure.

### **3.4 Material Properties**

The material properties of the test specimens were required to calculate the capacity of the test specimens and to include into the finite element models. Tension coupons from the gusset plates, splice members, and bracing members were obtained in accordance with CAN/CSA-G40.20-92 and testing was done as per the specifications outlined in ASTM A370-96. Four gusset plate coupons were taken (two in the direction of rolling, W1 and W2, and two in the transverse direction, W3 and W4), as well as two coupons from brace member and splice member sections. The gusset plates, splice plates, and bracing members were all designated as grade 350W steel. A summary of the material

properties obtained is listed in Table 3-4. The material strengths obtained for all three components of the test specimens are consistent with grade 350W steel.

### **3.5 Initial Imperfections**

The analytical investigation carried out by Walbridge *et al.* (1998) indicated that the magnitude of the gusset plate initial imperfections significantly affected the strength of the gusset plates in compression. Out-of-plane initial imperfections were therefore measured on each gusset plate and brace member before testing. Initial imperfection measurements were taken after the gusset plate, splice members, brace member, and framing members were assembled. In this way, any initial imperfections introduced by the assembly would be included. The out-of-plane initial imperfections of the gusset plate were measured with a depth gauge and referenced to a vertical plane to obtain the initial shape, see Figure 3-3. The vertical reference plane was provided by a 19mm thick plexi-glass sheet. The plexi-glass sheet was leveled in the vertical direction using a hand level and was secured parallel to the edge of the framing member flanges. The measured out-of-plane initial imperfections of the gusset plates in test specimens T-1, T-2, T-3, and T-4 are presented in Appendix A, Tables A-1, A-2, A-3, and A-4, respectively.

A surveying transit was used to measure the initial imperfections of the brace member at the locations shown in Figure 3-4. Since buckling of the brace member was governed by the weak axis, initial imperfections were measured in the out-of-plane direction only. Deviations of the centerline of the brace member were measured along its length. The centerline of the brace member was measured with respect to the flange edges of the brace member. It was assumed that the web to flange junction is parallel to the edge of

the flange. The validity of this assumption, however, is questionable since the permissible variation in the distance between the flange edge and centerline of the web of wide flange shapes can be as much as 5 mm (CAN/CSA-S16.1-94). The measured out-of-plane initial imperfections of the brace members are presented in Appendix A, Table A-5.

The material thickness and dimensions of the gusset plates, splice members, and brace members were also measured. Averages of the measured values were used subsequently in the finite element models and are listed in Table 3-1.

### 3.6 Test Set-up

The test set-up was designed to simulate a typical gusset plate – brace member subassembly in a concentrically braced frame and is similar to the set-ups used in earlier test programs by Yam and Cheng (1993) and Rabinovitch and Cheng (1993). A gusset plate under compressive load could fail by local buckling of its free edges, or if the brace member buckled out-of-plane, the plate could sway out-of-plane to accommodate the brace member end rotation. To allow for these modes of failure, the gusset plate–brace member connection needed to allow for out-of-plane movement. This was achieved by allowing free rotation of the brace member out-of-plane at the end of the member connected to the universal testing machine used to deliver the load to the test specimen. The boundary condition at the lower end was obtained by welding the gusset plate to the beam and column framing members. This assembly was subsequently bolted to a distributing beam using twenty 1-inch (25 mm) diameter ASTM A490 bolts. The distributing beam was anchored to a strong floor and provided the reaction for the beam-column-gusset plate assembly (see Figure 3-5).

The force effects that normally exist in the beam and column framing members were neglected in this test program. Work by Yam and Cheng (1993) indicated that these forces have little effect on the ultimate capacity and behavior of the gusset plate.

The axial load in the bracing member was delivered by a MTS universal testing machine. The tip of the brace member was welded to a tongue and attached to a clevis to allow for rotation of the bracing member about an axis in the plane of the gusset plate and out-of-plane displacement of the bracing member at the gusset plate connection. Although rotation was not permitted about the strong axis of the brace member, it was felt that this behavior would not govern and could therefore be neglected. Because the load was delivered in the vertical direction, the test specimens were positioned under the universal testing machine with the bracing member in the vertical direction as shown in Figure 3-5.

Due to application of tension and compression loads, the distributing beam was anchored to the laboratory strong floor using tension reaction frames as shown in Figure 3-5. Initially, the reaction frames incorporated load cells for a static check of the test assembly. However, the frames did not behave as expected and were altered for the testing of Specimens T-2, T-3, and T-4. Some of the problems encountered, and their immediate remedies were as follows:

- The distributing beam translated laterally in the West direction during load application. To prevent this undesirable translation, a lateral support mechanism was added to the beam at the East end.
- The distributing beam deflected excessively under compressive loads. This problem was solved by adding a third support at mid-span.

- The initial preload applied to the tension supports relaxed during testing. Since there was no way of measuring this relaxation, the load cells did not perform predictably. Some shear was also introduced into the load cells as a result of the lateral drift. As mentioned above, the load cells were removed for the subsequent tests.

The boundary conditions and restraints used for test specimens T-2, T-3, and T-4 are shown in Figure 3-6. The compression force applied to the bracing member was transferred directly to the strong floor, while the distributing beam reaction frames resisted the tensile forces. Lateral restraint was provided to the distributing beam as well as the tension reaction frame. These boundary conditions resulted in a more stable and predictable system.

### **3.7 Instrumentation**

The test specimens were instrumented using linear variable displacement transformers (LVDT), cable transducers (CT), strain gauges, and dial gauges. LVDT's, positioned as shown in Figures 3-5 and 3-6, measured in-plane displacements of the subassemblies and the test frame. Two LVDT's were set up to measure the vertical displacement of the brace member – gusset plate subassembly and the gusset plate with respect to the end plate used to attach the beam and column assembly to the distributing beam. In this way, the brace member – gusset plate subassembly and gusset plate deflections were isolated from the base plate and distributing beam deflections, as well as the slip experienced in the clevis pin connection. The performance of the slip critical connections could also be monitored. Due to the importance of these measurements, dial gauges were also used to record the same deformations at regular intervals throughout testing of specimens T-2,

T-3, and T-4. The vertical deflection of the distributing beam at center span for test T-1 was also monitored. For tests T-2, T-3, T-4, the distributing beam vertical deflection was not monitored.

The out-of-plane deformation of the gusset plate and brace members was measured using cable transducers. The out-of-plane deformation along the free edges of the gusset plate was measured using six cable transducers at the locations indicated in Figure 3-7. The cable transducers were mounted on a temporary frame mounted to the beam and column members as shown in Figure 3-8. The position of these cable transducers was the same for all four tests. The brace member out-of-plane deflection in test specimens T-3 and T-4 was measured using four cable transducers attached to a temporary frame. The assembly used to support these cable transducers is shown in Figure 3-9.

Strains in the gusset plate, edge stiffeners, and brace member were measured using linear and rosette electrical resistance strain gauges. The location of the strain gauges was chosen based on previous experiments and results of the finite element analysis models by Walbridge *et al.* (1998). Four rosettes were mounted on each gusset plate to determine the principal strain orientations since it was desirable to determine if the principal strain orientation was altered by the addition of free edge stiffeners. The strains in the stiffeners were measured to determine if yielding testing in the free edge stiffeners occurred. One pair of strain gauges was mounted on either side of the gusset plate directly below the end of splice member (Figure 3-10) to determine the amount of bending induced in the gusset plate. These gauges served to indicate when buckling occurred as well as the value of the maximum stresses in the plate during loading (see Figure 3-10). Strain gauges were

mounted on the brace member flanges to detect local buckling and overall buckling of the member. The location of the strain gauges for the brace members is shown in Figure 3-11. The output from the strain gauges, LVDT's, applied load and stroke, and cable transducers was monitored using a FLUKE data acquisition system.

### 3.8 Test Procedure

The load on the bracing member was applied using a MTS 6000 universal testing machine under stroke control. The rate of loading ranged from 1 mm/minute to 5 mm/minute, as measured by the stroke of the testing machine. The load rate chosen during a test was based on the behavior of the specimen under the prescribed loads. When the maximum compressive or tensile load was approached, the rate of loading was decreased, and during the unloading branch of a cycle, the rate was increased. Loading was paused when manual measurements of load and displacements were taken. The load history applied could be considered quasi-static, therefore the speed of testing could be considered to have a negligible effect on the results (Davis *et al.*, 1982).

The testing program derived for this study followed the Applied Technology Council recommendations for the cyclic seismic testing of components of steel structures (Applied Technology Council - 24, 1992). All four subassemblies were subjected to similar load histories. The load was applied by imposing a predetermined in-plane axial displacement to the brace member. The amount of displacement was chosen based on the expected tensile capacity of each member in the subassembly. The loading history included six cycles of elastic loading, with the first set of three cycles starting with tension followed by compression to the same displacement level as the tension

displacement. Following the elastic loading, a series of inelastic cycles were imposed. Each inelastic cycle was repeated three times at each level of displacement. After the maximum load was achieved in compression the number of loading cycles in each block of cycles was reduced to two. This loading procedure was continued until a stable compression load capacity was achieved. The magnitude of the tension displacement was held constant in the final cycles to prevent a tension failure in the connection before the plate had experienced large deformations in compression. When the stable compression load capacity was achieved, the specimen was loaded in tension until failure occurred. Failure was defined as the point at which the assembly lost its tensile load carrying capacity. Figures 3-12 through 3-15 depict the deformation spectrum adopted for each test.



**Table 3-1  
Specimen Description**

Test Specimen	Gusset Plate Dimensions (mm)	Free Edge Stiffener Width x Length (mm)	Brace Member Length (mm)	Splice Member Length (mm)
T-1	450 x 550 x 9.51	50.69 x 9.49	1100	1010
T-2	450 x 550 x 9.61	-	1100	1010
T-3	450 x 550 x 9.48	50.45 x 9.52	5250	1010
T-4	450 x 550 x 9.53	-	5250	1010

**Table 3-2  
Bolted Connection Slip Resistance**

Connection	Details	Slip Resistance (kN) 5% Probability of Slip	
		Class A Surface Clean Mill Scale	Class B Surface Blast-cleaned
Splice Member to Gusset Plate	10 – ASTM A490 1 in. (25 mm) diameter bolts	1431	2362
Brace Member to Splice Member	14 – ASTM A490 7/8 in. (22 mm) diameter bolts	1502	2481

Calculated as per CAN/CSA-S16.1-M94, Clause 13.12

**Table 3-3  
Welding Processes and Specifications**

<b>Gusset Plate to Framing Members</b>	<b>Single Pass</b>
	E-48018 electrodes x 3.2mm 125 A DCEP; 22V; 75-100mm/min
<b>Brace Member to Tongue</b>	<b>Full Penetration Multipass Welds</b>
	<u>Inside:</u> 10mm – 3 pass fillet
	Root E-48018 electrodes x 2.5mm 100 A DCEP; 22V; 100-125mm/min
	Cap E-48018 electrodes x 3.2mm 125 A DCEP; 22V; 75-100mm/min
	<u>Outside:</u> Single Bevel Groove Weld
	Root E-48018 electrodes x 2.5mm 100 A DCEP; 22V; 100-125mm/min Fill E-48018 electrodes x 3.2mm 125 A DCEP; 22V; 75-100mm/min Cap E-48018 electrodes x 4.0mm 160 A DCEP; 22V; 75-100mm/min

Note: Welding process used in all cases - Shielded Metal Arc Welding

**Table 3-4  
Material Properties**

Component	Yield Stress $F_y$ (MPa)		Ultimate Static Stress $F_u$ (MPa)	Elastic Modulus $E$ (MPa)
	Static	Dynamic		
Gusset Plate W1	417	435	482	208 400
Gusset Plate W2	424	441	491	215 500
Gusset Plate W3	408	425	478	192 900
Gusset Plate W4	409	430	484	192 600
<i>Mean</i>	<i>415</i>	<i>433</i>	<i>484</i>	<i>202 200</i>
<i>Coefficient of Variation %</i>	<i>1.9</i>	<i>1.6</i>	<i>1.1</i>	<i>5.3</i>
Brace Member	390	404	535	207 900
Brace Member	389	405	533	201 200
<i>Mean</i>	<i>390</i>	<i>405</i>	<i>534</i>	<i>204 500</i>
Splice Member	344	360	482	206 300
Splice Member	339	358	468	192 100
<i>Mean</i>	<i>342</i>	<i>359</i>	<i>475</i>	<i>199 200</i>

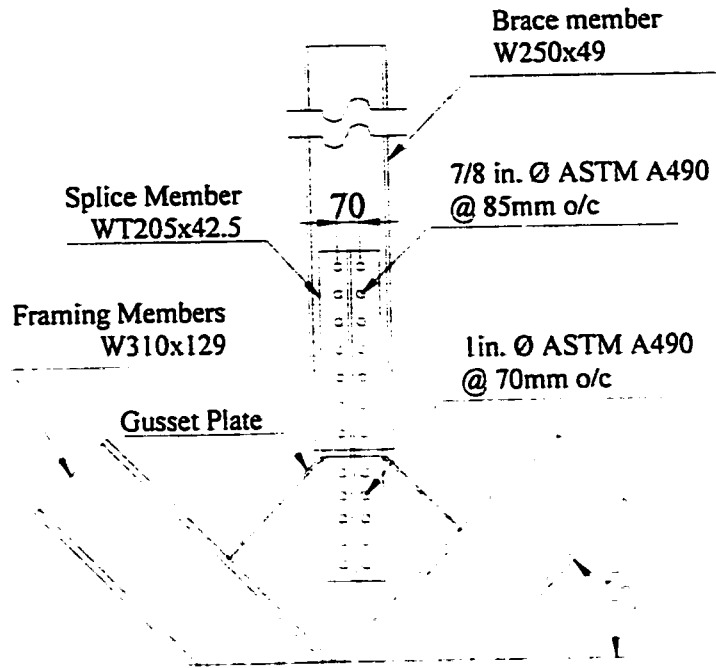


**Figure 3-1: Subassembly Details**

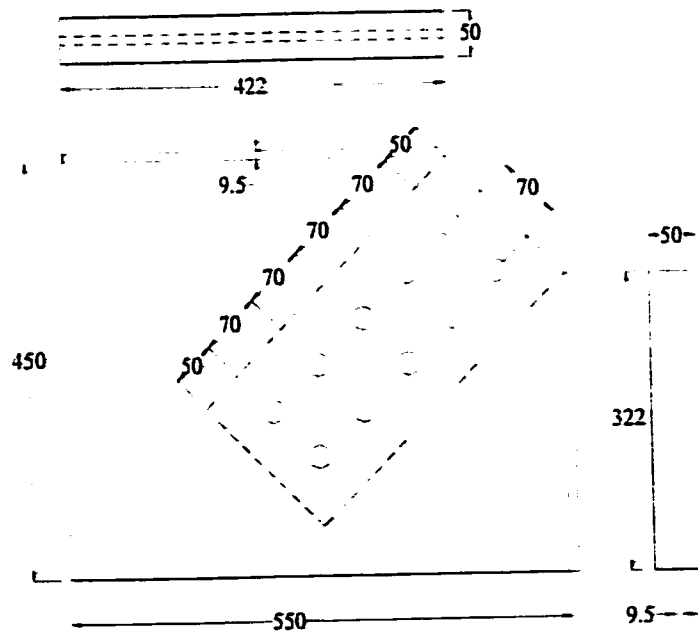


**Figure 3-2: Gusset Plate Geometry**

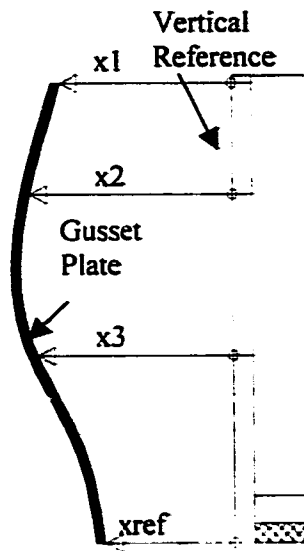


**Figure 3-3a: Profile of gusset plate showing typical imperfection measurements**

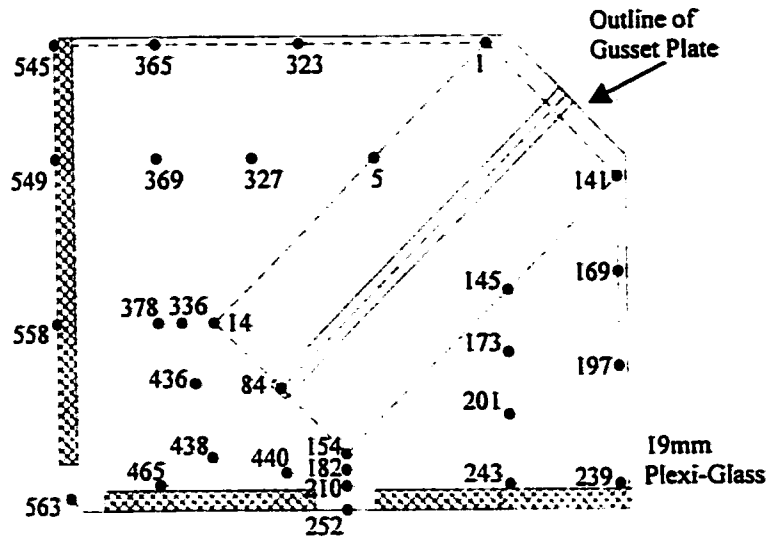


**Figure 3-3b: Finite element nodes where measurements were taken**

**Figure 3-3: Initial Imperfection Measurement**

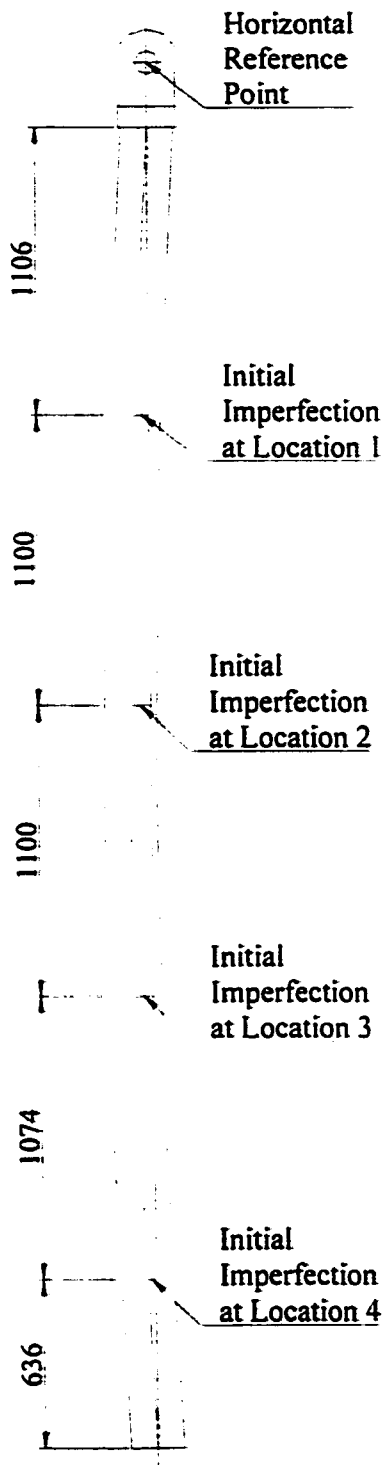


**Figure 3-4: Location of Initial Imperfection Measurements on Brace Member**

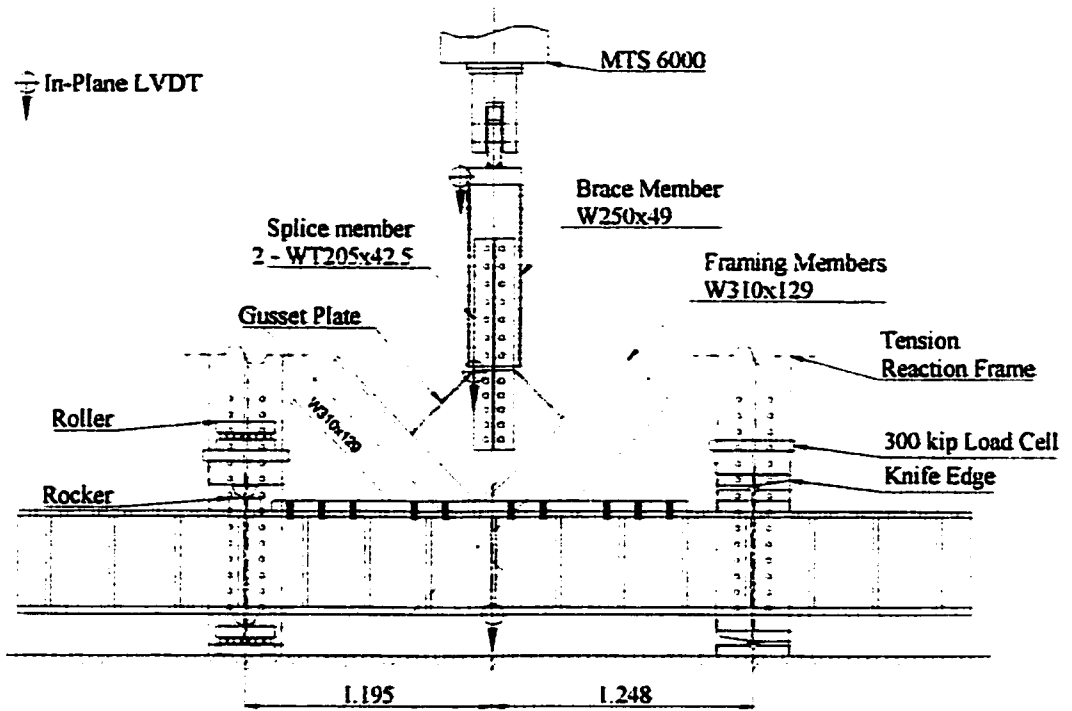


**Figure 3-5: Test Set-up for Specimen T-1**

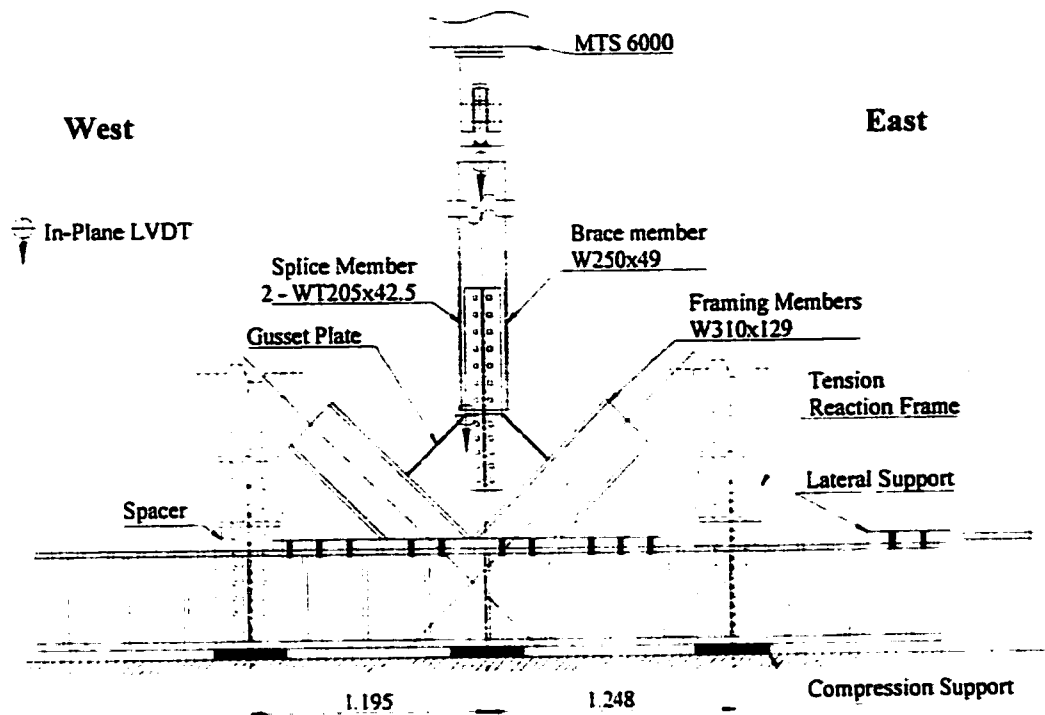


**Figure 3-6: Test Set-up for Specimens T-2, T-3, and T-4**



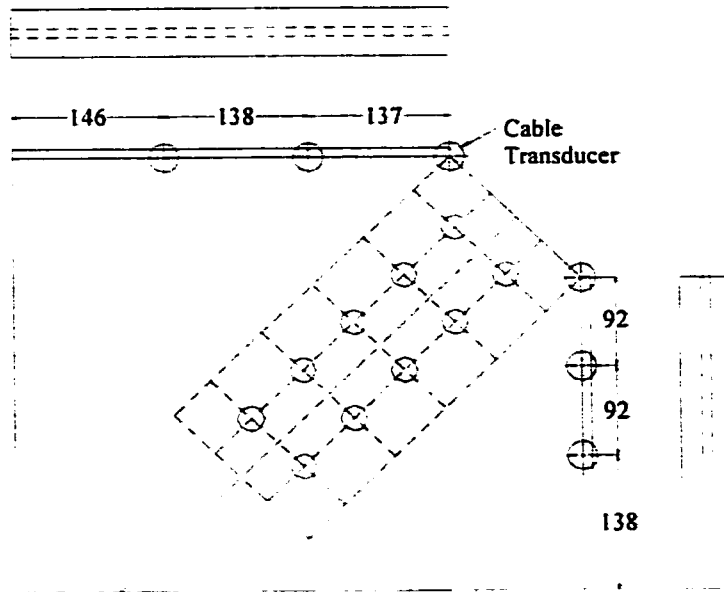


**Figure 3-7: Cable Transducer Location**

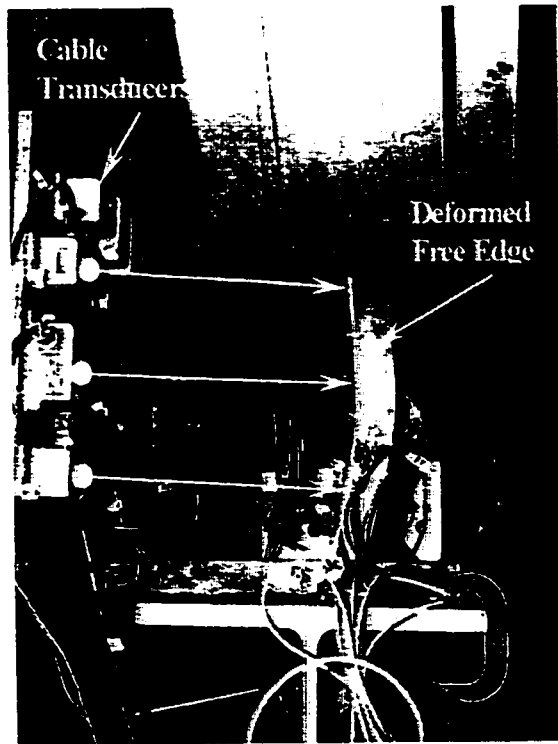


**Figure 3-8: Cable Transducer Frame -- Gusset Plate**

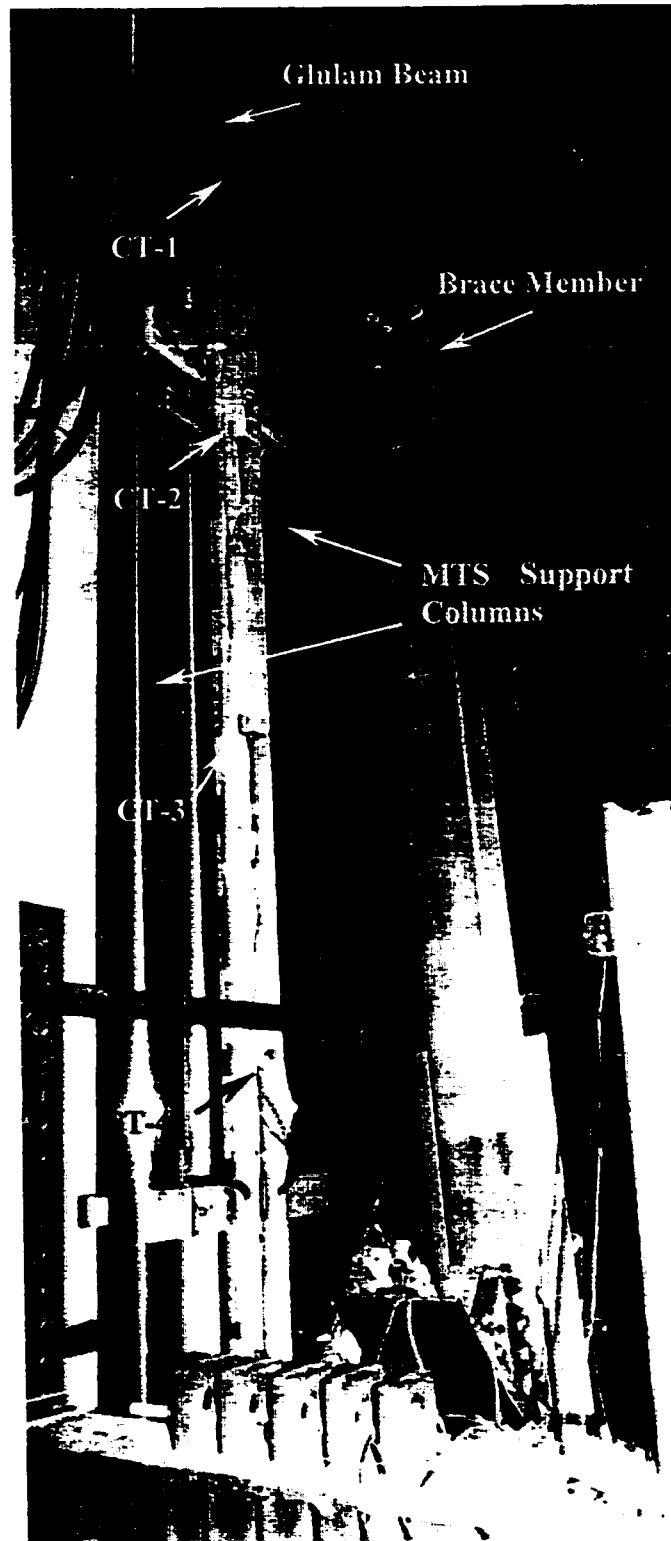
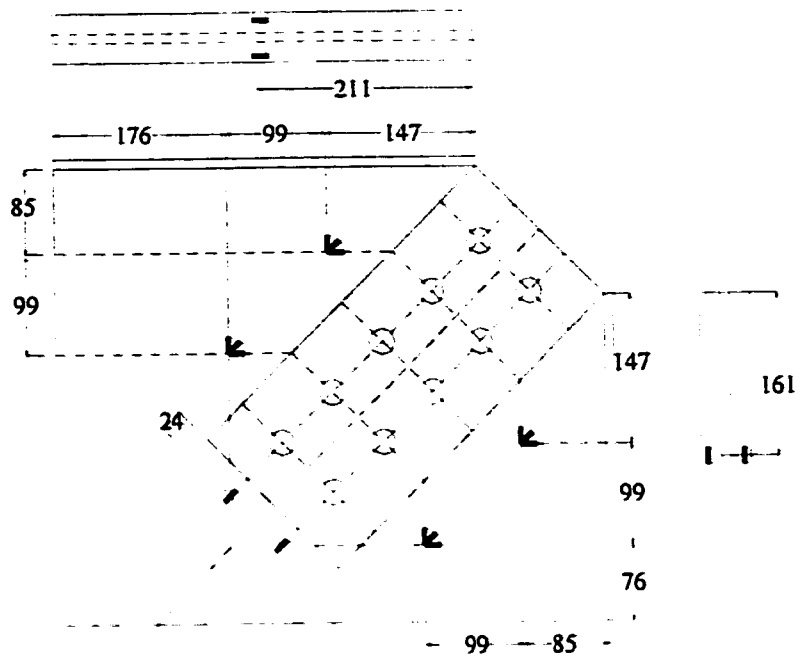


**Figure 3-9: Cable Transducer Frame – Brace Member**



\*Note: Linear Strain Gauges  
at last row of bolts are on  
both sides of Gusset Plate

**Figure 3-10: Strain Gauge Location on Gusset Plate**

South Face - Web

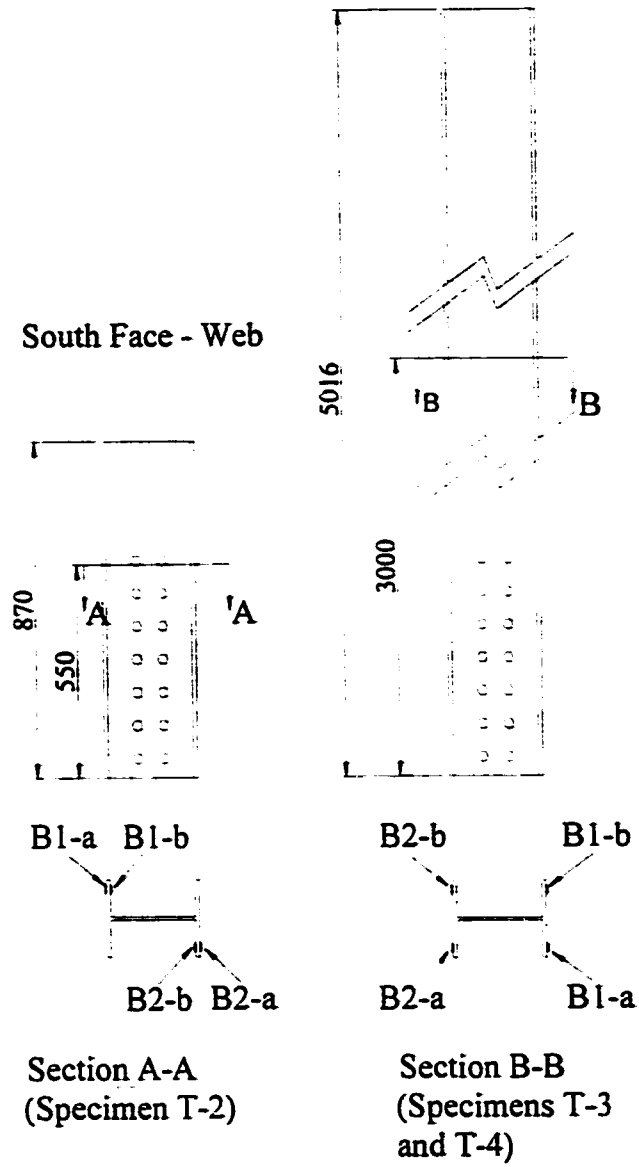


**Figure 3-11: Strain Gauge Position on Brace Members for Specimens T-2, T-3, and T-4**

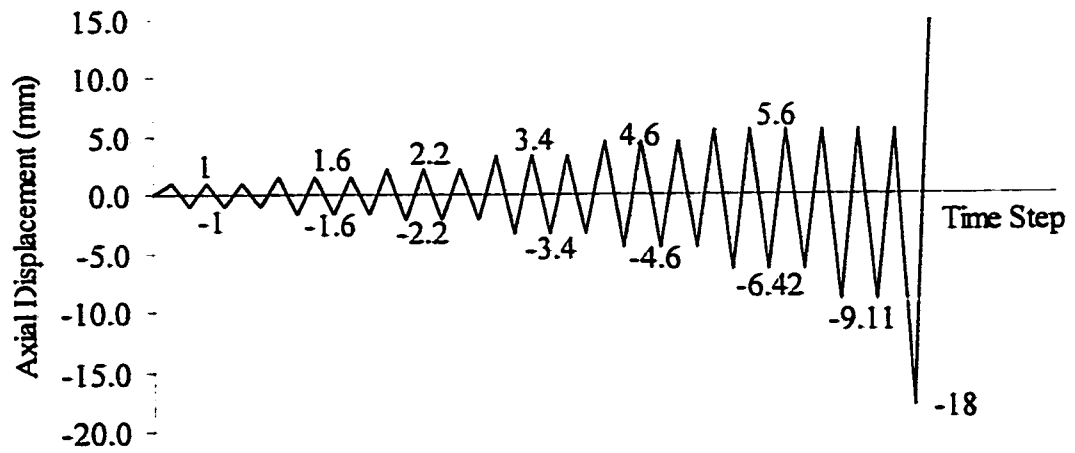


**Figure 3-12: Deformation Spectrum Applied to Specimen T-1**

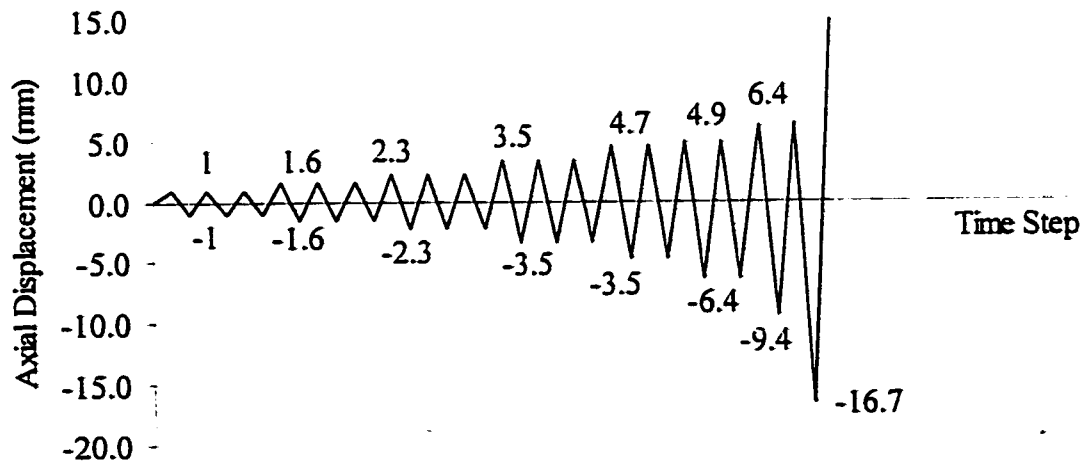


**Figure 3-13: Deformation Spectrum Applied to Specimen T-2**

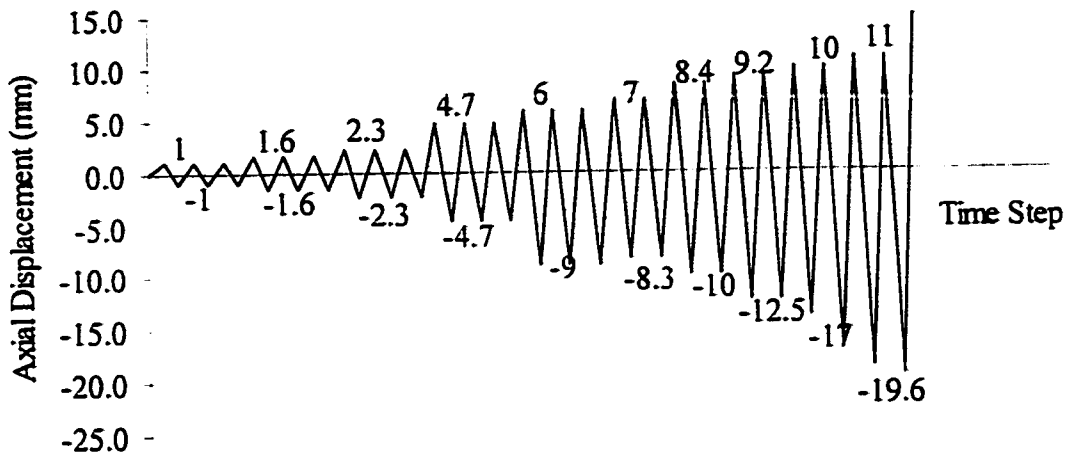


**Figure 3-14: Deformation Spectrum Applied to Specimen T-3**

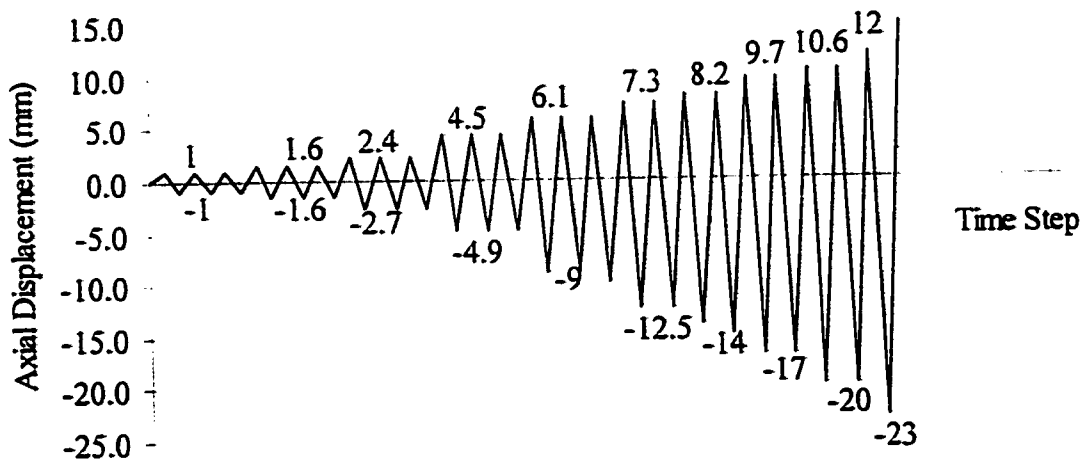


**Figure 3-15: Deformation Spectrum Applied to Specimen T-4**

## CHAPTER 4

### EXPERIMENTAL RESULTS

#### 4.1 Introduction

The data collected and the observations made during the four tests described in the previous chapter are presented in this chapter. The load versus deformation hysteresis response of the test specimens and the buckling configuration of the brace members and gusset plates are presented to help validate the finite element models proposed by Walbridge *et al.* (1998). The validation of these finite element models will be presented in Chapter 6. Measured strains and the direction of the principal strains in the gusset plates are also presented to add to the previous research by Rabinovitch and Cheng (1993) on the effect of the free edge stiffeners. The deformations and strains at specific load levels will be used as the basis of comparison between the tests. The load levels that will be used include the Whitmore yield load in tension and compression, as well as Thornton's buckling capacity of the gusset plates. Additional load levels that will be used include the loads at which yielding in the gusset plates and brace members were first detected during testing, and the experimental buckling loads of the brace members and gusset plates. Yielding in the test specimens was detected using strain gauges mounted on the gusset plate and bracing member. The use of a whitewash to visually detect yielding was not possible since the mill scale, usually present on hot rolled steel, was removed during the fabrication of test specimens.

In addition to the data collected, qualitative observations were made and are reported in this chapter. Further discussion of the test results relating to the objectives of this thesis will be presented in Chapter 6.

## **4.2 Load-Deformation Behavior**

All the test specimens were subjected to similar displacement histories. Each specimen was subjected to six cycles of elastic loading followed by a series of inelastic cycles. Specimens T-1, T-2, T-3, and T-4 were subjected to a total of 21, 18, 25 and 25 displacement cycles, respectively. The cycles were discontinued after the compressive load carrying capacity had become stable following buckling. The decrease in the compressive load capacity between the final two compressive cycles was 4, 5, 6, and 6 percent for Specimens T-1, T-2, T-3, and T-4, respectively.

Load versus deformation hysteresis curves for the test specimens were obtained for the deformation of the gusset plate alone, as well as for the deformation of the gusset plate – brace member assembly. The deformation of the gusset plate and the gusset plate – brace member assembly in Specimen T-1 was measured with linear variable displacement transducers. However, problems with this instrumentation were detected after testing and could not be corrected. Therefore, in the following tests, the axial deformations of the gusset plate and the gusset plate – brace member assemblies were measured with linear variable displacement transducers and dial gauges to rectify the problem. The measured axial deformations of the assembly include possible bolt slip of the gusset plate – splice member connection, whereas the axial deformations recorded for the gusset plate excluded bolt slip in the connection. The load versus deformation plots



for the gusset plate for Specimens T-1 to T-4 are shown in Figures 4-1 to 4-4, respectively, and the load versus deformation plots for the assemblies are presented in Figures 4-5 to 4-8.

The load versus deformation plots show that the imposed deformations in tension and compression were not symmetrical. The imposed tensile displacement was increased at the same rate as the compressive displacement up to the calculated ultimate tensile load capacity of the gusset plate based on block shear failure. From that point, the compressive displacement was increased in the subsequent cycles, and the tensile displacement was held relatively constant. After a stable behavior was reached in compression, the specimens were brought to failure in tension. The maximum tensile capacity and compressive capacity obtained from each test specimen are summarized in Table 4-1.

Although the gusset plate response for Specimen T-1 is inconclusive (Figure 4-1) because of the malfunction of the displacement transducer, the response of the assembly, as seen in Figure 4-5, shows a drop in compressive load carrying capacity following buckling of the gusset plate. As the axial deformation in compression was increased in subsequent cycles, the load carrying capacity decreased. This behavior was observed in all test specimens. A plot of the peak compressive load in each load cycle versus peak displacement, presented in Figure 4-9, illustrates this behavior. Each point in Figure 4-9 corresponds to a different loading block. Figure 4-9 also indicates that, compared to Specimen T-1, the compressive load carrying capacity of Specimen T-2 decreases rapidly after buckling of the gusset plate and that Specimen T-2 has an overall compressive capacity lower than that of Specimen T-1. This difference can be attributed to the

presence of free edge stiffeners since this is the only difference between the two specimens. Secondly, a negligible difference is observed in the load carrying capacities and the post-buckling strengths between Specimens T-3 and T-4. Finally, the overall rate of decrease in the load carrying capacity for Specimens T-3 and T-4 is significantly greater than for Specimens T-1 and T-2.

All specimens were loaded to failure in tension with the exception of Specimen T-1. The specimens failed in block shear with tearing between the bolt holes in the last row of bolts. This can be seen clearly in Figure 4-10. All tests failed at approximately the same load level as shown in Table 4-1. The measured failure load is in excellent agreement with the tensile block shear failure load of 1776 kN calculated using the method presented by Hardash and Bjorhovde (1985). The test to predicted ratio for block shear failure varies from 1.02 to 1.04.

Although the bolted connections were designed as slip critical, slip did occur in the bolted connection between the gusset plate and splice member in Specimens T-1 and T-2. Specimen T-1 experienced bolt slip in cycle #11 at a tensile load of 1265 kN and Specimen T-2 experienced slip at 1251 kN in cycle #8. When slip occurred, the load dropped due to the slack created in the loading system and then began to increase again upon completion of the slip. The first hysteresis loop where slip was observed in Specimens T-1 and T-2 is shown in Figure 4-11. It should be noted that the load drop observed when slip occurred is not shown in the figures since load and displacements were not recorded during that part of the tests. The loads at which slip occurred were much lower than the calculated slip resistance of 2360 kN for the connections. A lower bolt preload than expected is believed to have allowed the bolted connections to slip.

(The full one third turn of the nut could not be applied during torquing of the bolts in the specimens and as a result, the required preload in the bolts was not achieved in Specimens T-1 and T-2.) In order to avoid this result in Specimens T-3 and T-4, the nuts were torqued using a torque wrench to achieve the full one third turn required. As a result, Specimens T-3 and T-4 did not experience significant slip in the bolted connection between the splice member and the gusset plate.

### **4.3 Energy Absorption**

The area under the load-deformation curves is a measure of the energy absorbed during cyclic loading. The energy absorbed by each specimen was calculated for each test by integrating over the load versus displacement curve for each cycle of loading. The total area,  $A_1$  and  $A_2$ , as seen in Figure 4-12, was calculated for each displacement cycle. The calculated energy was then summed with the previous cycles and plotted against the maximum compressive displacement reached in that cycle ( $-\delta$ ). The cumulative energy absorbed by the specimen calculated in this way is presented in Figure 4-13(a).

An alternate way of presenting this information is to present the amount of energy absorbed in the tension and compression regions of the plots separately. The cumulative energy absorbed by each test specimen calculated in this manner is plotted in Figure 4-13(b). Although Specimens T-1 and T-2 are plotted with T-3 and T-4, they cannot be compared to these specimens. Specimens T-1 and T-2 were not designed with the same compressive capacity as T-3 and T-4. Therefore, a comparison of the amount of energy absorbed by Specimens T-1 and T-2 with T-3 and T-4 cannot be made. However, comparisons can be made between Specimens T-1 and T-2, and also between Specimens

T-3 and T-4 to determine the effect of free edge stiffeners. A comparison of the data for T-1 versus T-2 and T-3 with T-4 indicates that stiffeners have no effect on the amount of energy the assembly absorbs in tension. In compression, however, the stiffeners increase significantly the amount of energy absorbed. As expected, for the cases with the gusset plate as the weak element in compression, the stiffeners seem to have a negligible effect at small axial displacements, with increasing effectiveness at larger axial displacements. These results will be discussed further in Chapter 6.

In the research conducted by Rabinovitch and Cheng (1993), slip in the gusset plate-to-splice member connection was also determined to be an important factor in the amount of energy that could be absorbed by the system. By plotting separately the cumulative energy absorbed by the assembly and by the gusset plate for Specimen T-2 (see Figure 4-14) the effect of bolt slip can be assessed. The difference between these two plots represents the contribution of bolt slip to the energy absorbed by the assembly. Bolt slip will be discussed in more detail in Chapter 6.

#### **4.4 Out-of-Plane Deformation**

Cable transducers were used to monitor the out-of-plane deformations of the gusset plate in all the test specimens, as well as the brace member deformations in Specimens T-3 and T-4. It was expected that the free edges of the gusset plate would buckle and deform significantly out-of-plane in Specimens T-1 and T-2 since the gusset plate was designed to buckle. In Specimens T-3 and T-4, the gusset plate was expected to sway out-of-plane as a result of the brace member end rotation after buckling. The assemblies behaved as predicted. In Specimens T-1 and T-2, the gusset plates buckled in compression.

Buckling of the plate in these specimens took place at the end of the splice members and along the free edges. In Specimens T-3 and T-4, the brace member buckled elastically.

The deformed shape of the gusset plate free edges at yield of the gusset plate, calculated according to Thornton's method, and at the peak compressive capacity of the gusset plate (Table 4-2) are shown in Figures 4-15 and 4-16 for Specimens T-1 and T-2, respectively. Figures 4-17a and 4-17b show the deformed long free edge of the gusset plate at the peak compressive load of the final compression cycle for Specimens T-1 and T-2, respectively. The deformed shape of the gusset plate free edges at buckling of the brace member in Specimens T-3 and T-4 is shown in Figures 4-18 and 4-19, respectively. Only one curve is presented because the brace member cross-section did not yield before buckling. Figures 4-20a and 4-20b show the deformed long free edge of the gusset plate at the peak load of the final compression cycle for Specimens T-3 and T-4, respectively. A comparison of Figures 4-15 and 4-16 with Figures 4-18 and 4-19 indicates that the curvature over most of the plate length is small, and that the out-of-plane deformations are large when buckling of the brace member is the load limiting mechanism. Also, the gusset plate curvature is significantly larger and out-of-plane deflections are smaller when the load limiting mechanism in compression is buckling of the gusset plate.

The brace member out-of-plane deflections were also monitored during testing. The brace member from Specimens T-1 and T-2 did not buckle, but remained straight and rotated out-of-plane as the gusset plate buckled. The out-of-plane rotation of the brace member measured at the theoretical Thornton load, at the gusset plate buckling load, and at the peak load of the last compression cycle have been tabulated in Table 4-3. Twist about the axis of the brace member was also detected during the tests due to the

difference in stiffness of the gusset plate free edges. This behavior was also noted in Specimens T-3 and T-4.

The out-of-plane deflected shape of the brace member in Specimens T-3 and T-4 are shown in Figures 4-21 and 4-22, respectively. The deflected shape is plotted at first yield in the gusset plate, at buckling of the brace member, and at the peak of the last compression cycle. The deformed shapes of the brace members in Specimens T-3 and T-4 were very similar. The gusset plates in both tests did not buckle, but swayed out-of-plane as the end of the brace member rotated. The inflection points formed at the same location along the brace, and the location of the maximum out-of-plane deflection occurred at approximately mid-span in both specimens. However, the out-of-plane deformation of Specimen T-4 was greater than for Specimen T-3. As loading progressed, the system became softer and, for the same axial displacement level, the out-of-plane displacement increased with the number of cycles. Figure 4-23 depicts this progressive deformation for Specimen T-4 by plotting the peak out-of-plane deflected shape for each cycle of load blocks 5 to 9. The first number of the designation represents the loading block, and the second number is the cycle number within the block. Figure 4-24 shows the deflected shape of T-4 at the peak compressive load in cycle #21 (the eighth load block, second cycle).

#### **4.5 Strain Gauge Data**

Strains were measured in the gusset plates and brace members with single grid and rosette electrical resistance strain gauges. The strain data were used to determine the start

of yielding in the brace member and the gusset plate. The strain gauges were also used to determine the magnitude and direction of the principal strains in the gusset plates.

#### ***4.5.1 Strains in Gusset Plate and Brace Member***

Single grid strain gauges were used at the base of the splice member on the gusset plate to monitor strains at the points of expected peak strains in the gusset plate (refer to Figure 3-10). Four gauges were placed in this location on each specimen. A summary of the averages of these strains at specific load levels is presented in Table 4-4. The load levels chosen include the calculated Whitmore yield load in tension and compression, the Thornton load in compression, as well as the experimental buckling load (either gusset plate buckling or brace buckling). The strain data indicate that higher tensile strains develop in the gusset plate when the plate is designed as the weak element. A comparison of T-1 with T-2 and T-3 with T-4 at buckling also indicates that plates with free edge stiffeners exhibit larger compressive strains than the unstiffened gusset plates.

The strain gauges were also used to indicate the start of yielding in the gusset plate and brace member. The load and compression displacement of the gusset plate-brace member assembly at which first yield was detected either in the brace member or gusset plate are presented in Table 4-5. From this data, it can be seen that the gusset plates and brace members both yield at lower load levels and at smaller axial displacements when free edge stiffeners are present due to the increased stiffness of the gusset plate.

A recent paper by Astanteh-Asl (1998) states that in a weak gusset – strong brace system, the gusset plate would be expected to buckle elastically thus resulting in little energy absorption. However, the results of this experiment demonstrate that this is not the case.

The gusset plates in test specimens T-1 and T-2, designed with the gusset plate as the weak compression element, yielded well before buckling of the gusset plate. The first signs of yielding occurred in the region beneath the end of the splice member connected to the gusset plate, the location of maximum stress predicted by Whitmore (1952). This was determined based on the strain gauge data obtained during testing.

Strain rosettes were used to determine the magnitude and direction of the principal strains in the gusset plates. The effect of the free edge stiffeners on the stress distribution in the plate could thus be monitored. The load levels chosen for comparison are the Whitmore yield load in tension and compression, as well as the yield load of the brace member in compression. Thornton's load was not used since the strains in the gusset plate were approximately equal to those at the compressive Whitmore yield load level. Tables 4-6, 4-7 and 4-8 present the principal strain direction and magnitude for each of the load levels listed above. These test results indicate that the free edge stiffeners affect the stress distribution in the plate. There is a significant effect in tension when the gusset plate is designed as the weak element, and in compression whether or not the gusset plate is designed as the weak element. Figures 4-25 and 4-26 show the principal strain magnitude and directions in the gusset plates of Specimens T-1 and T-2 at the Whitmore compressive yield level. Figures 4-27 and 4-28 present the principal strain magnitudes and directions in the gusset plates in Specimens T-3 and T-4 at the compressive brace yield load level. These figures indicate that when stiffeners are used, the stress has the tendency to flow to the stiffeners and then to the framing members, rather than to the framing members directly. This will be discussed further in Chapter 6. This redistribution of stresses results in a more evenly distributed stress field over the plate



area, rather than concentrated stresses at the base of the splice members when the free edges are not stiffened. A similar load transfer mechanism also exists when the brace member is designed as the weak element in compression, which results in higher stresses in the unstiffened gusset plate (refer to Table 4-4).

#### ***4.5.2 Strains in Free Edge Stiffeners***

Test specimens T-1 and T-3 included free edge stiffeners. Two strain gauges were placed on each stiffener, as shown in Figure 3-10, to monitor the strains. These strains are presented in Table 4-9 at various load levels. The load levels chosen included yielding of the gusset plate, buckling of the gusset plate or brace member, and the maximum tensile load achieved during the tests. This data shows that large strains existed in the stiffeners at the maximum tensile load as well as at the gusset plate buckling load. The stiffeners, however, did not buckle. This observation reinforces the stress redistribution referenced to in the previous section.

**Table 4-1**  
**Maximum Test Loads Obtained (kN)**

	T-1	T-2	T-3	T-4
Tension	—	+1819	+1837	+1841
Compression	-1951	-1690	-1350	-1322

**Table 4-2**  
**Load Levels Used for Comparison (kN)**

	T-1	T-2	T-3	T-4
Whitmore Yield Load**	±1549	±1549	±1549	±1549
Thornton Buckling Load**	-1525	-1525	-1525	-1525
First Yield in Gusset Plate*	-1412	-1434	-1160	-1295
First Yield in Brace Member*	—	—	-839	-872
Gusset Plate Buckling*	-1951	-1690	—	—
Brace Member Buckling*	—	—	-1350	-1322

\*\*Calculated values.

\*Experimental values.

**Table 4-3**  
**Brace Member Rotations for Tests T-1 and T-2**

Load Level	T-1	T-2
Thornton Buckling Load	0.05 °	0.08°
Gusset Plate Buckling	0.26 °	0.13°
Last Compression Cycle	1.37°	1.87°

**Table 4-4**  
**Maximum Strains Measured in Gusset Plate ( $\mu\epsilon$ )**

Load Level	T-1	T-2	T-3	T-4
Whitmore Yield (tension)	1125	867	743	855
Whitmore Yield (compression)	-1657	-2107	*	*
Thornton Buckling (compression)	-1657	-2075	*	*
Gusset Plate Buckling	-3601	-2502	—	—
Brace Member Buckling	—	—	-2220	-1863

\*Brace member buckled before reaching yield of the gusset plate in compression.

**Table 4-5**  
**Loads and Axial Assembly Displacements at Which First Yield was Detected**

	Gusset Plate		Brace Member	
	Load (kN)	Displacement (mm)	Load (kN)	Displacement (mm)
T-1	-1412	-1.3	—	—
T-2	-1434	-1.8	—	—
T-3	-1160	-3.9	-838	-8.1
T-4	-1295	-4.9	-872	-8.2

**Table 4-6**  
**Principal Strain Magnitudes and Directions**  
**at Whitmore Yield Load (Tension)**

	Rosette 1			Rosette 2		
	$\epsilon_{\max}$ ( $\mu\epsilon$ )	$\epsilon_{\min}$ ( $\mu\epsilon$ )	Direction of Principal Strain (degrees)	$\epsilon_{\max}$ ( $\mu\epsilon$ )	$\epsilon_{\min}$ ( $\mu\epsilon$ )	Direction of Principal Strain (degrees)
T-1	1553	-413	10	1662	-47	10
T-2	1487	-483	351	1456	-61	336
T-3	1699	-58	353	1535	-402	333
T-4	1394	-460	348	1536	-150	340

	Rosette 3			Rosette 4		
	$\epsilon_{\max}$ ( $\mu\epsilon$ )	$\epsilon_{\min}$ ( $\mu\epsilon$ )	Direction of Principal Strain (degrees)	$\epsilon_{\max}$ ( $\mu\epsilon$ )	$\epsilon_{\min}$ ( $\mu\epsilon$ )	Direction of Principal Strain (degrees)
T-1	2494	-347	347	2404	-116	348
T-2	1923	-439	11	1844	-161	20
T-3	2261	-21	6	2003	-491	16
T-4	1539	-472	6	1758	-315	16

Note: all angles are measured clockwise with respect to axis parallel to the long edge of the plate

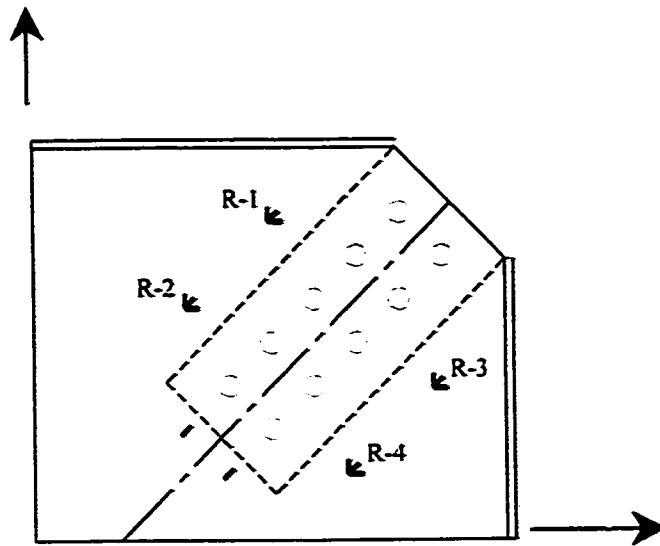


**Table 4-7**  
**Principal Strain Magnitudes and Directions**  
**at Whitmore Yield Load (Compression)**

	Rosette 1			Rosette 2		
	$\epsilon_{\max}$ ( $\mu\epsilon$ )	$\epsilon_{\min}$ ( $\mu\epsilon$ )	Direction of Principal Strain (degrees)	$\epsilon_{\max}$ ( $\mu\epsilon$ )	$\epsilon_{\min}$ ( $\mu\epsilon$ )	Direction of Principal Strain (degrees)
T-1	809	-881	10	569	-410	32
T-2	351	-757	353	322	-809	345

	Rosette 3			Rosette 4		
	$\epsilon_{\max}$ ( $\mu\epsilon$ )	$\epsilon_{\min}$ ( $\mu\epsilon$ )	Direction of Principal Strain (degrees)	$\epsilon_{\max}$ ( $\mu\epsilon$ )	$\epsilon_{\min}$ ( $\mu\epsilon$ )	Direction of Principal Strain (degrees)
T-1	501	-1265	354	277	-843	338
T-2	245	-398	16	279	-1017	11

Note: all angles are measured clockwise with respect to axis parallel to the long edge of the plate

**Table 4-8**  
**Principal Strain Magnitudes and Directions**  
**at Brace Yield Load (Compression)**

	Rosette 1			Rosette 2		
	$\epsilon_{\max}$ ( $\mu\epsilon$ )	$\epsilon_{\min}$ ( $\mu\epsilon$ )	Direction of Principal Strain (degrees)	$\epsilon_{\max}$ ( $\mu\epsilon$ )	$\epsilon_{\min}$ ( $\mu\epsilon$ )	Direction of Principal Strain (degrees)
T-3	-133	-854	26	-30	-924	327
T-4	276	-1666	15	-34	-1010	33

	Rosette 3			Rosette 4		
	$\epsilon_{\max}$ ( $\mu\epsilon$ )	$\epsilon_{\min}$ ( $\mu\epsilon$ )	Direction of Principal Strain (degrees)	$\epsilon_{\max}$ ( $\mu\epsilon$ )	$\epsilon_{\min}$ ( $\mu\epsilon$ )	Direction of Principal Strain (degrees)
T-3	0	-486	1	496	-732	8
T-4	82	-1009	341	452	-438	3

Note: all angles are measured clockwise with respect to axis parallel to the long edge of the plate

**Table 4-9**  
**Average of Strains in Free Edge Stiffeners ( $\mu\epsilon$ )**

Load Level	Long Free Edge		Short Free Edge	
	T-1	T-3	T-1	T-3
First Yield in Gusset Plate	-553	-535	-950	-566
Gusset Plate Buckling	-1665	—	-2459	—
Brace Member Buckling	—	-606	—	-657
Maximum Tensile load	-1344	-2568	-2148	-2565

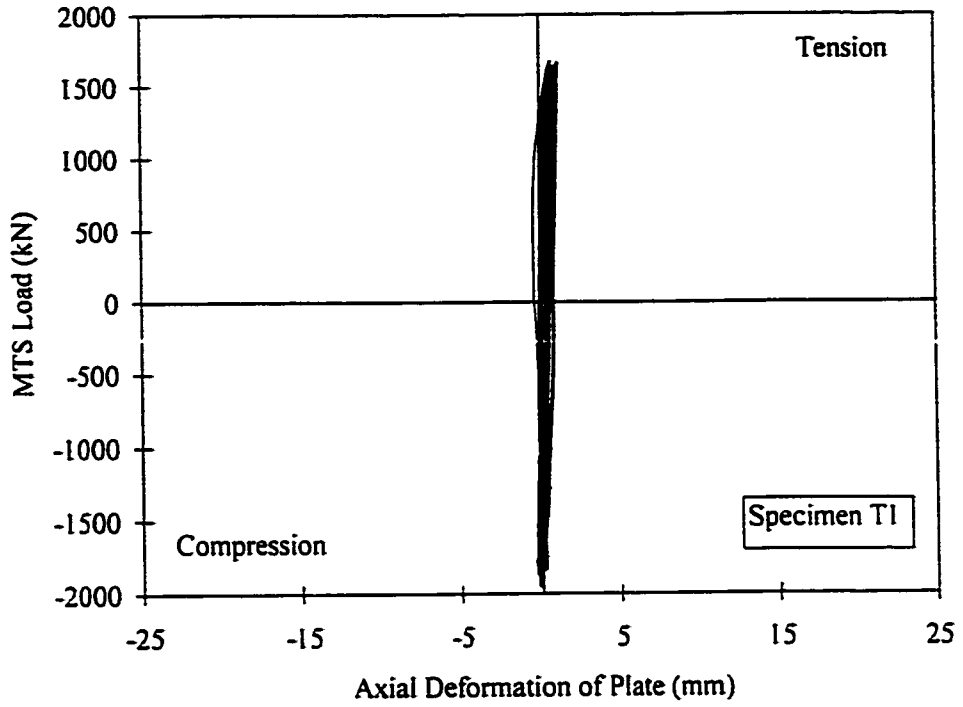


**Figure 4-1: Load versus Deformation Relationship for Gusset Plate: Specimen T-1**

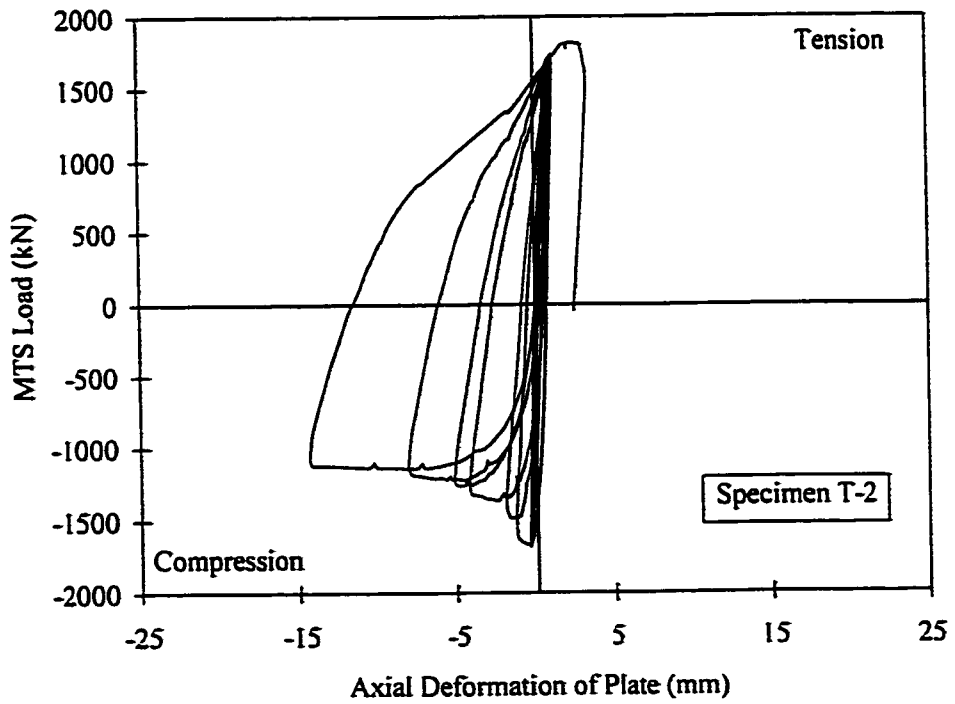


**Figure 4-2: Load versus Deformation Relationship for Gusset Plate: Specimen T-2**

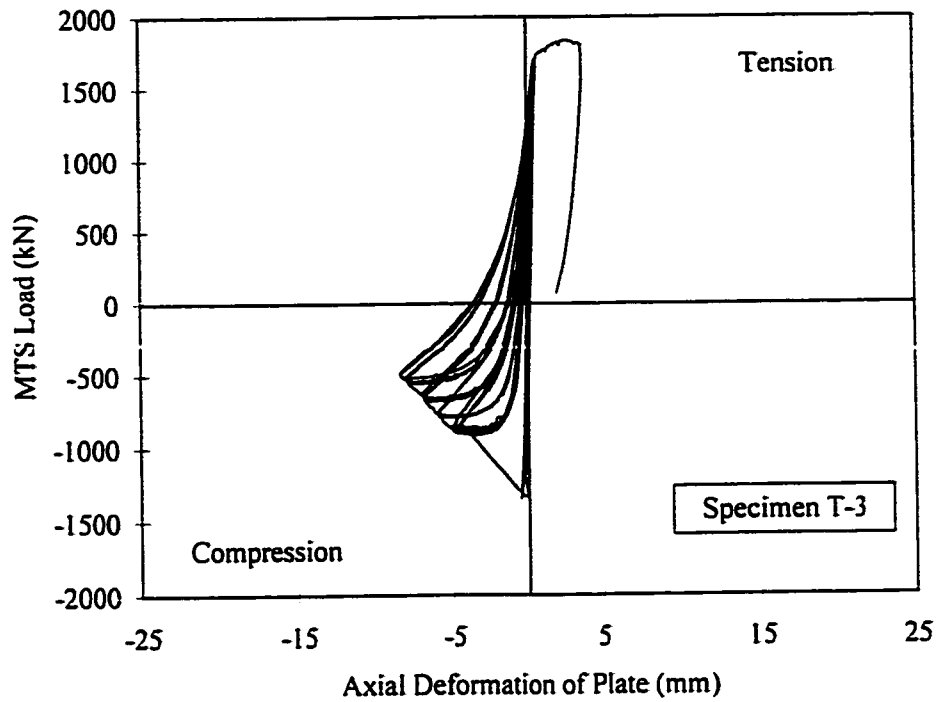


**Figure 4-3: Load versus Deformation Relationship for Gusset Plate: Specimen T-3**

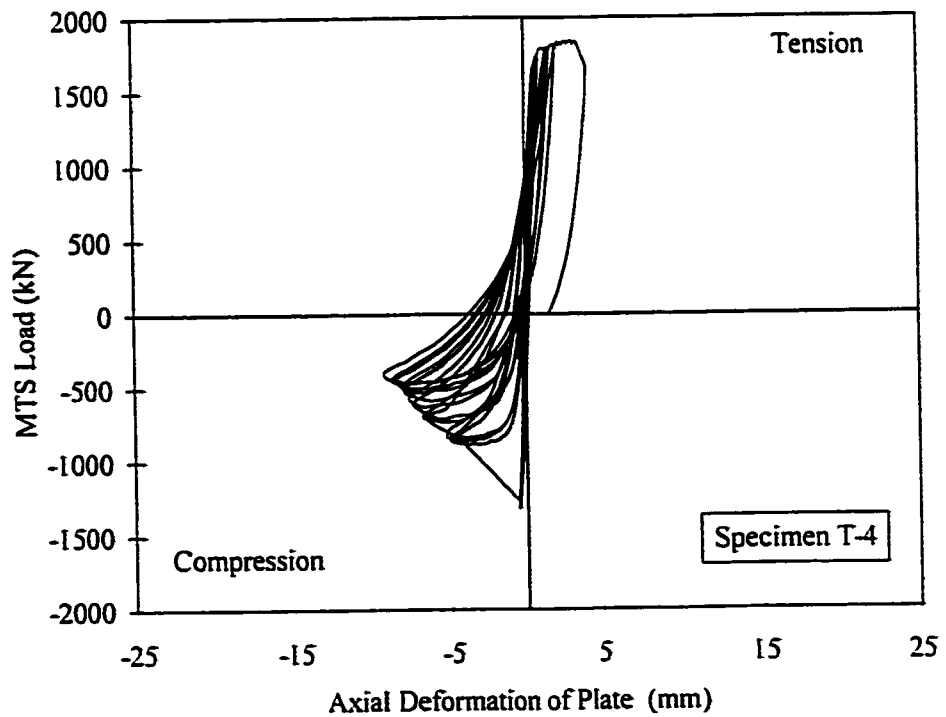


**Figure 4-4: Load versus Deformation Relationship for Gusset Plate: Specimen T-4**



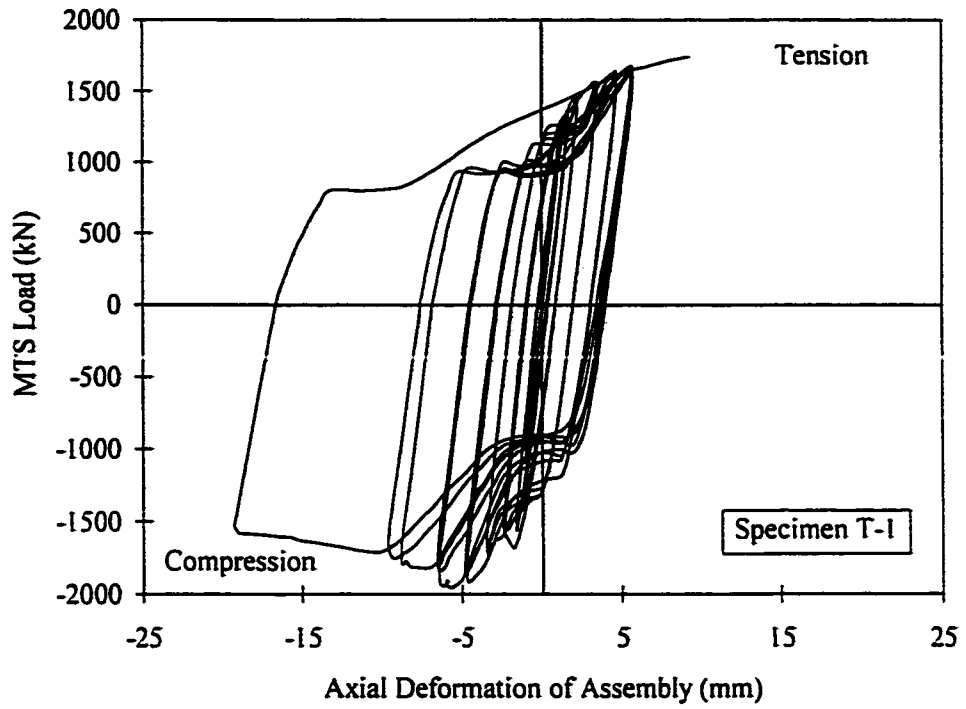


**Figure 4-5: Load versus Deformation Relationship for Assembly: Specimen T-1**

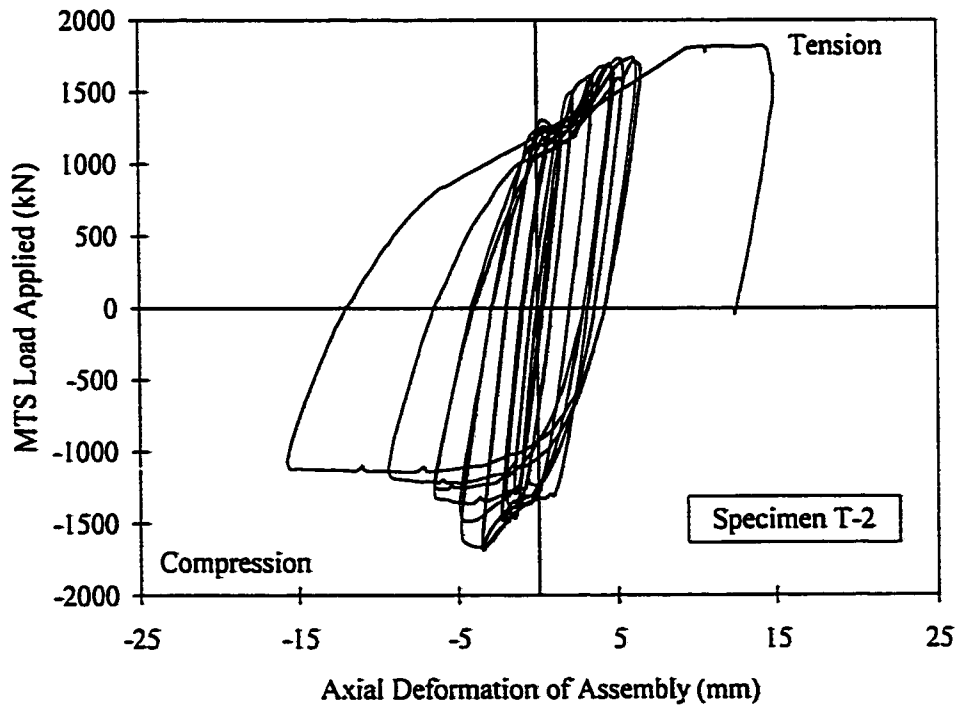


**Figure 4-6: Load versus Deformation Relationship for Assembly: Specimen T-2**

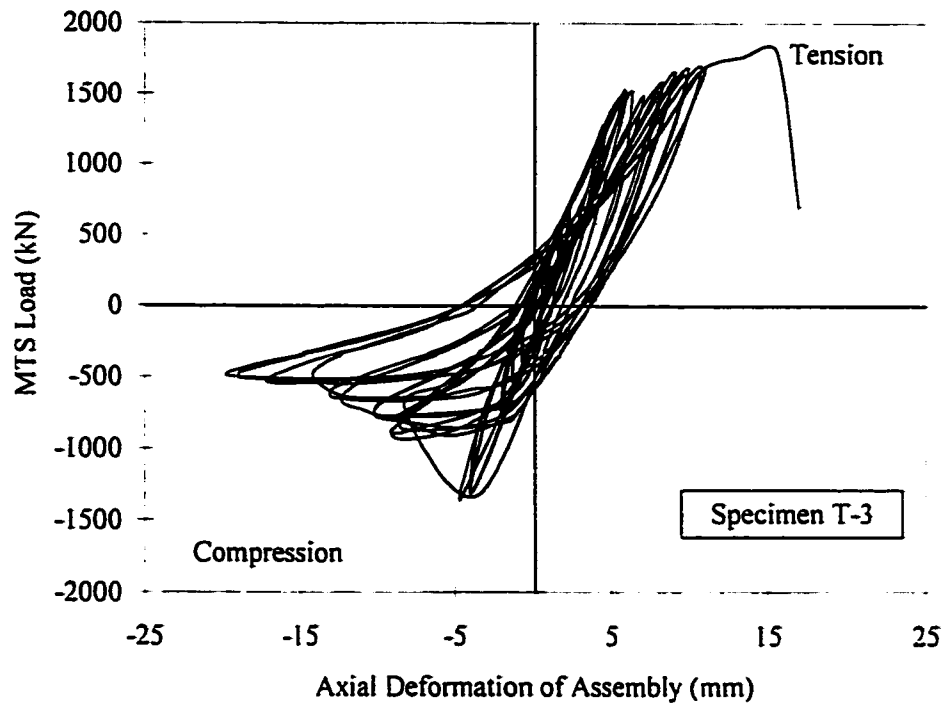


**Figure 4-7: Load versus Deformation Relationship for Assembly: Specimen T-3**

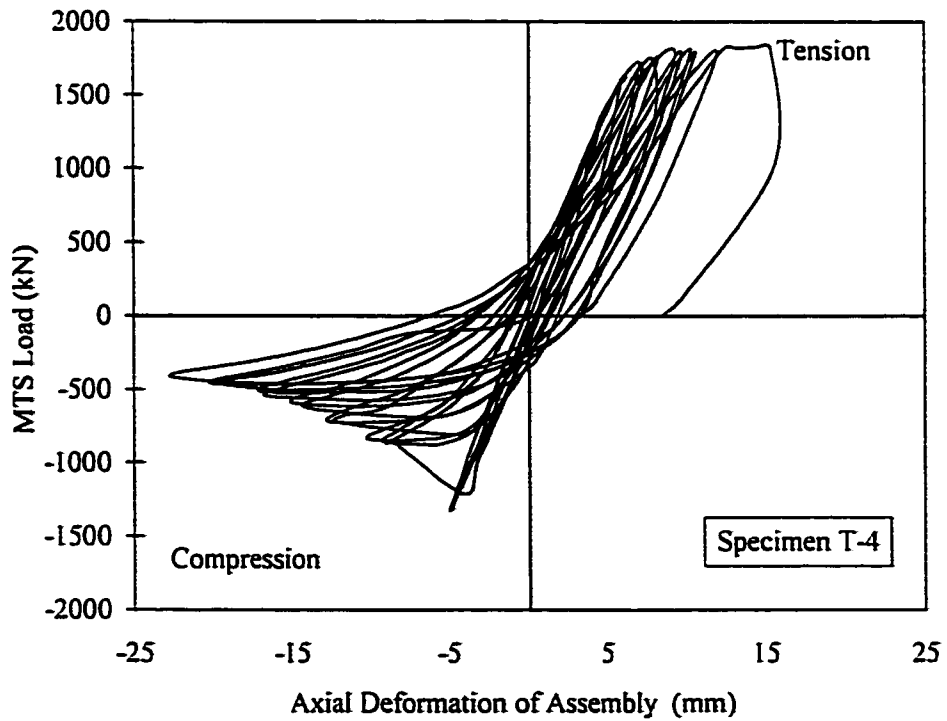


**Figure 4-8: Load versus Deformation Relationship for Assembly: Specimen T-4**

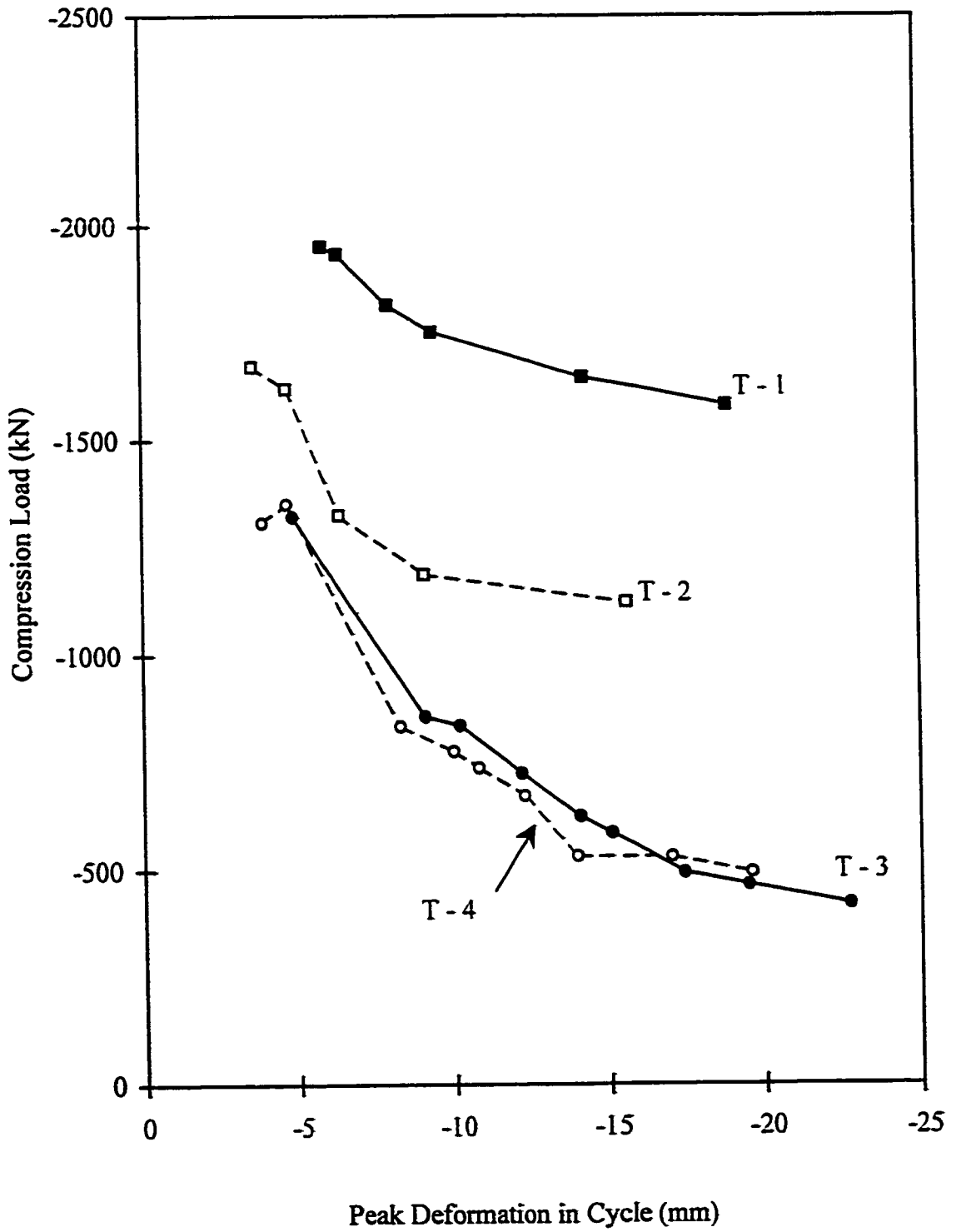


**Figure 4-9: Deterioration of Buckling Load Due to Applied Cycles**



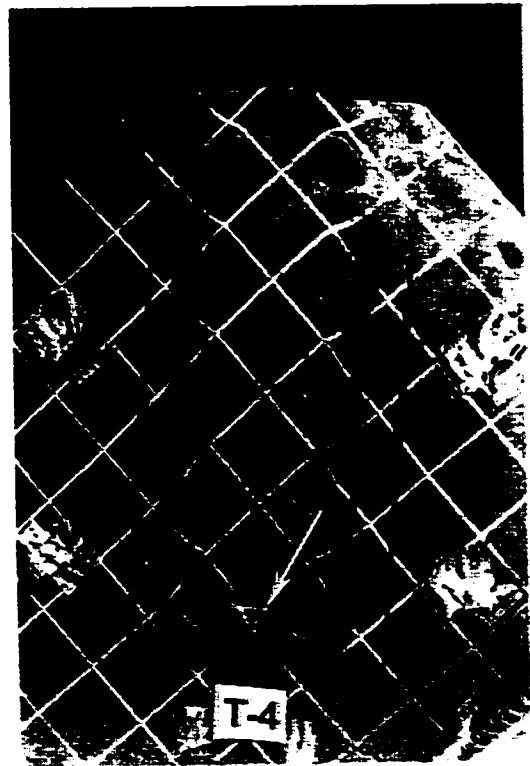
(a)



(b)

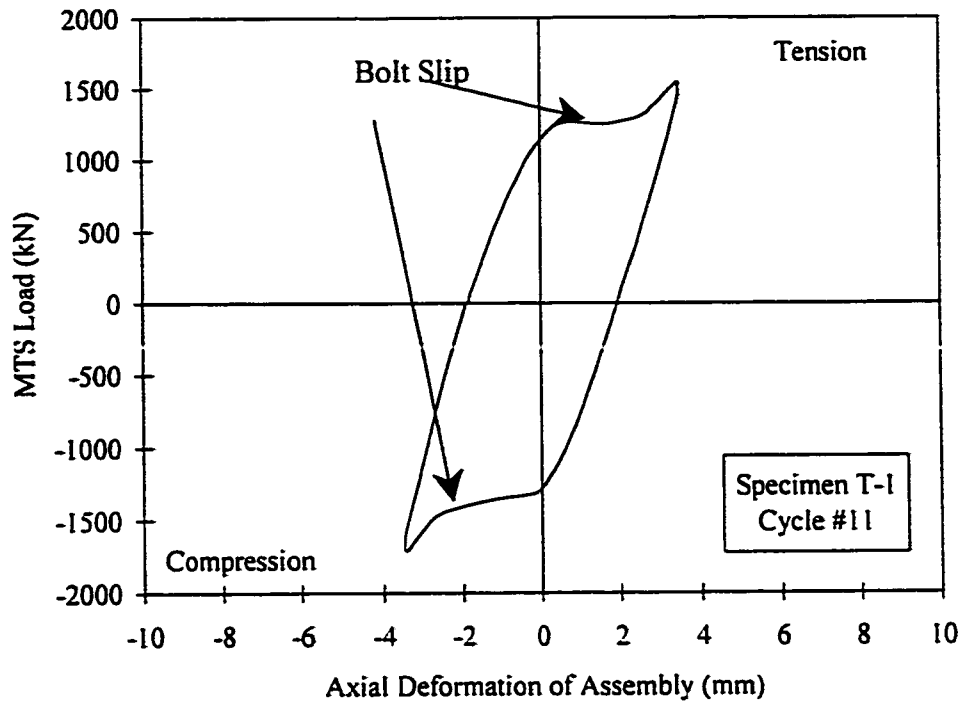


(c)

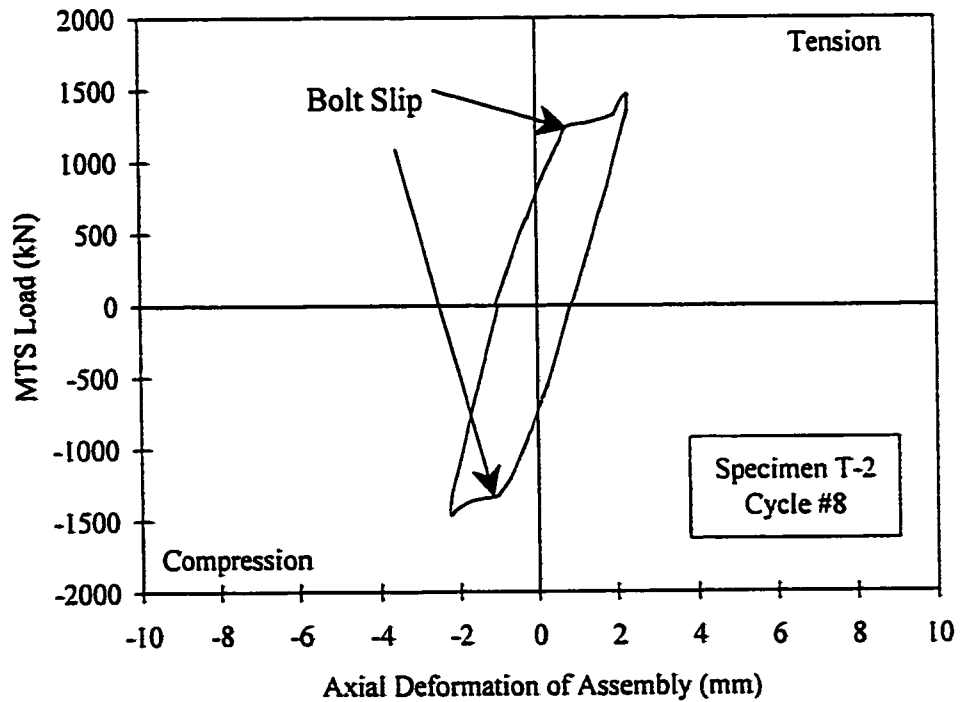


(d)

**Figure 4-10: Failed Gusset Plate Specimens**



(a) Specimen T-1: Cycle #11



(b) Specimen T-2: Cycle #8

Figure 4-11: Cycle at Which Bolt Slip First Occurs in Specimens T-1 and T-2

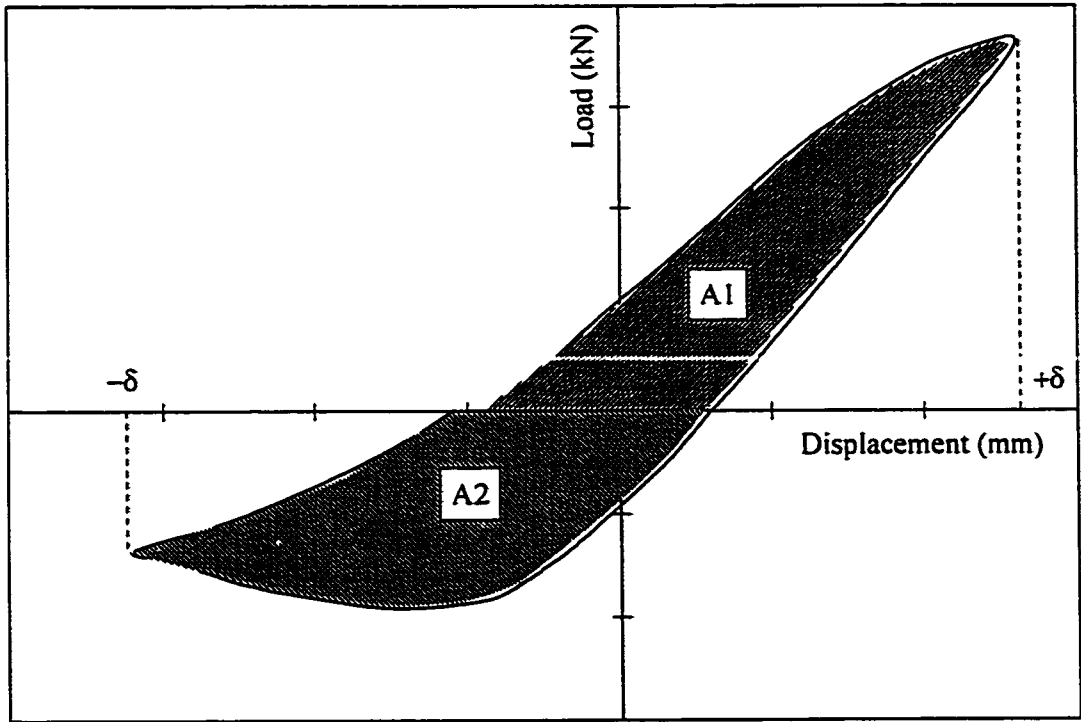
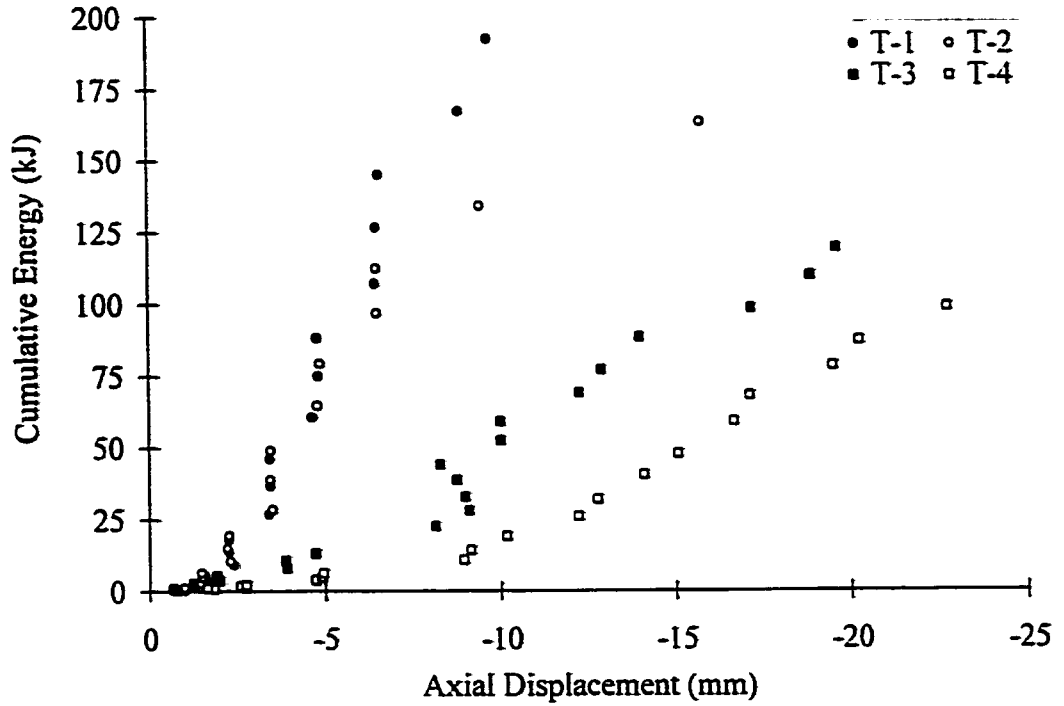
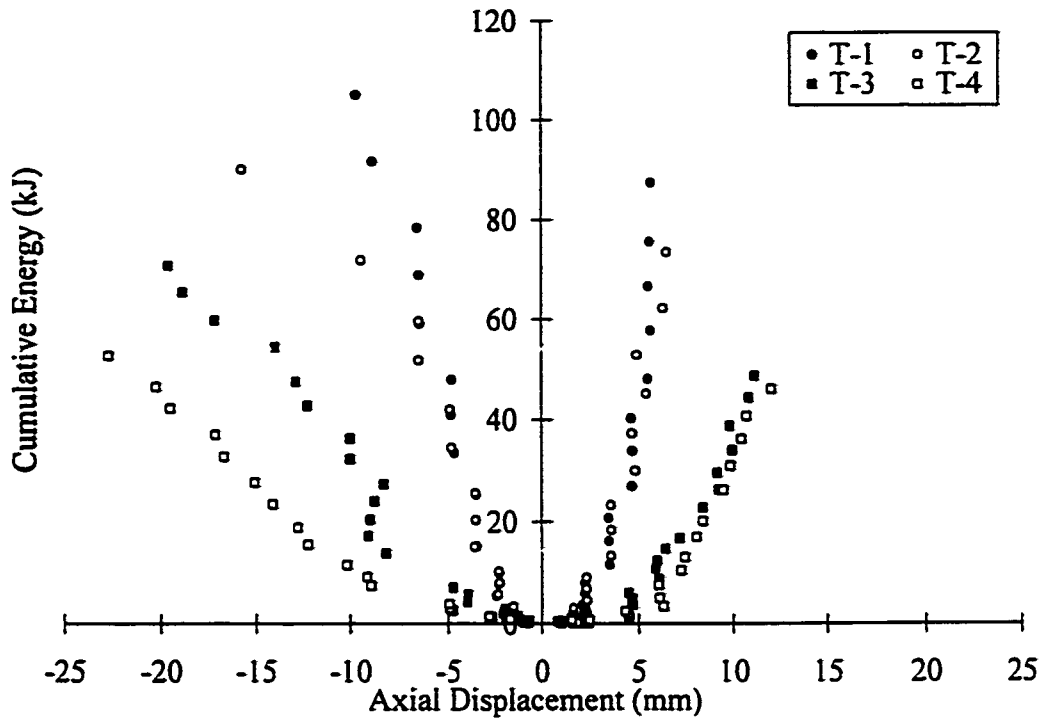


**Figure 4-12: Determination of Energy Absorbed**



**(a) Cumulative Energy Absorbed by Specimens**



(b) Tension and Compression Energy Absorbed by Specimens

Figure 4-13: Cumulative Energy Dissipated by Test Specimens

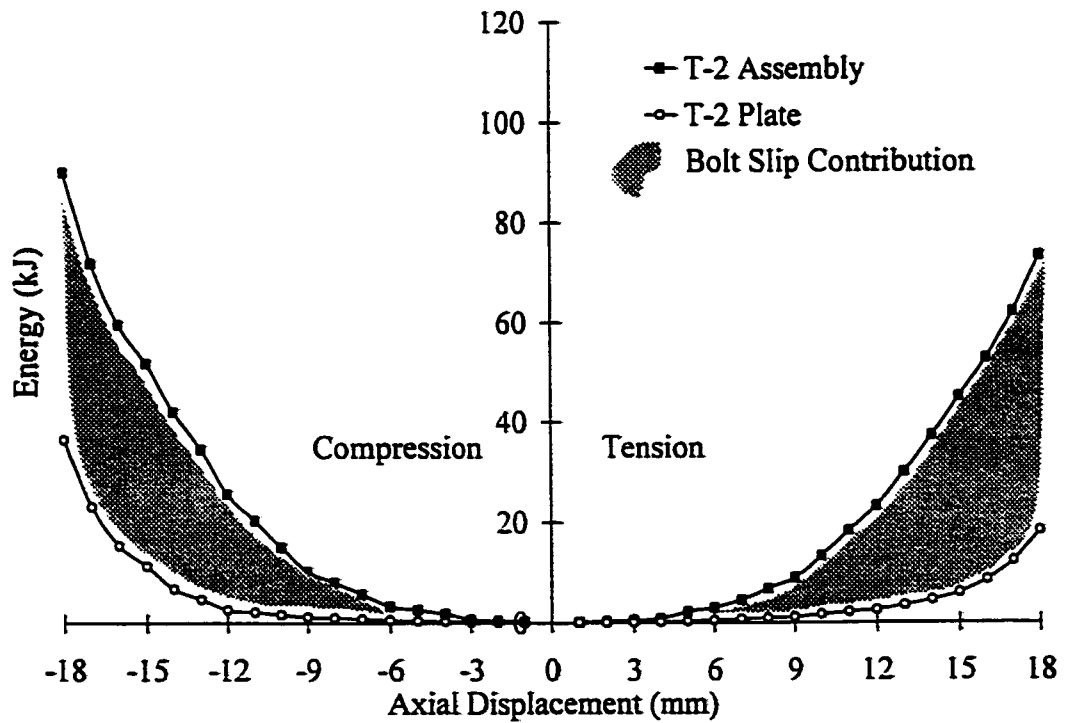
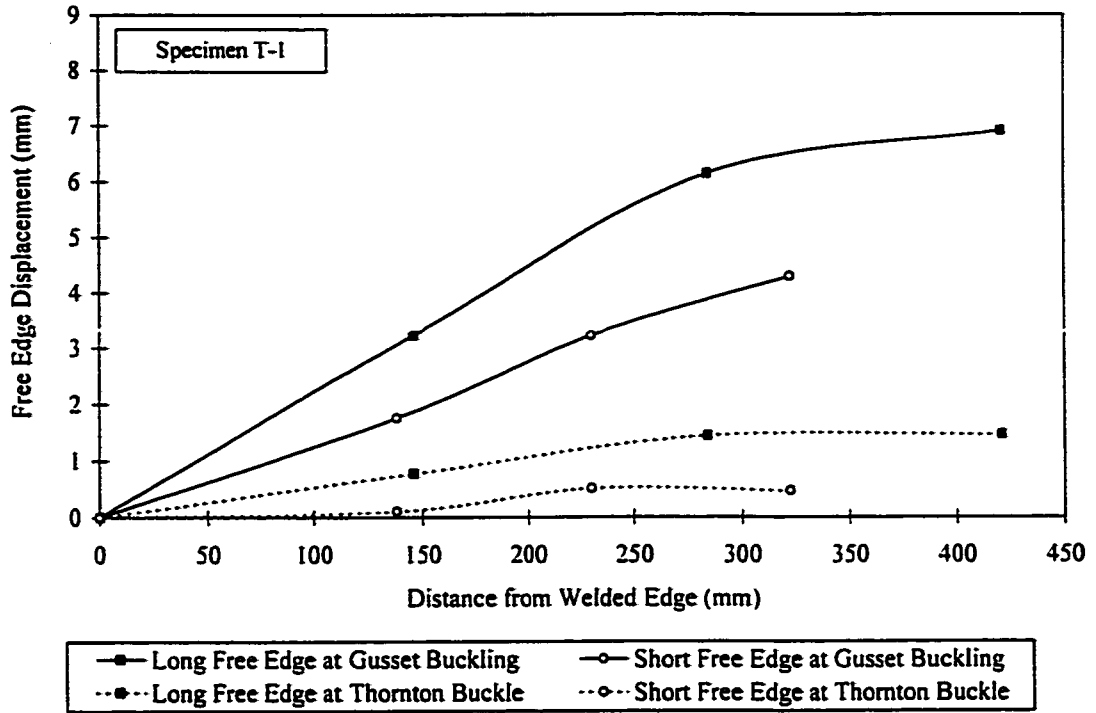
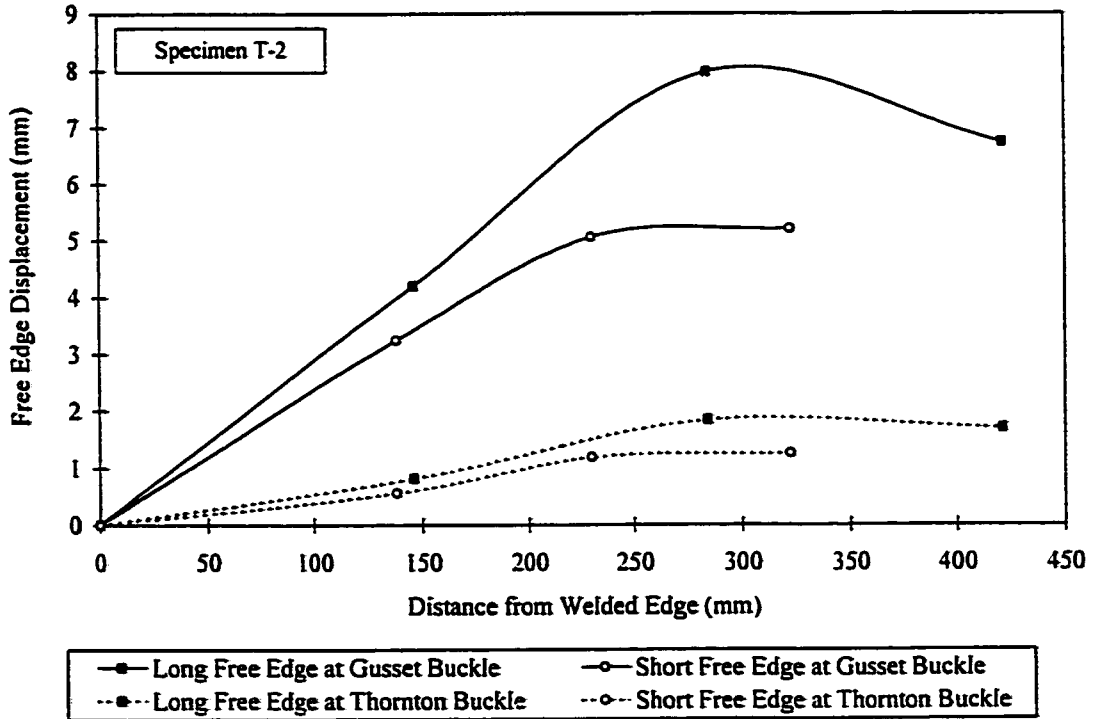


Figure 4-14: Effect of Bolt Slip on the Cumulative Energy Absorption Capacity of the Assembly

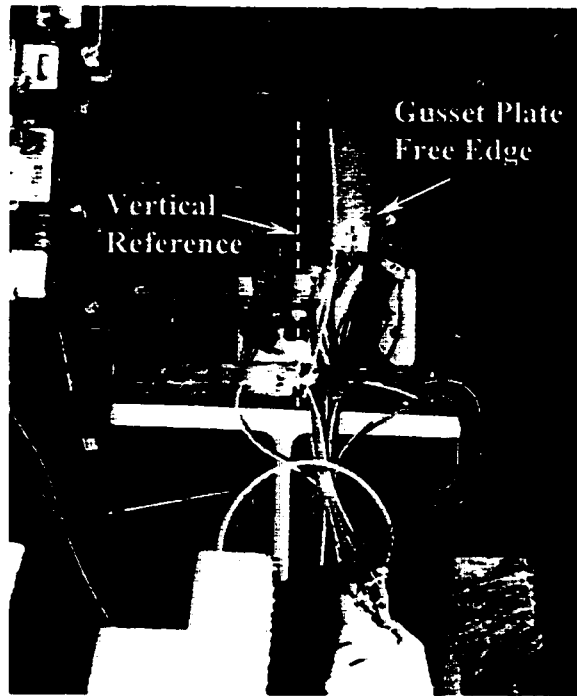


**Figure 4-15: Out-of-Plane Deformation of Gusset Plate Free Edges – Specimen T-1**

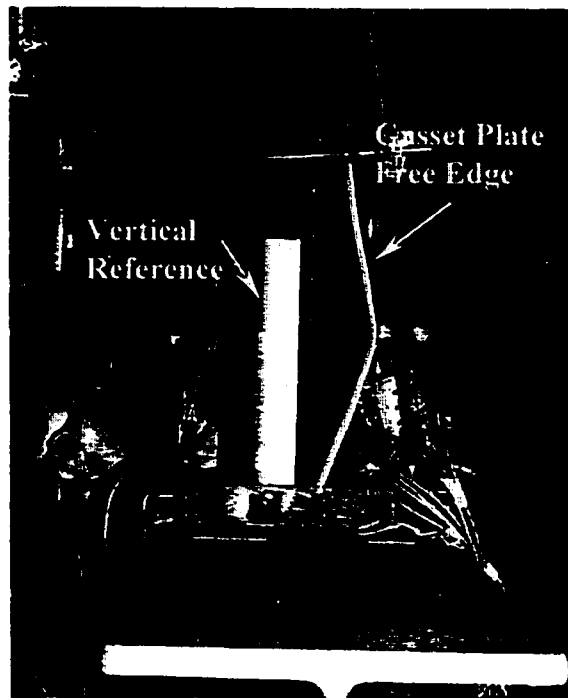


**Figure 4-16: Out-of-Plane Deformation of Gusset Plate Free Edges – Specimen T-2**





(a) Specimen T-1



(b) Specimen T-2

Figure 4-17: Deformed Shape of Gusset Plate Long Free Edge

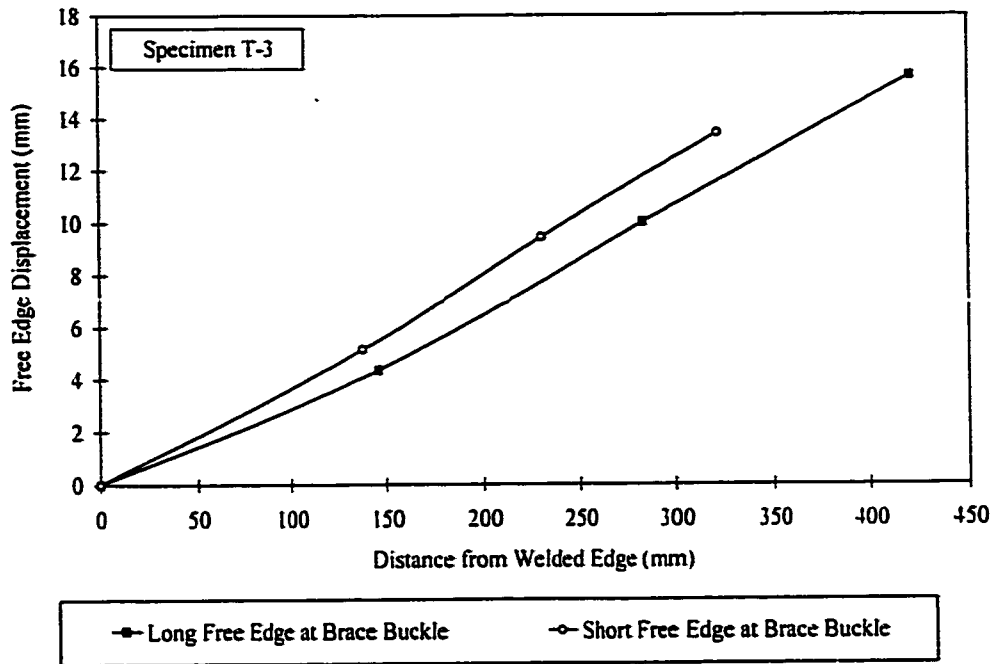


**Figure 4-18: Out-of-Plane Deformation of Gusset Plate Free Edges – Specimen T-3**

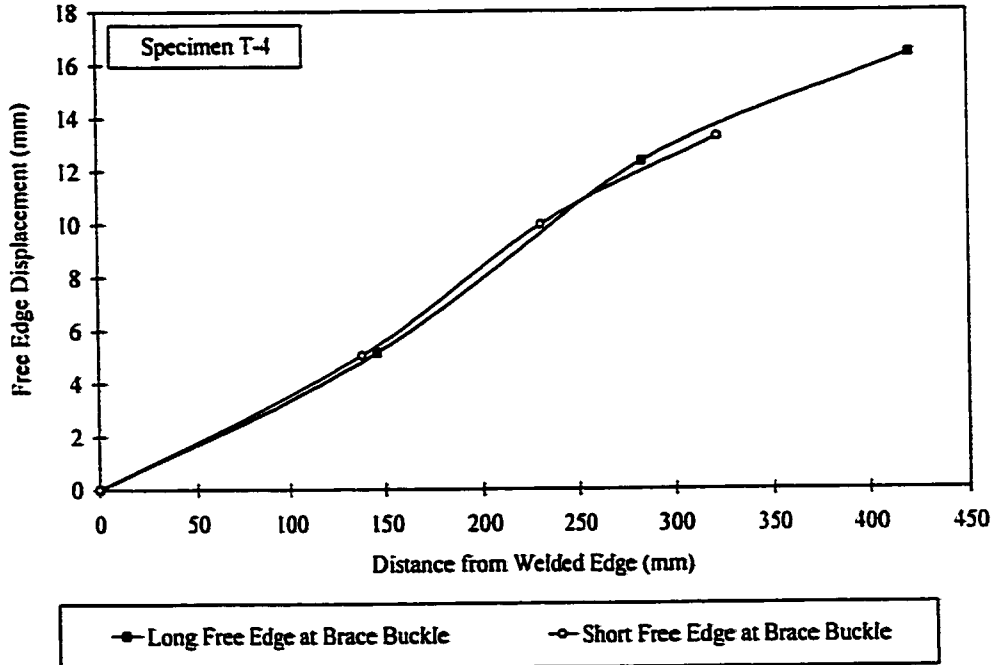
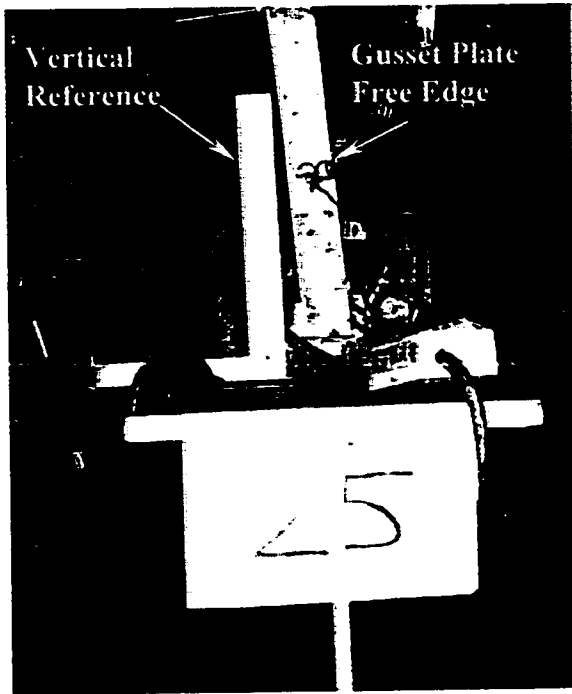
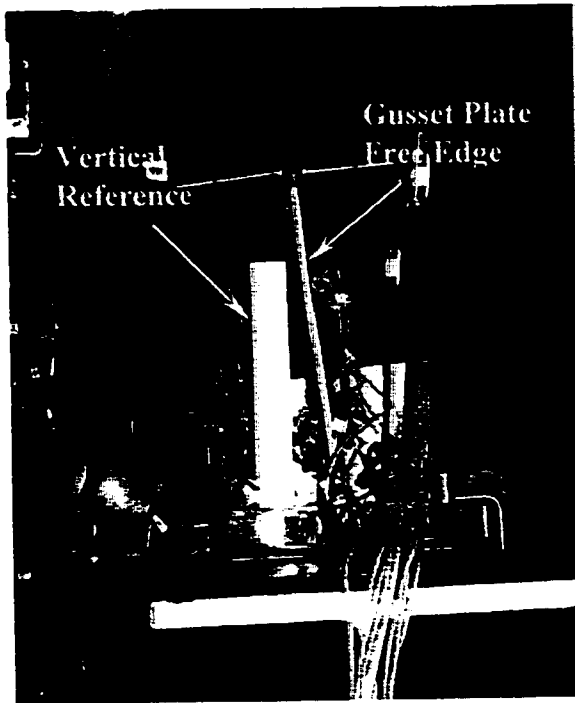


**Figure 4-19: Out-of-Plane Deformation of Gusset Plate Free Edges – Specimen T-4**



(a) Specimen T-3



(b) Specimen T-4

**Figure 4-20: Out-of-Plane Deformation of Gusset Plate Free Edges**

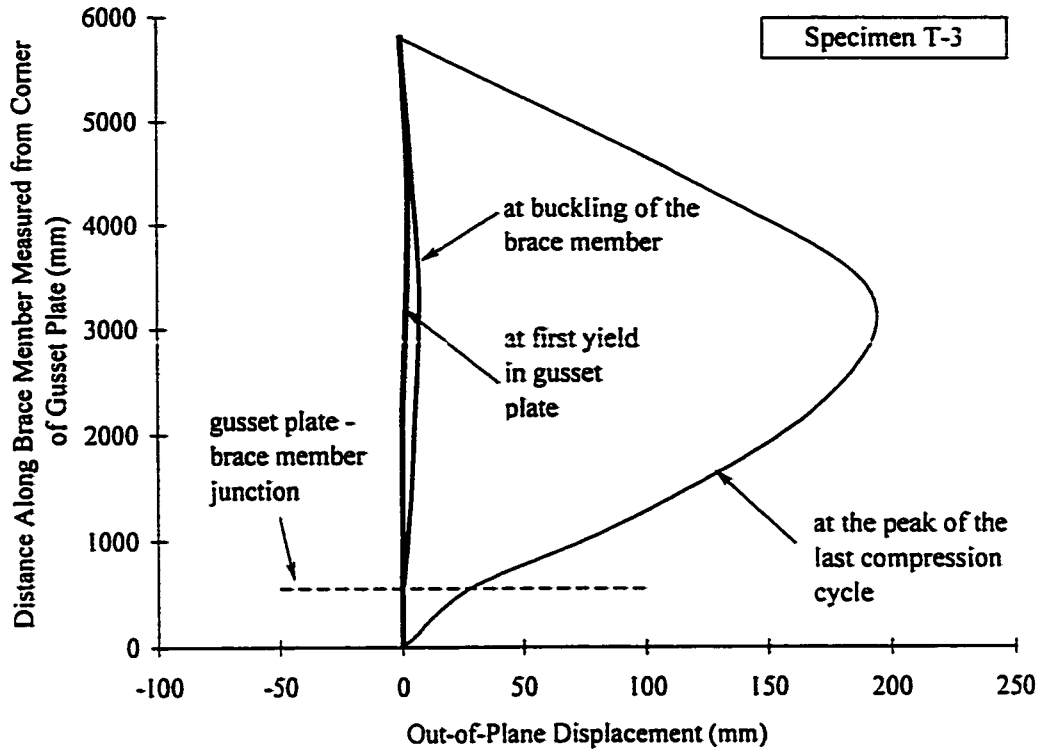


**Figure 4-21: Out-of-Plane Deformation of Brace Member – Specimen T-3**

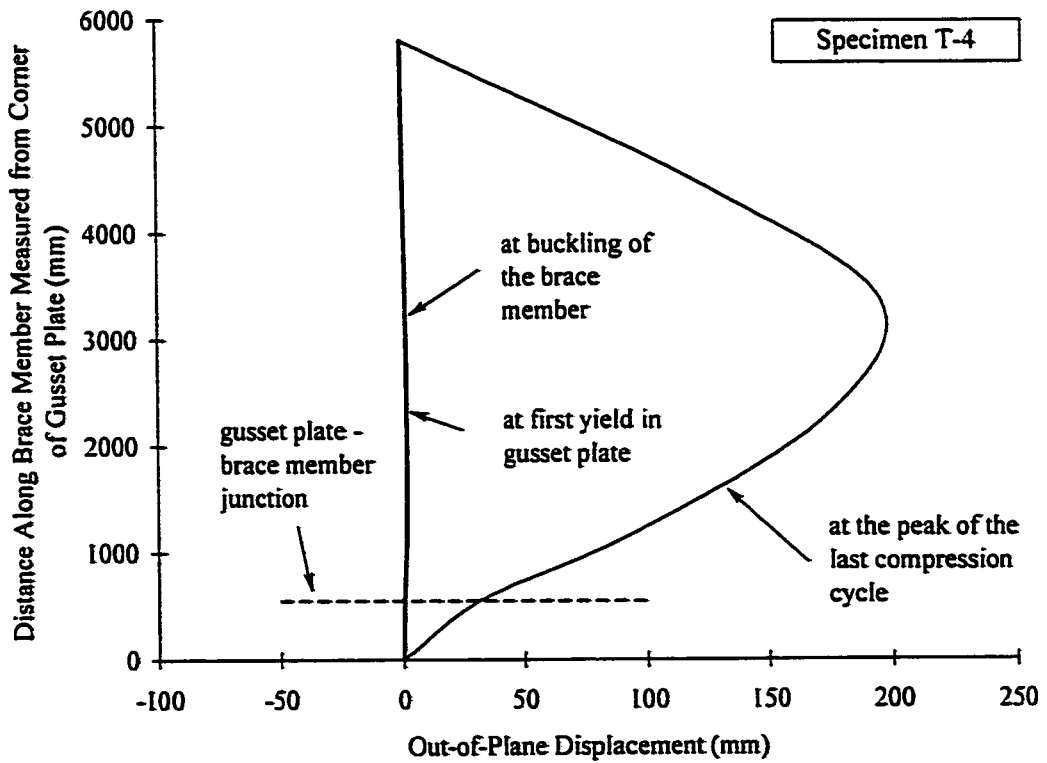


**Figure 4-22: Out-of-Plane Deformation of Brace Member – Specimen T-4**

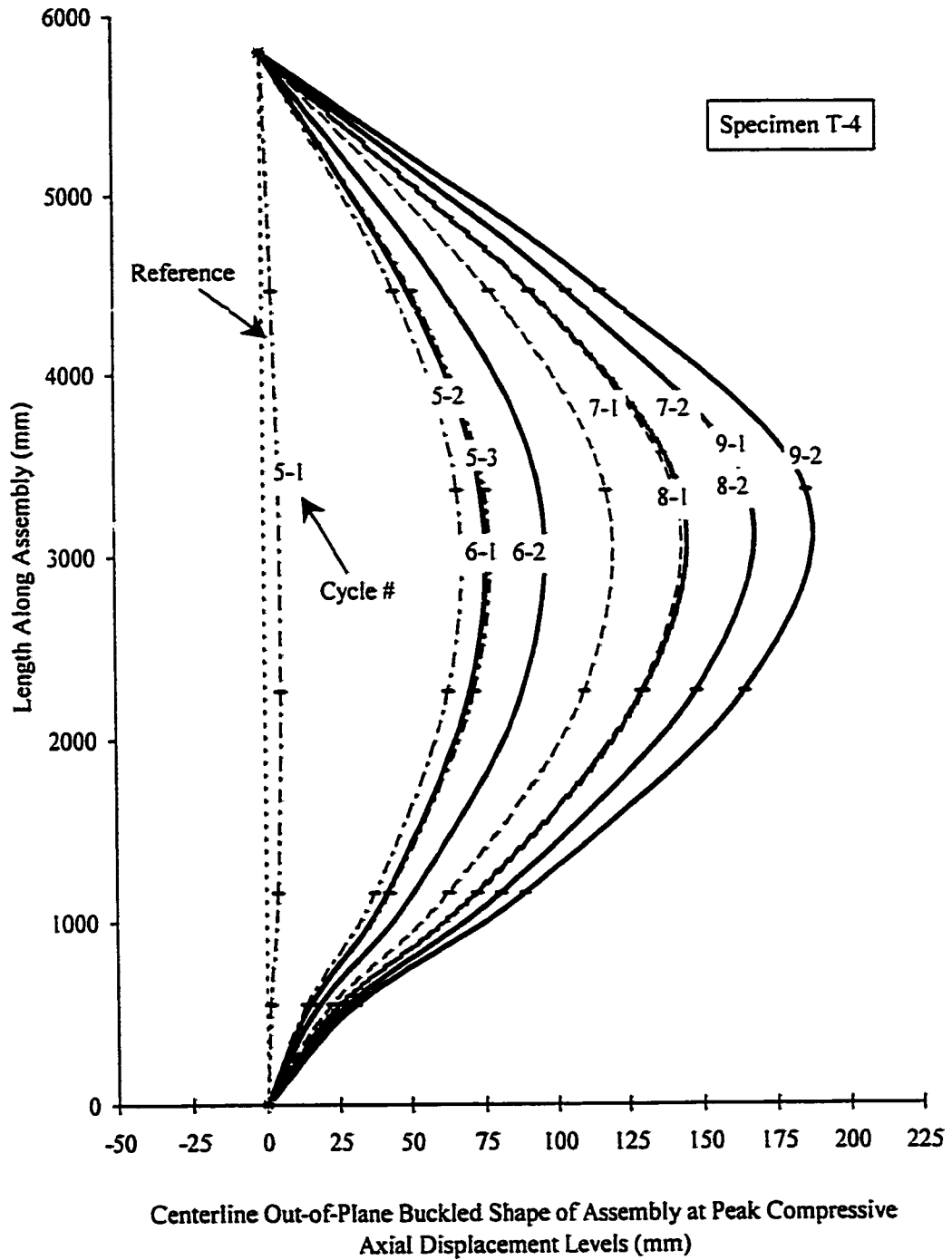


**Figure 4-23: Out-of-Plane Deformation of Brace Member at Specific Displacement Levels – Specimen T-4**



**Figure 4-24: Out-of-Plane Deformation of Assembly– Specimen T-3 at Peak Compression - Cycle 21**

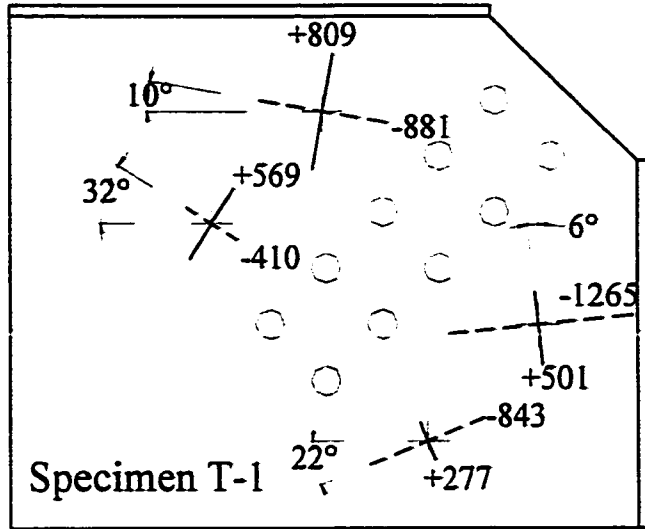


**Figure 4-25: Principal Strain Magnitudes and Directions at Whitmore Compressive Yield Level - Specimen T-1**

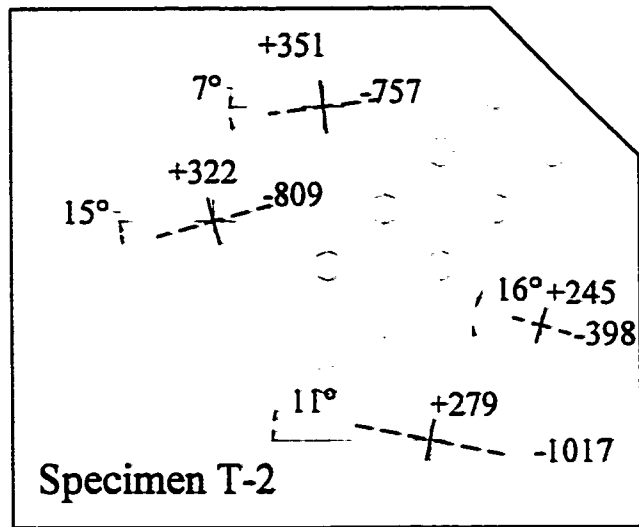


**Figure 4-26: Principal Strain Magnitudes and Directions at Whitmore Compressive Yield Level - Specimen T-2**

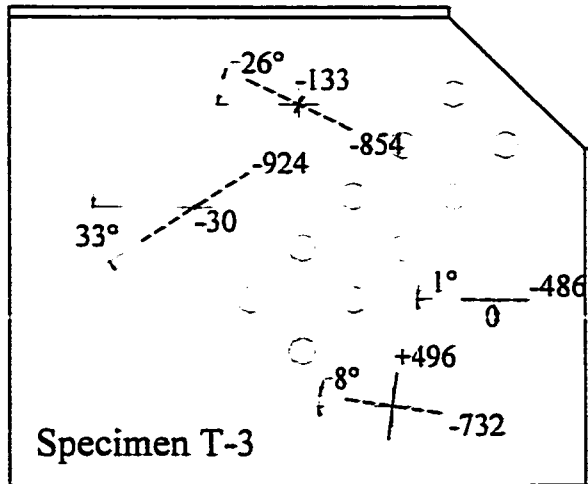


**Figure 4-27: Principal Strain Magnitudes and Directions at Whitmore Compressive Yield Level - Specimen T-3**

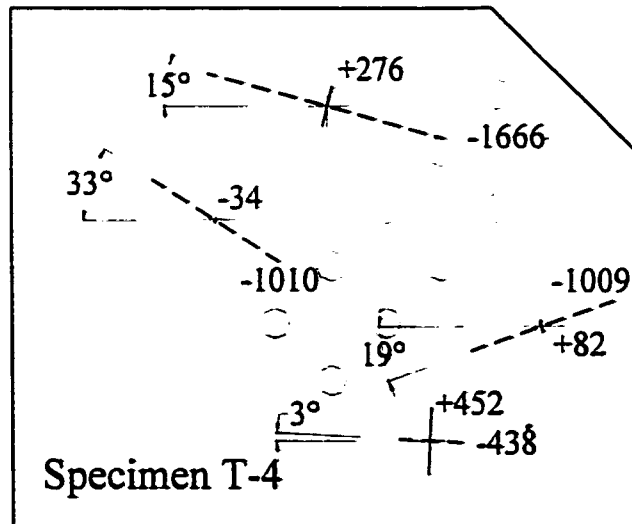


**Figure 4-28: Principal Strain Magnitudes and Directions at Whitmore Compressive Yield Level - Specimen T-4**



## CHAPTER 5

### FINITE ELEMENT ANALYSIS

#### 5.1 Introduction

The finite element analysis presented in this chapter consists of two parts. An analysis was first performed using previously validated models presented by Walbridge *et al.* (1998) to determine the size of the free edge stiffeners to include in the testing program. The results of this analysis will be described in Section 5.2. Secondly, the finite element models of the gusset plate and brace member, proposed by Walbridge and *et al.* (1998), were modified to reflect the geometry and boundary conditions of the test specimens presented in Chapter 3. The geometry, boundary conditions, initial imperfections, and material properties included in these models will be presented in Section 5.3. Results of the finite element analysis and the comparison with the test results presented in Chapter 4 will be presented in Chapter 6. The validation of these models is of particular interest because it enables the researcher to test many parameters affecting the strength and behavior of gusset plate connections without the need to perform costly full-scale tests. Some of these parameters include the presence and size of free edge stiffeners and other factors that influence the gusset plate – brace member interaction.

The gusset plate specimens tested in the experimental program described in Chapter 4 were modeled using the commercial finite element code ABAQUS (Hibbitt *et al.* 1996). The analysis was conducted on a SUN SPARC workstation.

## 5.2 Preliminary Finite Element Analysis for Stiffener Selection

A preliminary finite element study was performed to select an appropriate size of gusset plate free edge stiffeners for Specimens T-1 and T-3. CAN/CSA-S16.1-M94 has no provisions for the design of free edge stiffeners. However, codes do exist that provide recommendations for the addition of gusset plate free edge stiffeners when gusset plates are subjected to compressive loads. For example, the Ontario Highway Bridge Design Code (1990), Clause 10-16.5.1, states that: “the unsupported edge of a gusset plate shall be stiffened if the length exceeds  $930/\sqrt{F_y}$  times its thickness”. Similarly, CAN3-S6-M (1983), Clause 7.25.4.4, states that: “if the edge of the gusset plate, which may be subjected to compression, exceeds  $945/\sqrt{F_y}$  times its thickness, the edge shall be stiffened”. These codes, however, do not provide guidelines for determining the size or the amount of stiffening that should be provided. Therefore, this preliminary analysis was conducted to select an adequate gusset plate free edge stiffener size for testing.

Three Series of finite element models were constructed. Each model included the beam and column framing members, the gusset plate, free edge stiffeners, and splice members. The first set of models included the splice members but no bracing member and was subjected to monotonic compressive loading. The second and third sets of models included the brace member and were loaded under monotonic compressive loading and cyclic loading, respectively. All the models were designed with the gusset plate as the weak compressive element. Each set of numerical models looked at the effect of varying the stiffener slenderness ratio, expressed as the width-to-thickness ratio,  $2b/t_{st}$  where  $2b$  is

the full width of the stiffener and  $t_{st}$  its thickness. The first series of analyses also looked at the effect of the stiffener thickness to gusset plate thickness ratio,  $t_{st}/t$ .

### **5.2.1 Model Description**

All the finite element models used in this preliminary analysis are based on models of unstiffened gusset plates validated by Walbridge *et al.* (1998) and modified to include gusset plate free edge stiffeners of varying dimensions. Each model included the beam and column framing members and a 450 mm x 550 mm gusset plate with an imposed quarter sine wave initial imperfection with a maximum out-of-plane magnitude of 2 mm. Brace members, consisting of a W200x59 shape, 2595 mm long, were included in two of the models. The model of the brace member incorporated initial imperfections consisting of a half sine wave with a maximum magnitude of  $L_b/1400$ , where  $L_b$  is the length of the brace member. The models were discretized using a four node, finite strain, shell element and the mesh size was the same as the one adopted by Walbridge *et al.* (1998). This mesh was found to be adequate to ensure convergence. Figure 5-1 shows typical models used for this analysis.

The model was loaded by imposing an in-plane axial displacement at the locations identified in Figure 5-1. The point of loading was restrained from translating out-of-plane (coordinate 3 direction), free to translate in the axial direction, and free to rotate about all three coordinate axes. The translational degree of freedom in the 3-direction,  $u_3$ , was therefore eliminated at the points of loading. The intersection of the beam and column members was fixed in all directions.

In the study performed by Walbridge *et al.* (1998), an elastic-perfect plastic material model was found to most closely predict the test results presented by Rabinovitch and Cheng (1993) for cyclic loading, and isotropic strain hardening material models most closely predicted Yam and Cheng's (1993) monotonic compression test results. Therefore, an isotropic strain hardening material model was used for the monotonic compression models, and an elastic-perfect plastic material model was used for the specimens subjected to cyclic loading. A summary of the models used in this preliminary analysis is shown in Table 5-1.

### ***5.2.2 Results of the Preliminary Analysis***

The first Series of analyses was performed to investigate the effect of stiffener size on the strength and behavior of gusset plates of varying thickness. The gusset plate connections were modeled without the brace member and were subjected to monotonic compressive loading. Plate thickness and stiffener dimensions were varied as shown in Table 5-1. The gusset plate thickness was chosen based on practical limits. In the experiments performed by Rabinovitch and Cheng (1993), the stiffener thickness was limited to the thickness of the gusset plate ( $t_{st}/t = 1$ ). Therefore, to study the effect of the  $t_{st}/t$  ratio, stiffeners with a thickness equal to, greater than, or smaller than the gusset plate thickness were included into this study. A stiffener width was then chosen to limit the  $2b/t_{st}$  ratio to a maximum of 6.0, and a minimum of 2.0. This seemed to result in practical stiffener dimensions.

The load versus gusset plate axial displacement behavior obtained from the analysis of the first set of analyses are plotted in Figure 5-2. These preliminary results indicate that:

- the peak compressive strength of the gusset plate is not significantly affected by the presence of free edge stiffeners;
- free edge stiffeners increase the post-buckling capacity of the gusset plate;
- the size of the free edge stiffeners, either expressed by its width to thickness ratio,  $2b/t_{st}$ , or by its area, does not affect significantly the buckling and post-buckling behavior of the gusset plate.

The results presented in Figure 5-2 also suggest that the use of large stiffeners is not justified because the resulting increase in post-buckling strength is not significant compared to a smaller stiffener.

Figure 5-2 also illustrates the effect of varying the gusset plate thickness. The results from three different gusset plate thicknesses, namely 9, 12, and 15 mm are presented and are designated as the mc9, mc12, and mc15 series, respectively. The results obtained for the 15 mm gusset plate indicate that the effect of free edge stiffeners may be reduced for gusset plates of larger thickness. The post-buckling strength of the 15 mm gusset plate was not affected much by the selected stiffeners. There is also no noted effect of the stiffener to gusset plate thickness ratio,  $t_{st}/t$ .

Based on the results from Series I, only the width of the stiffener,  $2b$ , was varied for Series II and III. The gusset plate thickness was kept constant at 12 mm and the stiffener thickness was taken as 9 mm. The specimens investigated in Series II and Series III included a W200x59 brace member with an overall length of 2595 mm and free edge stiffeners with various  $2b/t_{st}$  values. Table 5-1 presents a description of the specimens

investigated in these Series. The models from Series II were loaded monotonically in compression whereas the models from Series III were loaded cyclically. The deformation history used in Series III is shown in Figure 5-3. Figures 5-4 and 5-5 show the analysis results of Series II and III, respectively. Results similar to those of Series I were observed. The sudden drop in load carrying capacity of models mc12BS5 and mc12BS2 can be attributed to the buckling of the brace member after more load was applied following gusset plate buckling. Detailed numerical results of Series I, II, and III are presented in Appendix B.

Based on these results, it was felt that a stiffener with a thickness equal to that of the gusset plate, and a width of 50 mm would be adequate for testing.

### **5.3 Description of the Finite Element Models**

Finite element models of the test specimens described in Chapter 4 were developed to test the finite element models proposed in earlier work by Walbridge *et al.* (1998). By comparing the finite element analysis results with the experimental results presented in Chapter 4, the numerical models can be tested. Since the effect of boundary conditions, loading sequence, and mesh size were investigated by Walbridge *et al.* (1998), only a summary of the models used in this investigation will be presented in the following paragraphs.

#### **5.3.1 Elements and Mesh**

The finite element mesh used to model test specimens T-1 and T-2 is shown in Figure 5-6 and the mesh for T-3 and T-4 is presented in Figure 5-7. As for the preliminary analysis,

the components of the test assembly, including the framing members, gusset plate, free edge stiffeners, splice members, and the brace member, were modeled using the ABAQUS shell element S4R. The S4R element is a four node, doubly curved shell element that accounts for finite element strains and allows for a change in element thickness. This element has six degrees of freedom at each node (three displacement components and three rotation components). The S4R element is a reduced integration element with a single integration point at the centroid of the element. The cross-sectional behavior of the homogeneous shell element is calculated using Simpson's rule with five integration points through the thickness of the element (Hibbitt *et al.*, 1996).

The bolts connecting the splice member to the gusset plate and the splice member to the brace member were modeled using rigid links to connect the nodes on the splice member to the nodes on the gusset plate corresponding to the location of the bolts. In this way, the nodes were forced to translate by the same magnitude and in the same direction in the coordinate axis-1 and axis-2 directions. The locations of the rigid links are shown in Figure 5-8. No attempt was made to model the bolt holes in the model and the bolt slip observed in Specimens T-1 and T-2.

To ensure compatibility of the out-of-plane displacements between the splice members, the gusset plate, and the brace member rigid links were used at "contact" points between the gusset plate and the splice member, as well as between the brace member and the splice member. The locations of these links are shown in Figure 5-9.

The nodes at the intersection of the beam and column framing members were restrained in all six degrees of freedom, rotation ( $\theta_1, \theta_2, \theta_3$ ) and translation ( $u_1, u_2, u_3$ ), along the

coordinate axis shown. One end of the brace member was connected to the splice member, and the other end was restrained from out-of-plane translation ( $u_3$ ), and free in all other degrees of freedom ( $\theta_1, \theta_2, \theta_3, u_1, u_2$ ). The load was applied to the assembly by imposing an in-plane axial deformation, in the longitudinal direction of the brace member, at the restrained node in the brace member. Figure 5-10 shows the imposed restraints, the coordinate axis, as well as the point of load application in a typical model.

### ***5.3.2 Initial Imperfections***

Out-of-plane initial imperfections of the gusset plate and the brace member were measured for each test specimen. The locations of the initial imperfection measurements of the gusset plate were shown in Figure 3-3. The measurements obtained at these points were mapped onto the finite element mesh and incorporated into the finite element model. The measurements are summarized in Appendix A. Figures 5-11 through 5-14 show the out-of-plane initial imperfections of the gusset plates for the four test specimens. The imperfections shown in the figures are referenced to an undeformed plate and magnified 50 times for clarity.

### ***5.3.3 Material Models***

Tension coupon tests were performed to obtain the engineering stress-strain data for the gusset plates, splice members, as well as the brace members. In order to incorporate the measured material properties into the finite element models, the material test results were transformed to true stress and logarithmic strain values. This conversion is accomplished by the following formulae, where  $\sigma_{\text{true}}$  is the true stress,  $\sigma_{\text{nom}}$  is the engineering stress



obtained from the tension coupon test,  $E$  is the modulus of elasticity of the material,  $\epsilon_{nom}$  is the engineering strain, and  $\epsilon_{ln}$  is the logarithmic strain.

$$\sigma_{true} = \sigma_{nom} (1 + \epsilon_{nom}) \quad (5-1)$$

$$\epsilon_{ln} = \ln (1 + \epsilon_{nom}) - \sigma_{true} / E \quad (5-2)$$

Both isotropic strain hardening models as well as elastic perfectly plastic models were used in the numerical models. The isotropic strain hardening model over predicted the peak strengths of the assemblies and did not exhibit larger stiffness. The elastic-perfectly plastic material model was found to predict Rabinovitch and Cheng's (1993) experimental results most accurately (Walbridge *et al.*, 1998) and thus was ultimately used in these models. The material models used in the finite element analysis and the original engineering stress-strain curves obtained from coupon tests for each component, gusset plates, brace members, and splice members, are shown in Figure 5-15.

#### 5.4 Analysis

Specimens T-1 and T-2 were designed with the gusset plate as the weak element in compression and were subjected to cyclic loading. The analysis of these specimens was performed using Newton's method to solve the nonlinear equilibrium equations. Specimens T-3 and T-4, however, were designed such that the brace member was the weak element in compression. In order to model this type of behavior (possibly unstable), the modified Riks method implemented in ABAQUS was used in the analysis. A standard Newton approach was used up until buckling, then the solution strategy was switched to Riks' procedure to carry the solution through buckling. In order to accomplish this, the analysis had to be stopped after the cycle before buckling was

completed, then restarted to load the specimen in compression through buckling. Following completion of the Riks' step, the analysis was again stopped and restarted using the standard Newton's approach to complete the remaining displacement cycles.

Since the predicted behavior cannot match exactly the observed behavior during the tests, the loading history used for the analysis was not exactly the same as the one adopted for the tests. Instead, the displacement imposed to the model was such that the model buckled in the same displacement cycle as the test specimen. For most specimens, this occurred in displacement cycle #5. Before the buckling cycle, the displacements in the model were incremented equally in tension and compression. After the buckling cycle, the displacement was increased in compression and held constant in tension, as was the case during the tests. Also, in order to speed up the analysis, only one loading cycle was applied in each loading block. Walbridge *et al.* (1998) found that only a very small deterioration in behavior was observed during cycling within a loading block.

The results from each analysis included the load versus displacement behavior of the assembly and gusset plate, the out-of-plane deformed shape of the gusset plate free edges and brace members at the maximum compressive load, as well as the principal stress directions. The results of the finite element analysis will be presented and compared with the test results in Chapter 6.

**Table 5-1**  
**Description of Preliminary Finite Element Models**

**Series I – Monotonic Compression, Without Brace Member**

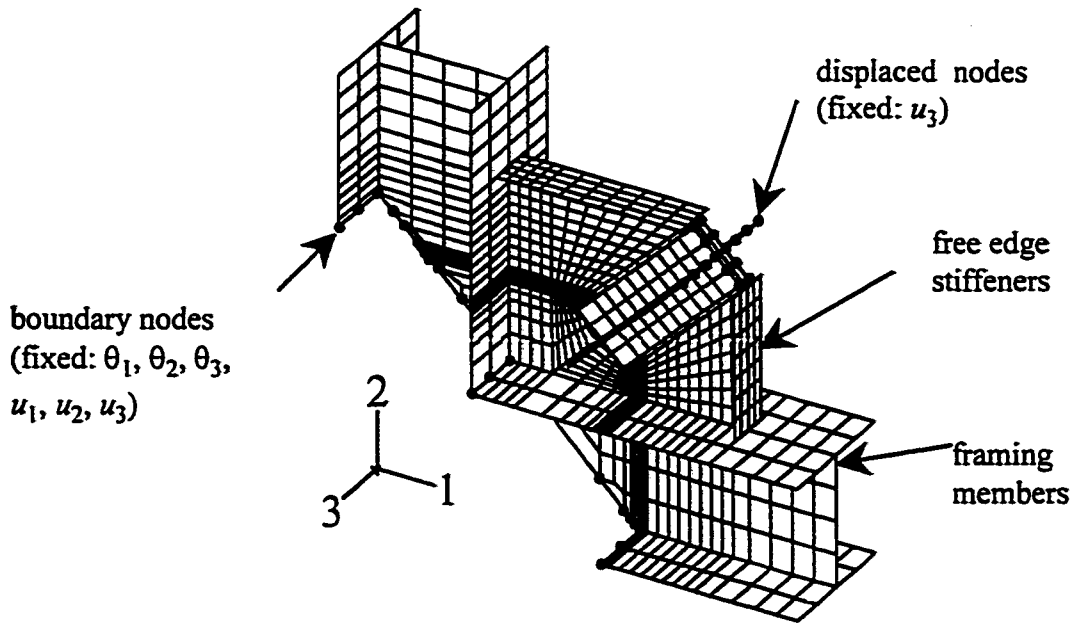
Model	Gusset Plate Thickness t (mm)	Stiffener Thickness t <sub>st</sub> (mm)	Stiffener Width 2b (mm)	2b / t <sub>st</sub>	t <sub>st</sub> / t
mc9	9	—	—	—	—
mc9S1	9	9	25.0	2.78	1.00
mc9S2	9	9	37.5	4.17	1.00
mc9S3	9	12	25.0	2.08	1.33
mc9S4	9	12	37.5	3.13	1.33
mc12	12	—	—	—	—
mc12S1	12	9	25.0	2.78	0.75
mc12S2	12	9	37.5	4.17	0.75
mc12S3	12	12	25.0	2.08	1.00
mc12S4	12	12	37.5	3.13	1.00
mc12S5	12	9	51.0	5.67	0.75
mc12S6	12	12	51.0	4.25	1.00
mc15	15	—	—	—	—
mc15S1	15	9	25.0	2.78	0.60
mc15S2	15	9	37.5	4.17	0.60
mc15S3	15	12	25.0	2.08	0.80
mc15S4	15	12	37.5	3.13	0.80

**Series II – Monotonic Compression, With Brace Member**

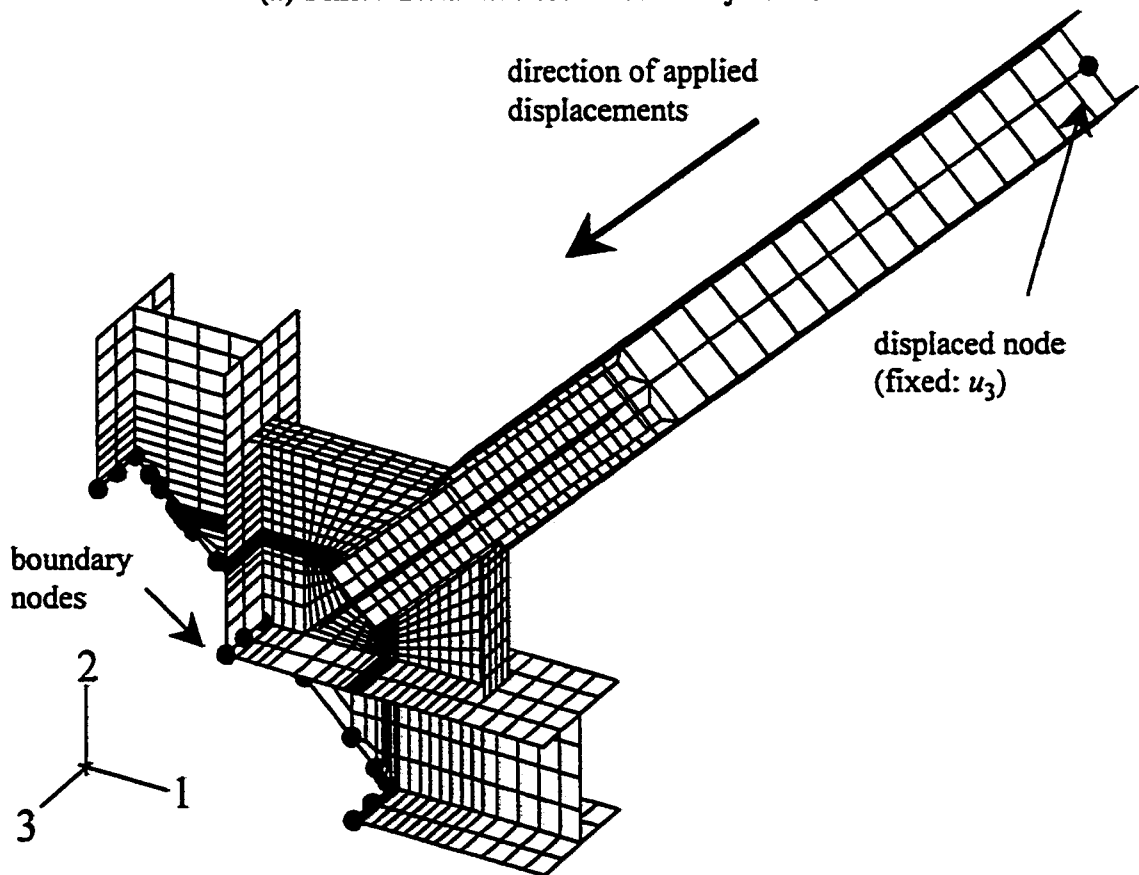
Model	Gusset Plate Thickness t (mm)	Stiffener Thickness t <sub>st</sub> (mm)	Stiffener Width 2b (mm)	2b / t <sub>st</sub>	Brace Member x 2595 mm
mc12B	12	—	—	—	W200 x 59
mc12BS1	12	9	25.0	2.78	W200 x 59
mc12BS2	12	9	37.5	4.17	W200 x 59
mc12BS5	12	9	51.0	5.67	W200 x 59

**Series III– Cyclic Loading, With Brace Member**

Model	Gusset Plate Thickness t (mm)	Stiffener Thickness t <sub>st</sub> (mm)	Stiffener Width 2b (mm)	2b / t <sub>st</sub>	Brace Member x 2595 mm
cy12	12	—	—	—	W200 x 59
cy12BS1	12	9	25.0	2.78	W200 x 59
cy12BS2	12	9	37.5	4.17	W200 x 59
cy12BS5	12	9	51.0	5.67	W200 x 59



(a) Finite Element Model for Analysis—Series I



(b) Finite Element Model for Analysis—Series II and III

Figure 5-1: Typical Finite Element Models

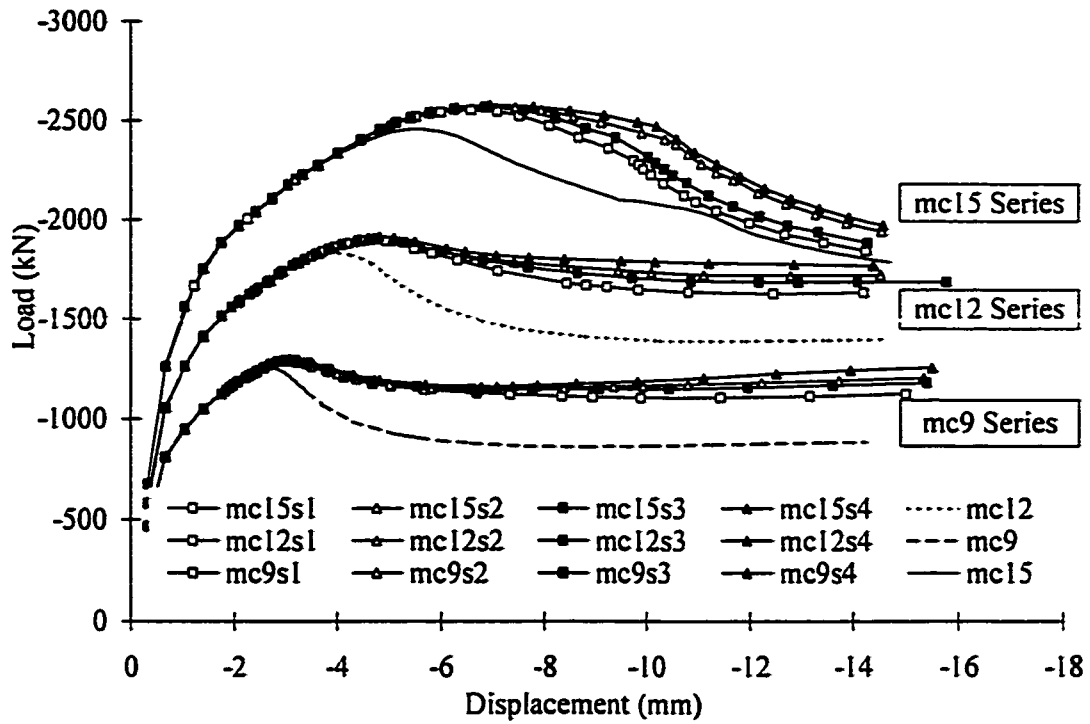


**Figure 5-2: Effect of Gusset Plate Thickness and Stiffener Dimensions on Gusset Plate Behavior**

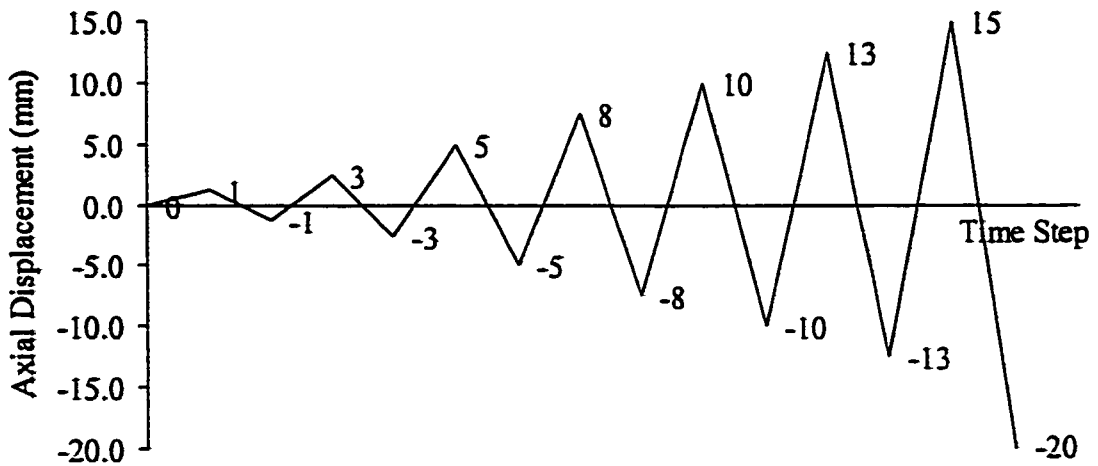


**Figure 5-3: Deformation Spectrum Applied to Series III**

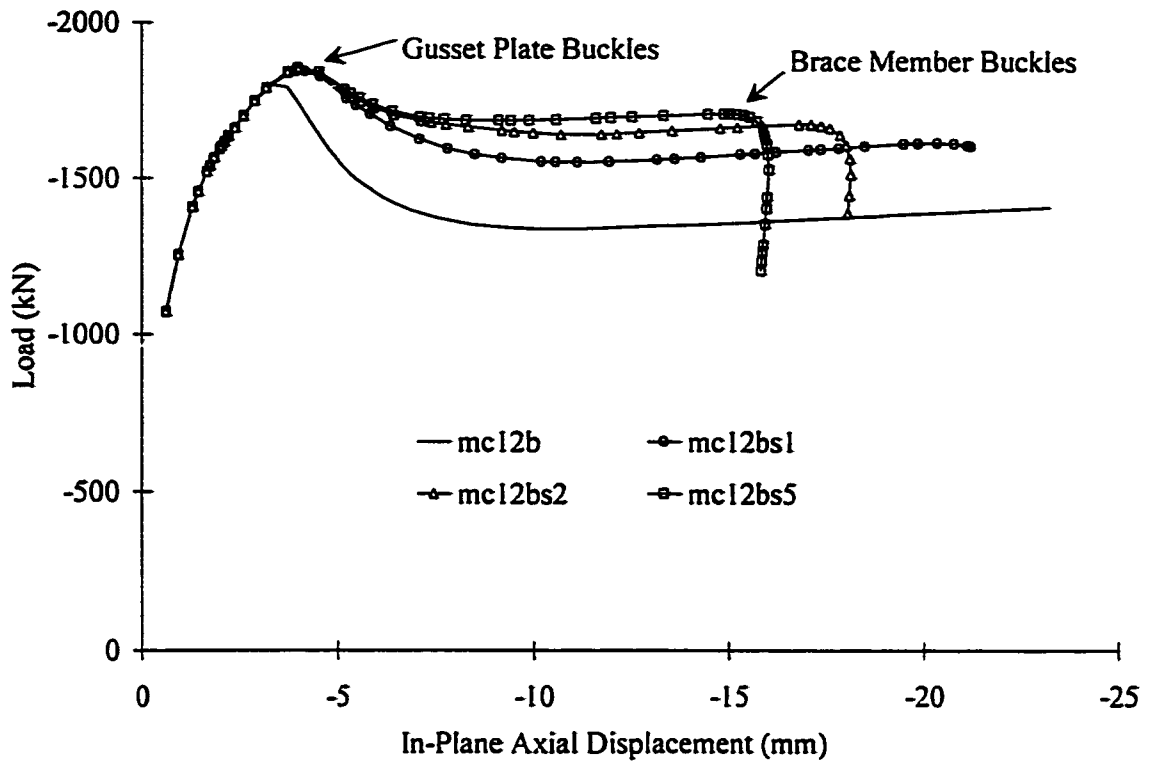


**Figure 5-4: Load versus Gusset Plate In-Plane Axial Displacement Relationship for Series II (With Brace Member) Under Monotonic Compressive Loading**

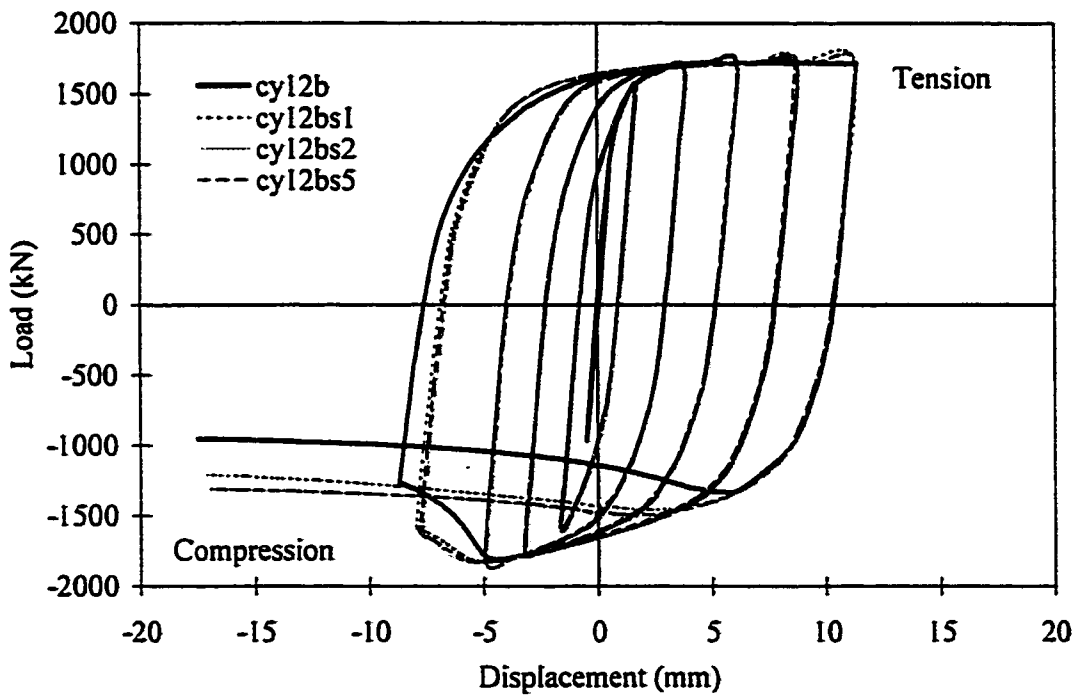


**Figure 5-5: Load versus Gusset Plate Axial Displacement Relationship for Series III (With Brace Member) Under Cyclic Loading**

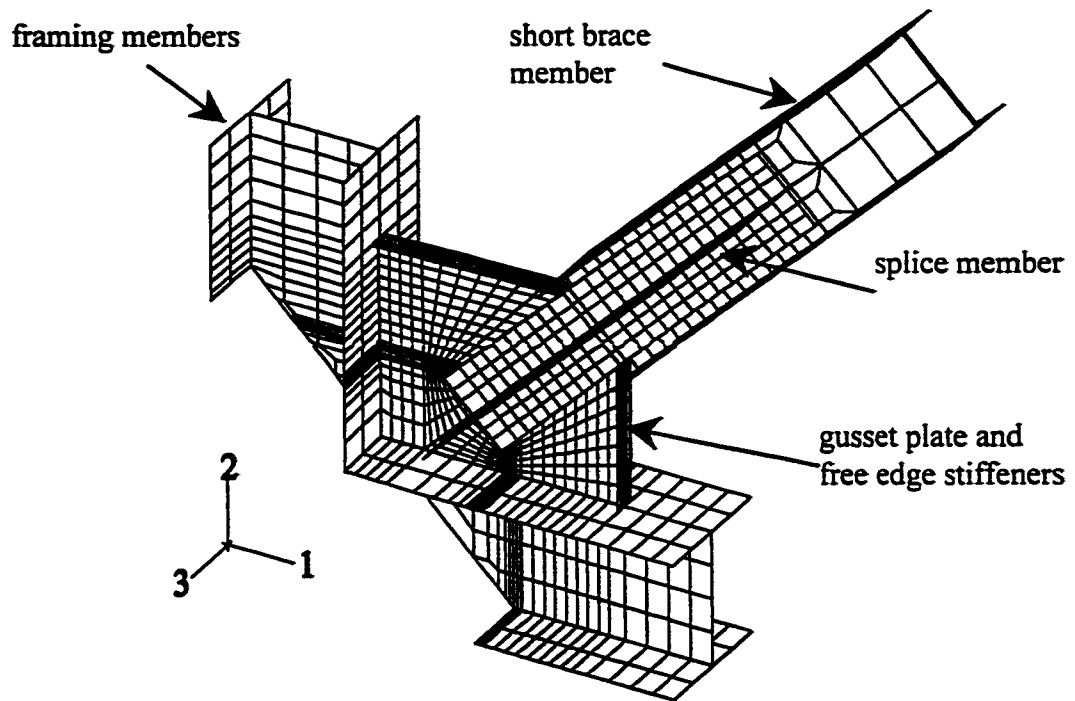


**Figure 5-6: Finite Element Model for Specimens T-1 and T-2**

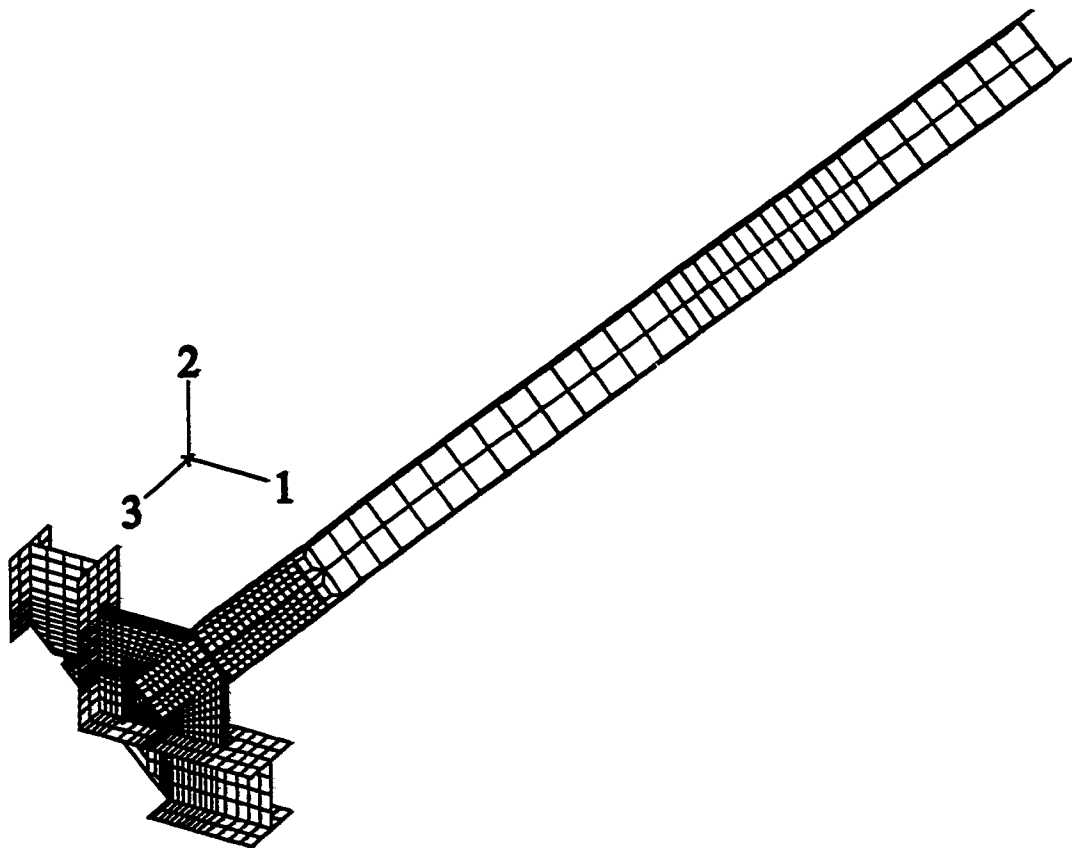


**Figure 5-7: Finite Element Model for Specimens T-3 and T-4**

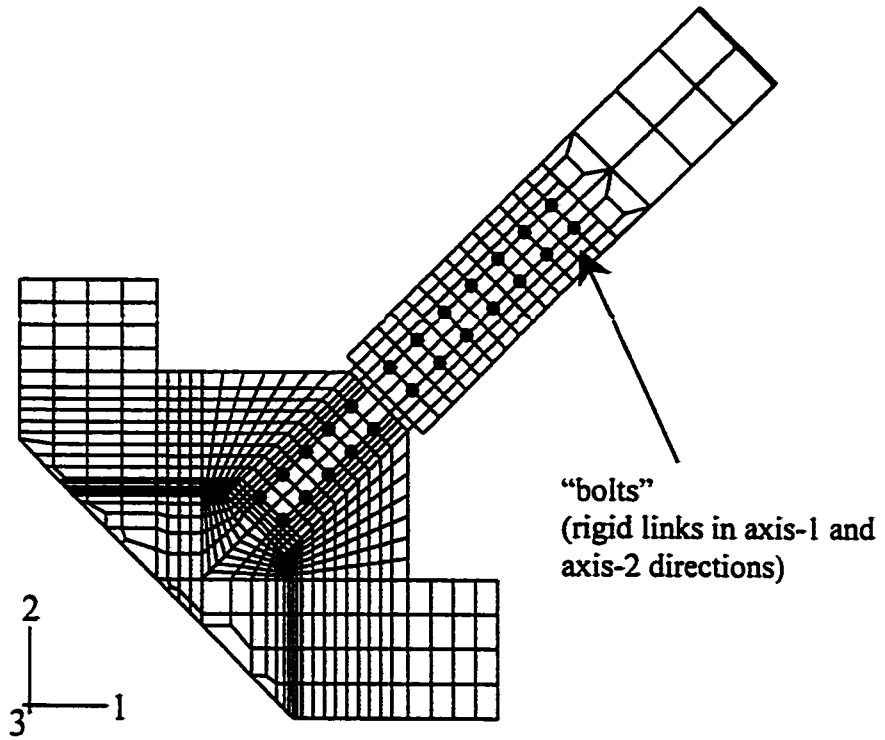


**Figure 5-8: Location of "Bolts" as Rigid Links in the Finite Element Models**

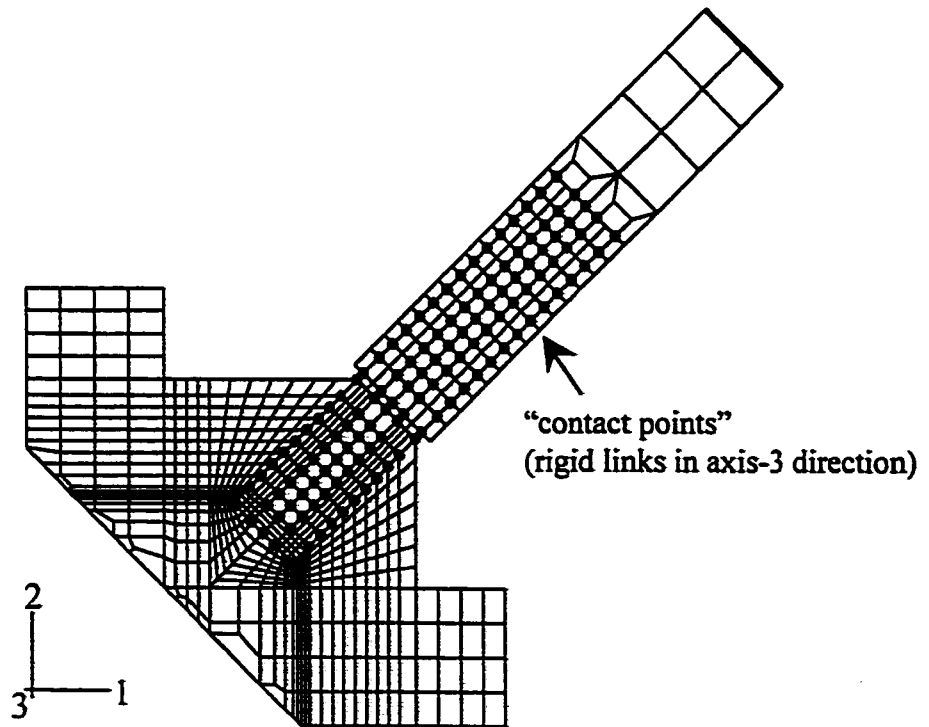


**Figure 5-9: Location of "Contact Points" in the Finite Element Models**



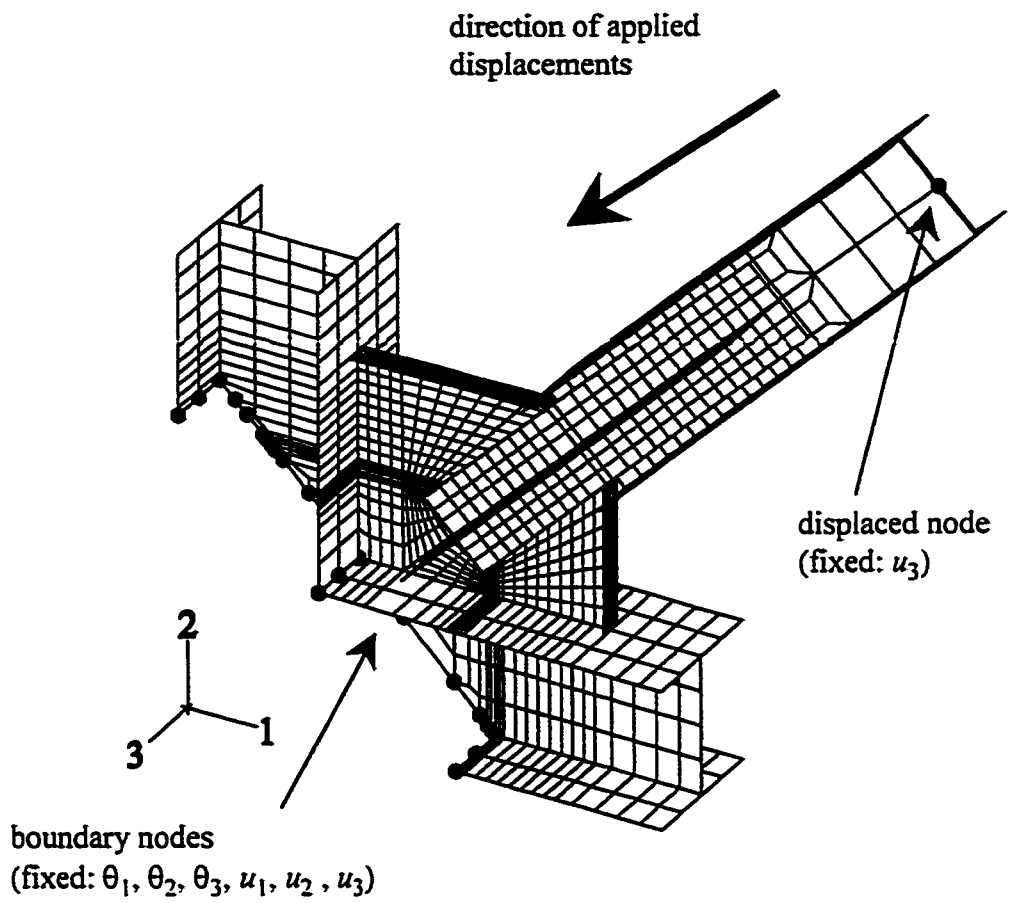


**Figure 5-10: Boundary Conditions and Point of Load Application**

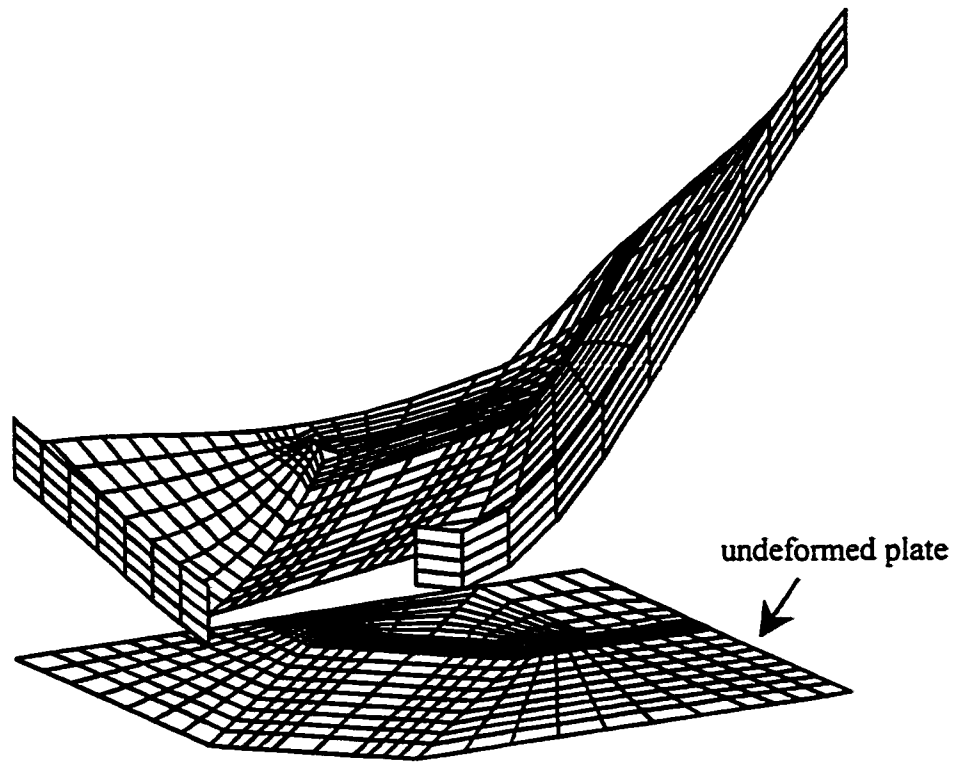


**Figure 5-11: Gusset Plate Out-of-Plane Initial Imperfection for Test Specimen T-1 (Magnified 50 Times)**

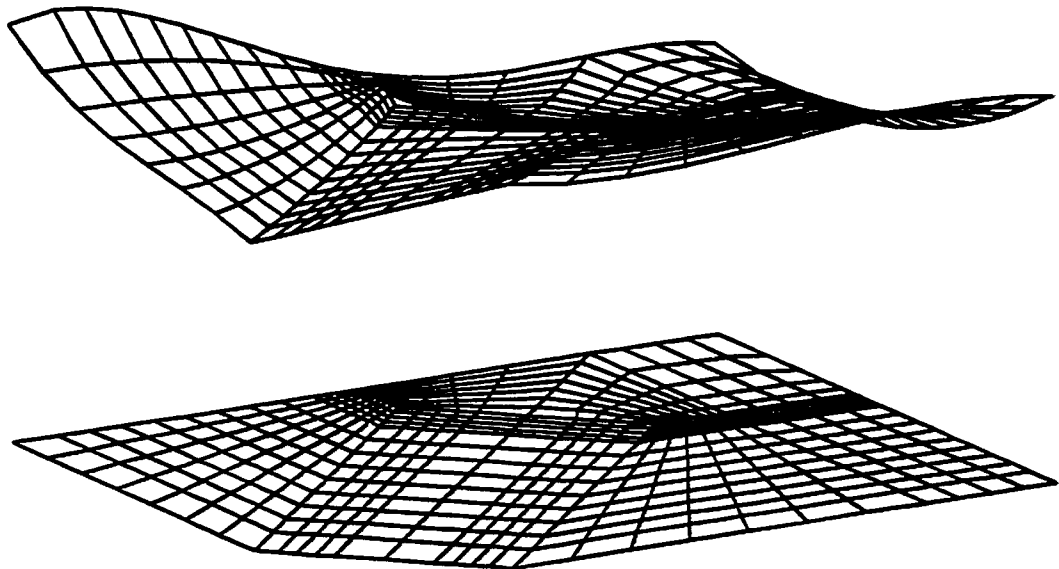


**Figure 5-12 : Gusset Plate Out-of-Plane Initial Imperfection for Test Specimen T-2 (Magnified 50 Times)**

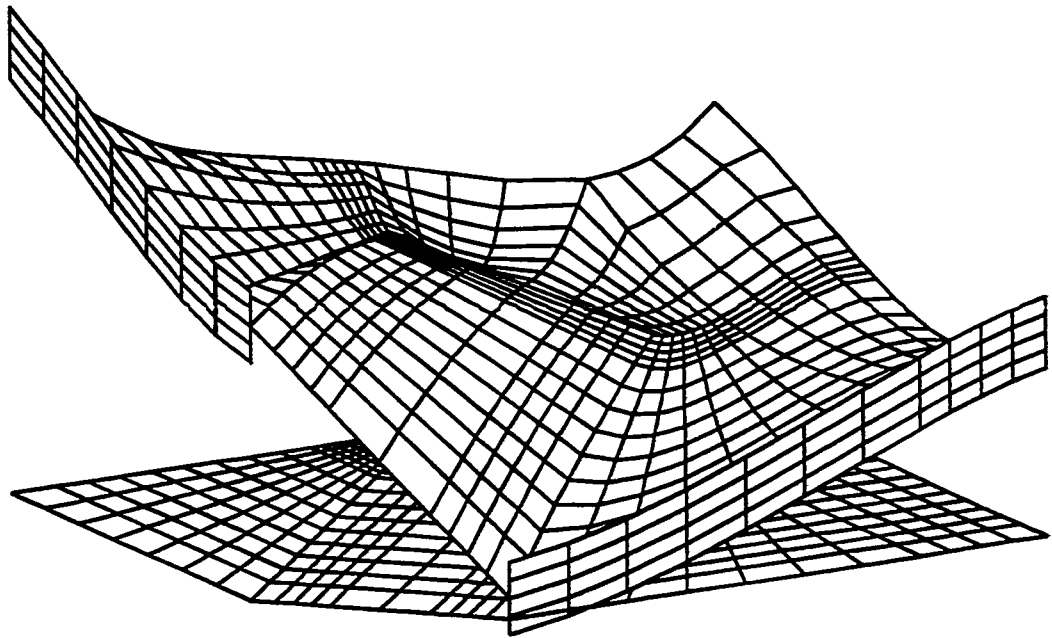


**Figure 5-13: Gusset Plate Out-of-Plane Initial Imperfection for Test Specimen T-3  
(Magnified 50 Times)**

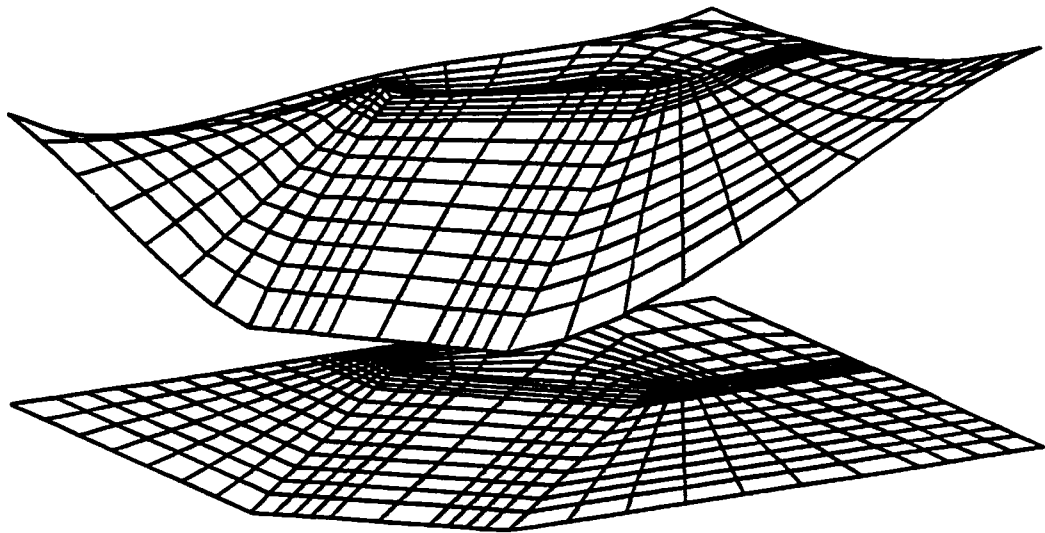
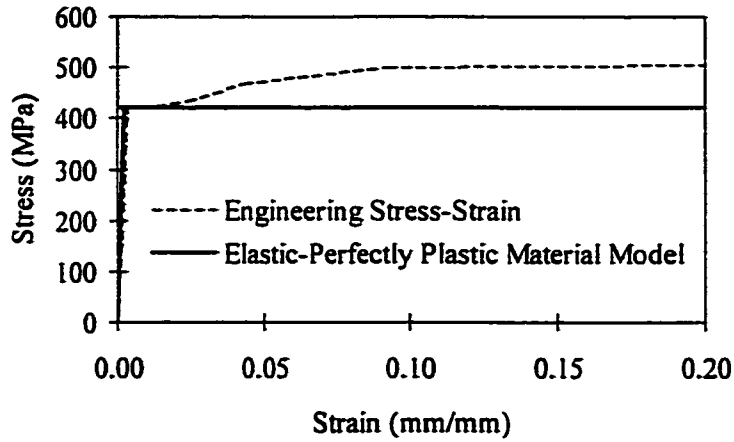
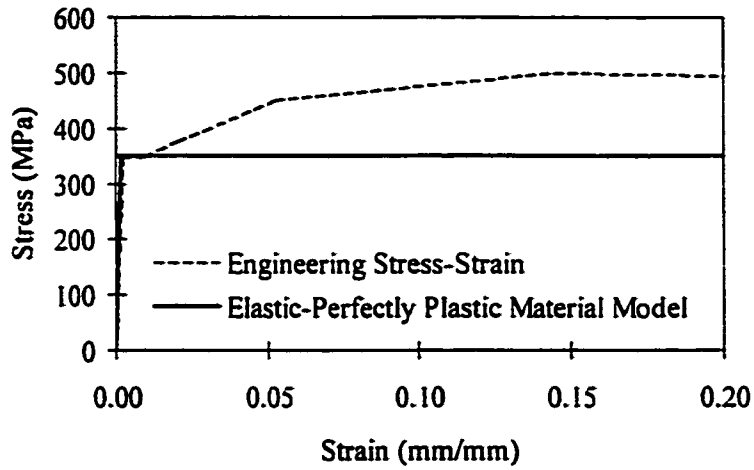


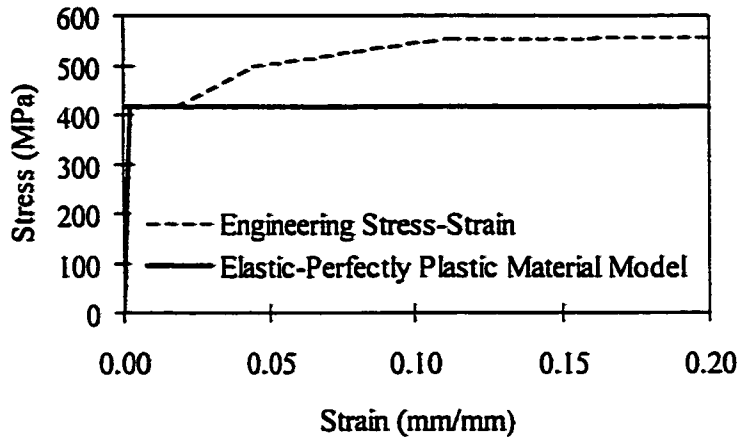
**Figure 5-14: Gusset Plate Out-of-Plane Initial Imperfection for Test Specimen T-4  
(Magnified 50 Times)**



**(a) Material Model for Gusset Plate**



**(b) Material Model for Splice Members**



**(c) Material Model for Brace Members**

**Figure 5-15: Stress versus Strain Curves used in the Finite Element Analysis**

## CHAPTER 6

### DISCUSSION

#### 6.1 Introduction

This chapter presents a discussion of the test results and a comparison of the test results with the behavior predicted using the numerical models presented in Chapter 5. A discussion of the test results with respect to the load versus displacement response, energy absorption, and out-of plane displacements is first presented in Section 6.2. Section 6.3 then presents the comparison between the test results and the predictions using the numerical models. These comparisons are based on the load versus displacement behavior, energy absorption characteristics, out-of-plane deformations of the gusset plate and brace member, as well as the direction of principal strains.

#### 6.2 Experimental Results

##### *6.2.1 Load versus Displacement Response*

The predicted tensile and compressive strengths of the assemblies are compared with the test results in Tables 6-1 and 6-2. Table 6-1 compares the maximum tensile strength reached by each specimen with the predicted strengths calculated using Whitmore's method, as well as the block shear models proposed by Hardash and Bjorhovde (1985) and CAN/CSA-S16.1 (1997) with the factor  $0.85\phi$  taken as 1.0. The test-to-predicted ratios range from 1.17 to 1.19 for the predictions using Whitmore's effective section, from 1.02 to 1.04 using the block shear model proposed by Hardash and Bjorhovde (1985), and from 1.35 to 1.37 using the block shear model in CAN/CSA-S16.1 (1997).

Based on these results, it is seen that the block shear model proposed by Hardash and Bjorhovde (1985) most accurately predicts the tensile strength of the connection. The tensile resistance predicted using Whitmore's approach is consistently conservative, although less conservative than the approach used in CAN/CSA-S16.1. The predictions from the two block shear models differ significantly. The block shear model used in CAN/CSA-S16.1 assumes that tensile failure and shear failure occur at the same time. Since rupture in shear is assumed, the ultimate shear strength is used on the net shear area for strength calculations. The block shear model proposed by Hardash and Bjorhovde, however, does not assume that failure in tension and in shear occur simultaneously. Since the shear area is not assumed to fail, the gross area is used rather than the net area. The shear stress acting on the shear area is somewhat lower than the ultimate shear stress. This latter model is consistent with the experimental observations that indicate that failure in tension occurs by rupture along the net tension area and large shear deformations along the length of the connection.

Table 6-2 compares the maximum compressive strengths reached by test specimens with the predicted strengths calculated using CAN/CSA-S16.1 (1997), Whitmore's method (this represents an upper bound to the capacity in compression), and Thornton's method. The results indicate that the predicted compressive capacity of Specimens T-1 and T-2, designed to fail by gusset plate buckling, is conservative using both Whitmore's and Thornton's methods. However, the strength is predicted more accurately for the unstiffened gusset plate (Specimen T-2) than for the stiffened gusset plate (Specimen T-1). The resulting average test-to-predicted ratios are 1.10 for Specimen T-2 and 1.27 for Specimen T-1. This trend is expected since these equations do not take into account the

benefits of free edge stiffeners. For specimens designed to fail by brace member buckling – Specimens T-3 and T-4 – the buckling strength of the brace member was calculated using the method outlined in CAN/CSA-S16.1 (1997) using an effective length factor of 0.7. These calculated strengths were also conservative with an average test-to-predicted ratio of 1.30 as shown in Table 6-2. This may have resulted due to friction in the top pin connection, which prevented it from acting as a true pin. This friction was observed during testing thus decreasing the effective length and resulting in a higher observed compressive capacity.

The test results presented in Table 6-2 indicate that free edge stiffeners significantly increase the compressive strength of gusset plate connections designed with the brace member as the strong element in compression. However, the benefit of free edge stiffeners is much less pronounced when the brace member is the weak element in compression. A comparison of the load versus displacement behavior between Specimens T-1 and T-2 and between T-3 and T-4 is shown in figures 6-1 and 6-2, respectively. Figure 6-1 indicates that the addition of free edge stiffeners to gusset plates designed as the weak element in compression increases the post-buckling strength (measured in the final compression cycle at -15 mm displacement) by 45% (from 1120 kN to 1630 kN) and the peak compressive load carrying capacity by 15%. This result is in agreement with the increase in strength observed by Rabinovitch and Cheng (1993) in their test specimen A-3, which showed a 19% increase in peak compressive strength after the addition of free edge stiffeners with a width-to-thickness ratio of 5.36. This increase in strength may be a result of the increased amount of material able to resist the compressive loads, or a result of the increased in-plane stiffness of the gusset plate.

The strain distribution in the gusset plate shows that more load is going to the stiffeners than directly to the framing members because the gusset plate is quite flexible.

Specimen T-1 was able to maintain its in-plane stiffness after many load cycles. The in-plane stiffness of test specimen T-1 during the final unloading from compression to tension, was 158% greater than that of Specimen T-2. The comparison between T-1 and T-2 presented in Figure 6-1 also indicates that the free edge stiffeners contribute to a more stable buckling response. This is believed to be the result of the reduced out-of-plane deformations in the gusset plates observed in the test specimens with free edge stiffeners. Out-of-plane deformations contribute to second order effects, which in turn result in a reduction of compressive strength both at buckling and post buckling stages.

As stated earlier, for cases in which the load limiting mechanism in compression is buckling of the brace member, the stiffness of the end connection may affect the effective length of the brace member in compression, hence the load carrying capacity and the behavior of the assembly. The test results presented in Chapter 4, however, do not show a significant effect of the additional rotational end restraint provided by the free edge stiffeners on the strength and behavior of the brace member. A comparison of the load versus displacement behavior of Specimens T-3 and T-4 in Figure 6-2 indicates that the tensile strength of Specimens T-3 and T-4 are within 1% of each other, and their peak compressive strengths are within 2%. The post buckling strengths of Specimens T-3 and T-4, as measured in the final compression cycle at 15 mm displacement, were -513 kN and -468 kN, respectively; a 10% difference. Based on this observation, the presence of free edge stiffeners seem to have a negligible effect on the tensile and compressive load carrying capacity of assemblies when buckling of the brace member is the load limiting



mechanism in compression. This observation cannot be generalized, however, since only one stiffener – gusset plate size combination was tested. The effect of gusset plate free edge stiffeners on the out-of-plane stiffness of the gusset plate - brace member connections and on the effective length of the brace member in compression, should therefore be investigated using additional combinations of stiffener size and gusset plate thickness.

The tensile strength of the gusset plate assemblies tested seemed to be relatively unaffected by the presence of free edge stiffeners. This is the case because the strength of the assembly in tension is governed by the connection strength and the stiffeners have little or no effect on either block shear failure of the gusset plate or on the net section failure of the brace member. The addition of free edge stiffeners also had a negligible effect on the tension behavior of the assemblies. An examination of the principal strain directions in the gusset plate when the brace member is in tension (refer to Table 4-7) indicates that the effect of free edge stiffeners on the stress flow in the gusset plate for Specimens T-1 and T-2 is small, and for Specimens T-3 and T-4 the effect is negligible. The stress flow directions indicate that the load path in the gusset plate is directed to the framing members primarily by the gusset plate rather than by the free edge stiffeners. Since the load path in the specimens is similar for the stiffened and unstiffened gusset plates their behavior in tension is similar.

### ***6.2.2 Energy Absorption***

The cumulative energy absorbed by the four test specimens, T-1 through T-4, was presented earlier in Figure 4-12. The comparison of Specimen T-1 with T-2, and T-3

with T-4 indicates that free edge stiffeners have no effect on the energy absorption capacity of the assembly in tension. In test specimens T-1 and T-2 it was noted that significant bolt slip occurred compared to test specimens T-3 and T-4. Since bolt slip is a contributing factor to the energy absorption capability of the assembly, bolt slip must be considered when comparing the energy absorption capabilities of the assemblies in tension.

In compression, free edge stiffeners have a significant effect on the amount of energy absorbed by the assemblies. A comparison of test specimen T-1 with T-2 in Figure 4-12 indicates that the effect of the free edge stiffeners is more significant at larger axial displacements than at smaller displacements. The free edges of the gusset plate do not experience large curvatures at smaller axial displacements and, therefore, the effect of free edge stiffeners in this range is small. At larger axial displacements, the larger free edge restraint provided by the stiffeners results in a higher peak compressive and post buckling strength, thus greater energy absorption capability. For the case where buckling of the brace member is the load limiting mechanism, the stiffeners seem to have an effect on the amount of energy that can be absorbed at all displacement levels. Upon application of the compressive loads, the gusset plate does not buckle at the free edges, but sways out of plane to allow for the brace end rotations and the stiffeners help to transfer the load from the brace member to the framing members.

It is important to note that in the calculations of energy capacity, the effect of bolt slip was not isolated and removed. This would not have an effect on the comparison between the test specimens if the bolt slip was equal in all test specimens or if the bolt slip contribution to the amount of energy dissipated was small. However, this is not the case.

In 1993, Rabinovitch and Cheng observed that slip in the gusset plate to splice member bolted connection could contribute significantly to the energy absorption capacity of the assembly and it is also supported by the test results presented in Figure 4-13. By taking the difference between the amount of energy absorbed by the assembly and the energy absorbed by the gusset plate in Specimen T-2, the contribution of bolt slip could be assessed. This indicates that approximately 80% of the total amount of energy absorbed by the assembly in tension and compression was due to bolt slip. Therefore, bolt slip must be considered when comparing the results of test specimens T-1 and T-2. Unfortunately, the amount of energy absorbed and the amount of bolt slip experienced by the gusset plate in Specimen T-1 could not be obtained due to problems experienced with the instrumentation during the test. Significant bolt slip also occurred in Specimen T-2, however, a comparison of energy absorption between test specimen T-1 and test specimen T-2 cannot be made. During testing, the amount of bolt slip that was observed in test specimens T-3 and T-4 was small and can be considered negligible. Thus, the observations made regarding test specimens T-2, T-3 and T-4 can be considered valid, and those regarding the energy absorption characteristics of Specimen T-1 and the comparison of T-1 and T-2 with T-3 and T-4 are inconclusive. Since bolt slip has been shown to significantly increase the energy absorption capabilities of assemblies subjected to cyclic loading, (Astaneh-Asl, 1998; Rabinovitch and Cheng, 1993) slip should be isolated and included in future experiments.

### ***6.2.3 Out-of-Plane Displacements***

The deformed shape of the gusset plate free edges, at the peak compressive load reached by the assemblies, is shown in figures 6-3 and 6-4. It is evident from Figure 6-3 that the out-of-plane deformation of the gusset plate free edges is greatly influenced by the presence of free edge stiffeners when the load limiting mechanism in compression is buckling of the gusset plate. Both the curvature and the deflections along the edge are smaller for the stiffened gusset plate in Specimen T-1 than for unstiffened Specimen T-2. The free edge stiffeners have the effect of limiting the amount of curvature in the plate free edges and therefore decreasing the amount of out-of-plane deformation. For the assemblies in which buckling of the brace member is the load limiting mechanism in compression (see Figure 6-4), the stiffeners have a negligible effect on the out-of-plane deformation. This is expected since curvature over most of the plate length is small. A comparison of test specimen T-3 with T-4 indicates that the stiffeners offer little additional restraint to the brace member end rotation.

Figure 6-5 depicts the out-of-plane deformation of the brace member for Specimens T-3 and T-4 at the final peak compressive load achieved before the specimen was brought to failure in tension. The magnitude of the out-of-plane deformation, the inflection point along the brace member, and the maximum deflection are unaffected by the presence of gusset plate stiffeners. This suggests that the presence of free edge stiffeners, for the geometry chosen in this experimental program, had a negligible effect on the stiffness of the end connection and thus had no effect on the buckling behavior of the brace member. This observation is in agreement with earlier observation about the effect of free edge stiffeners on the load carrying capacity and buckling behavior of Specimens T-3 and T-4.

The Ontario Highway Bridge Design Code (1990) and CAN3-S6-M (1983) recommend that the free edges of gusset plates should be stiffened if the free length exceeds  $930/\sqrt{F_y}$  or  $945/\sqrt{F_y}$  times its thickness, respectively. Although the free lengths of the gusset plates used in this test program did not exceed this criterion, free edge stiffeners were used and were found to improve the gusset plate behavior. Astaneh-Asl (1998) stated that the above criterion is adequate for monotonically loaded specimens, but that edge buckling will occur if the gusset plate is subjected to cyclic loading. In order to prevent buckling of the free edge prior to the gusset plate reaching its maximum compressive strength, Astaneh-Asl (1998) suggested reducing the allowable free length limit to approximately  $335/\sqrt{F_y}$  times its thickness. For the specimens tested, the length of the gusset plate free edge did not meet this criterion and the gusset plate yielded prior to the maximum compressive load being achieved.

### **6.3 Comparison of Finite Element Analysis Results with Test Results**

#### ***6.3.1 Load versus Displacement Behavior***

This section presents a comparison between the test results and predicted response of the assemblies. The observed and predicted load versus axial displacement relationships for the test specimens are compared in terms of the peak loads in tension and compression, the stiffness of the assemblies, overall buckling behavior and the amount of energy absorbed during cyclic loading.

Table 6-3 presents the predicted peak tensile and compressive loads, as well as the post-buckling strength, at an overall displacement of -15 mm measured at the point of loading.

The test to predicted ratios range from 0.98 to 1.02 for the peak load in tension and from 0.86 to 1.01 for the peak load in compression. The predicted maximum strength was in better agreement with the test results for the stiffened specimens than for the unstiffened specimens. The test to predicted ratios are 1.01 and 0.90 for the stiffened gusset plate specimens and 0.86 and 0.88 for the unstiffened gusset plate specimens. The test to predicted ratios for the post-buckling strength of the assemblies are also presented, ranging from 0.85 to 1.05, with an average of 0.94. Based on these results, the finite element models are seen to give very good predictions of tensile strength and good, although sometimes unconservative, estimates of the peak compressive and post buckling capacities of the gusset plate-brace member assemblies.

Figures 6-6 through 6-9 show comparisons between the test and predicted load versus axial displacement responses of the assemblies. The load versus axial displacement relationship of the assemblies for Specimens T-1 and T-2 are shown in figures 6-6 and 6-7, respectively. The finite element model predicted the axial displacement at onset of buckling for Specimens T-1 and T-2 to be 8.7 mm, and 9.0 mm, compared to 5.9 mm and 3.5 mm observed in the tests. The rates at which the compressive load carrying capacity decreased after buckling was modeled well, as seen in figures 6-6 and 6-7, and the post buckling strengths for Specimens T-1 and T-2 were predicted within 5%. The finite element models displayed a more flexible behavior than the test specimens in the elastic and inelastic ranges of both compressive and tensile loading. This is unexpected because finite element models typically exhibit stiffer behavior because it has fewer degrees of freedom than the actual structure and stores less strain energy. Although the stiffness in each cycle is not predicted well, the rate at which the stiffness of the assembly

deteriorates, subsequent to buckling, during the final cycles of loading is predicted well. By comparing the stiffness between the final consecutive unloading cycles, a stiffness deterioration rate can be approximated. A comparison of the stiffness deterioration rates of consecutive cycles between the test specimens and that predicted by the finite element models averages 15% and 14%, respectively for Specimen T-1, and 36% and 37%, respectively for Specimen T-2. They are in good agreement.

The load versus axial displacement relationship of the assemblies for Specimens T-3 and T-4 are shown in figures 6-8 and 6-9, respectively. The finite element model predicted the point at which the maximum compressive load occurred for both Specimens T-3 and T-4 to be 9.2 mm. The observed buckling displacement for Specimens T-3 and T-4 was 4.7 mm and 4.8 mm, respectively. As was observed in Specimens T-1 and T-2, the rates at which the compressive load carrying capacity diminished was modeled well, as seen in figures 6-8 and 6-9 and the test to predicted ratio for the post buckling strengths for Specimens T-3 and T-4 was approximately 0.86. The stiffness of the unloading portion of the load deformation plot was calculated using the slope of the trailing end. The stiffness is calculated as the slope of the load-deformation plot. The stiffness decrease between consecutive cycles in the test specimens and the finite element models during the unloading phase from compression to tension are 17% for Specimen T-3, and 5% for Specimen T-4. Therefore, as with Specimens T-1 and T-2, the elastic and inelastic stiffness predicted by the finite element model was lower than observed in the test specimens in both tension and compression and the stiffness deterioration rate subsequent to buckling, during the final cycles of loading, was predicted reasonably well.

### **6.3.2 Energy Absorption**

The amount of energy dissipated by the connection was calculated from the results of the finite element analysis and the test results. A comparison of the amount of energy absorbed at each displacement cycle by the test assemblies and the finite element models is presented in figures 6-10 to 6-15. Figures 6-10 and 6-11 display the amount of energy absorbed in each displacement cycle versus the peak compressive displacement in that cycle for Specimens T-1 and T-2, as well as T-3 and T-4, respectively. The amount of energy dissipated due to compressive displacements is separated from that absorbed by tensile displacement in figures 6-12 through 6-15. From these plots, the following observations can be made. The predicted amount of energy absorption from Specimens T-1 and T-2 as shown in figures 6-12 and 6-13, respectively, is lower than achieved in the tests, approximately 27% and 30% respectively. Since the finite element models exhibited less stiff behavior, this result is expected. The plots displaying the energy absorbed by test specimens T-3 and T-4 (figures 6-14 and 6-15) indicate that at very small displacements where the assembly is elastic, the predicted energy absorption is zero, as expected. In the test specimens, the amount of energy absorbed in the specimen is not zero when subjected to the elastic displacements due to the initial slack in the LVDT wire used to take the axial displacement measurement of the assembly. At larger tension displacements the predicted energy absorption is lower than the experimental results, due to the stiffness variation, averaging a difference of 28% and 16% for Specimens T-3 and T-4, respectively. In compression however, the predicted amount of energy absorbed exceeds that achieved by the test specimens, by as much as 100% at larger axial displacements. By examining the load versus displacement plots this result is



explained. The finite element models displayed more flexibility and buckled at a larger axial displacement. Consequently, the finite element models had a greater strength than the test specimen at each displacement level subsequent to buckling. Since the plot displays axial displacement along the abscissa, the predicted amount of energy absorbed by the assembly is greater than that absorbed by the test assembly. Overall, these figures indicate that the finite element models are able to predict the energy absorption characteristics of the assemblies adequately.

### ***6.3.3 Out-of-Plane Displacements***

Figures 6-16 and 6-17 depict the overall deformed shapes of the gusset plate for Specimens T-1 and T-2 at the maximum displacement of the final compression cycle. These deformed shapes are representative of the deformed shape observed in the test specimens. The deformed shapes of the gusset plate for Specimens T-3 and T-4 are not shown because the bracing member rather than the gusset plate buckled in these two specimens and no noticeable gusset plate deformation or sway was detected. In the test specimens, the gusset plates swayed out-of-plane to allow for the brace end rotations, whereas the gusset plate in the finite element model did not. The rotation of the distributing beam about its longitudinal axis may have contributed to this effect since this rotation was restricted in the finite element models.

Figures 6-18 and 6-19 show the buckled configuration of the brace member predicted by the finite element models for Specimens T-3 and T-4. It is noted that the point of maximum displacement does not coincide with that of the test specimen. In the test specimens, the point of maximum displacement occurred at approximately mid-length of

the brace member (Figure 6-5), whereas in the finite element model, this point occurred at approximately two thirds of the length from the gusset plate (figures 6-18 and 6-19). This, as well as the deformed shape of the gusset plate subsequent to buckling, suggests that the out-of-plane rotational stiffness of the gusset plate in the model is larger than the stiffness observed in the test specimen. A contributing factor to this is the rotation of the distributing beam in the test setup. However, since there would have been no rotation of the beam at small displacements, a problem in the model in terms of the stiffness of the gusset plate-brace member connection is indicated.

#### ***6.3.4 Principal Strain Directions***

The directions of principal strains for the test specimens were presented in Chapter 4. Major principal strains and their directions at onset of compression yielding in the gusset plate were also obtained from the finite element analysis and are presented in figures 6-20 to 6-23. According to the strain directions presented in the finite element plots, the compressive strain directions within the gusset plate are not significantly affected by the presence of free edge stiffeners. However, as noted in figures 6-20 to 6-23 and in Chapter 4, unstiffened gusset plates experience larger strains than stiffened gusset plates by allowing the redistribution of strains over a greater area. When figures 6-20 and 6-23 are compared to the principal strain directions obtained from the test specimens and plotted in figures 4-24 and 4-27, one can see that the principal directions coincide well.

**Table 6-1**  
**Comparison of Experimental Results with Predicted Strengths — Tension**

Specimen	Measured Ultimate Tensile Load, $P_u^+$ (kN)	$\frac{P_{u^+}}{P_{w^+}}$	$\frac{P_{u^+}}{R_n}$	$\frac{P_{u^+}}{T_r}$
T-1	1740*	1.12	0.98	1.29
T-2	1819	1.17	1.02	1.35
T-3	1837	1.19	1.03	1.36
T-4	1841	1.19	1.04	1.37

\* : The test specimen was not loaded to failure in tension.

$P_{w^+}$ : Whitmore Tensile Load (1549 kN)

$R_n$ : Block shear as per Hardash and Bjorhovde, 1985 (1776 kN)

$T_r$ : block shear as per CAN/CSA-S16.1, 1997 Clause 13.2 and  $0.85\phi = 1.0$  (1348 kN)

**Table 6-2**  
**Comparison of Experimental Results with Predicted Strengths — Compression**

Specimen	Measured Ultimate Compressive Load, $P_u^-$ (kN)	$\frac{P_{u^-}}{P_{w^-}}$	$\frac{P_{u^-}}{P_t}$	$\frac{P_{u^-}}{P_b}$
T-1	-1951	1.26	1.28	N.A.
T-2	-1690	1.09	1.11	N.A.
T-3	-1350	N.A.	N.A.	1.32
T-4	-1322	N.A.	N.A.	1.28

$P_{w^-}$ : Whitmore Compressive Load (-1549 kN)

$P_t$ : Thornton Load,  $K = 0.65$  (-1525 kN)

$P_b$ : brace strength as per CAN/CSA-S16.1 (1997), Clause 13.3.1 & Clause 27.4.3.2 with  $K = 0.7$  and  $0.85\phi = 1.0$  (-1026 kN)

**Table 6-3**  
**Comparison of Finite Element Results with Experimental Results**

Specimen	Finite Element Analysis Results (kN)			Comparison with Experimental Results		
	Maximum Comp. $P_{A-}$	Maximum Tension $P_{A+}$	Post Buckling $P_{PA}$	$\frac{P_u -}{P_{A-}}$	$\frac{P_u +}{P_{A+}}$	$\frac{P_{PE}}{P_{PA}}$
T-1	-1936	1857	-1552	1.01	0.94*	1.05
T-2	-1974	1854	-1132	0.86	0.98	0.99
T-3	-1497	1821	-609	0.90	1.01	0.87
T-4	-1497	1808	-596	0.88	1.02	0.85

\* : The test specimen was not loaded to failure in tension.

$P_{PE}$ : Experimental post-buckling strength at 15 mm in the final compression cycle

$P_{PA}$ : Predicted post-buckling strength at 15 mm in the final compression cycle

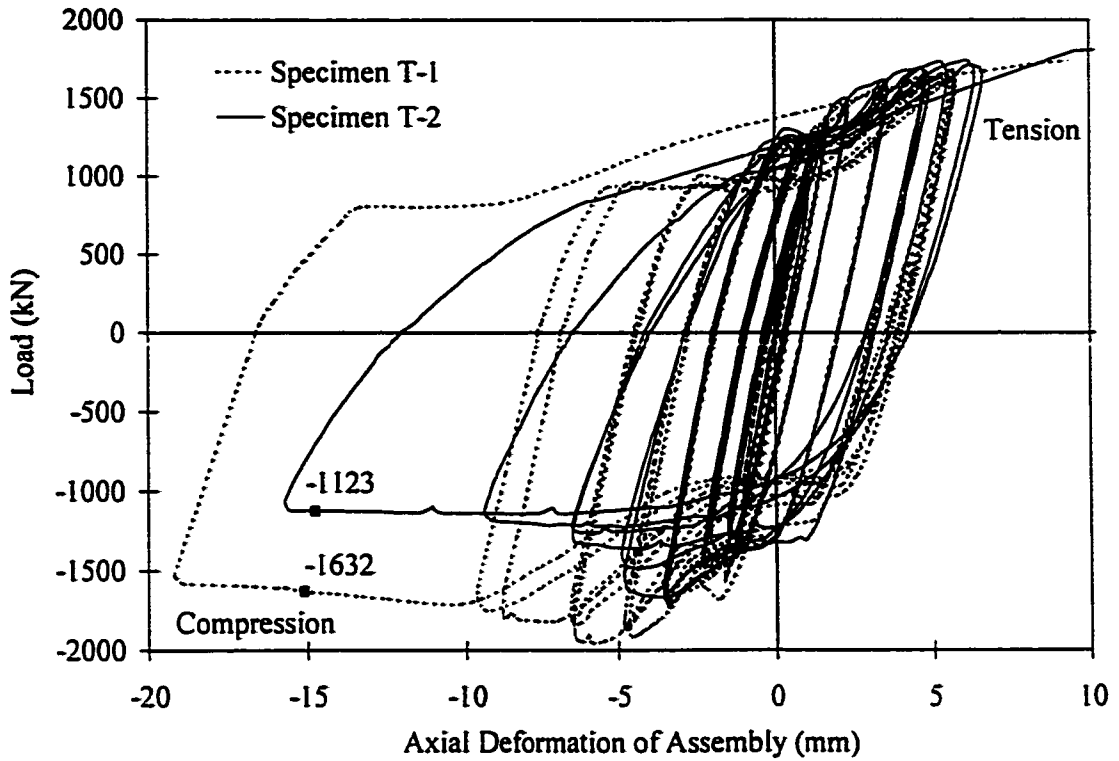


**Figure 6-1 : Load versus Deformation Relationship for Assembly:  
Specimens T-1 and T-2**

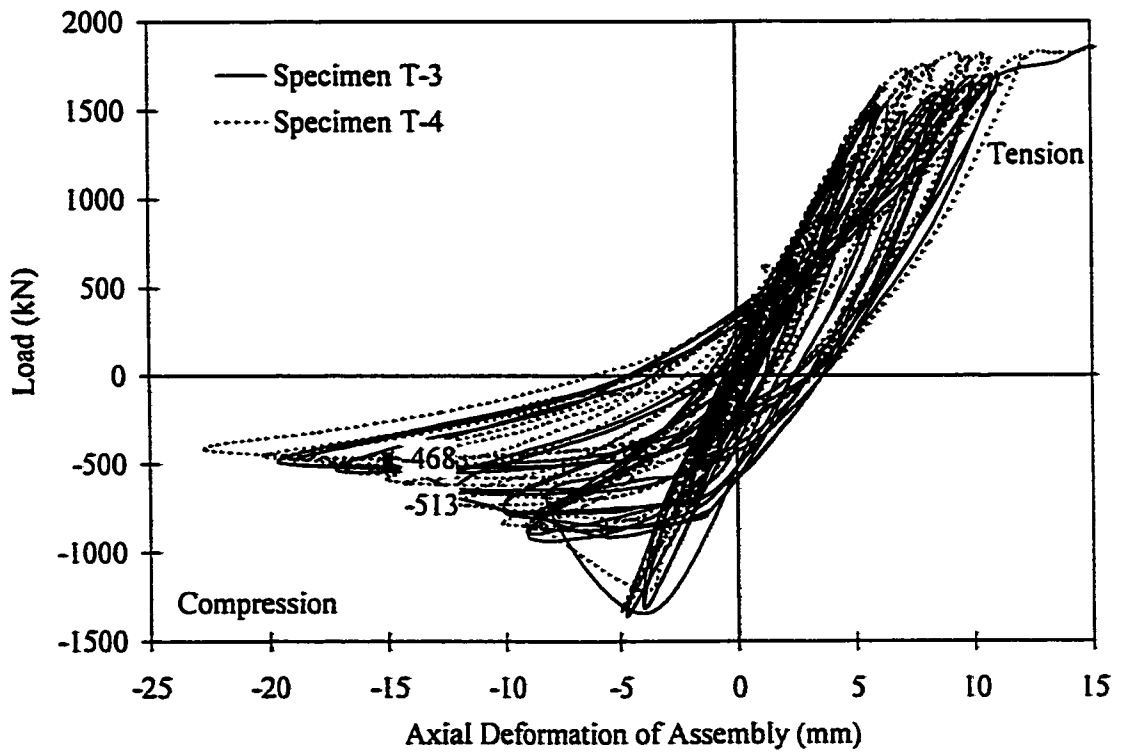


**Figure 6-2: Load versus Deformation Relationship for Assembly:  
Specimens T-3 and T-4**

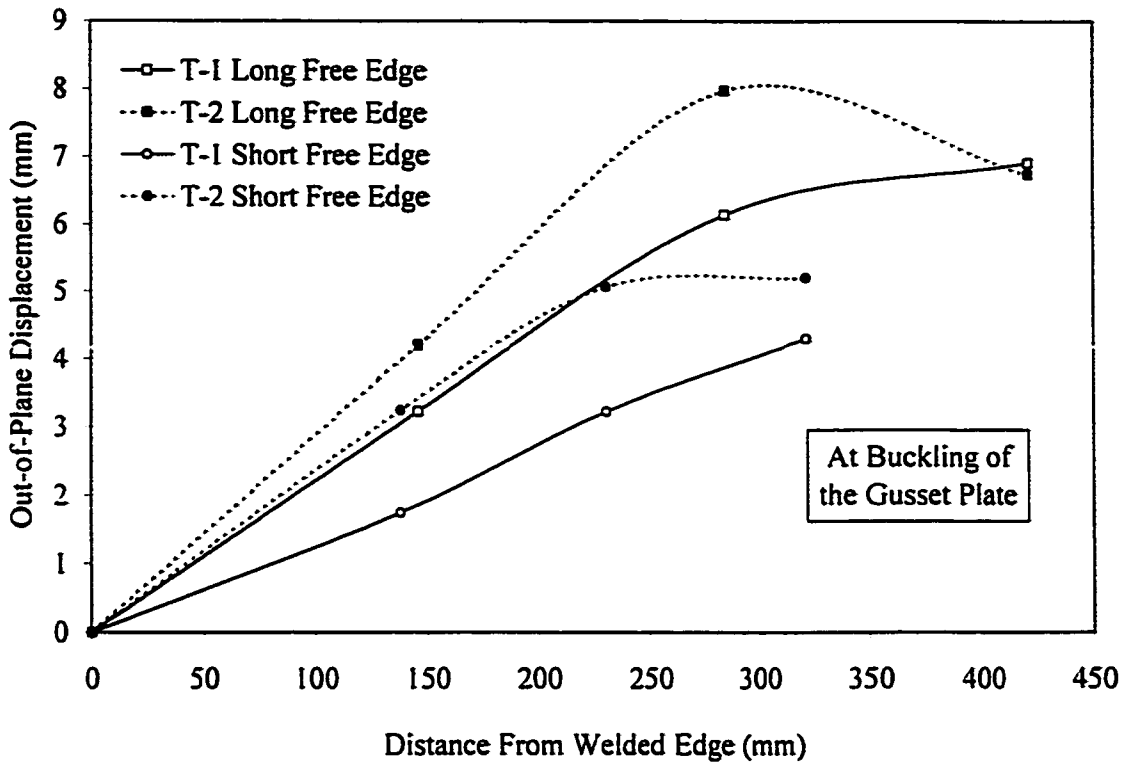


**Figure 6-3: Experimental Gusset Plate Free Edge Displacements at the Peak Compressive Load: Specimens T-1 and T-2**

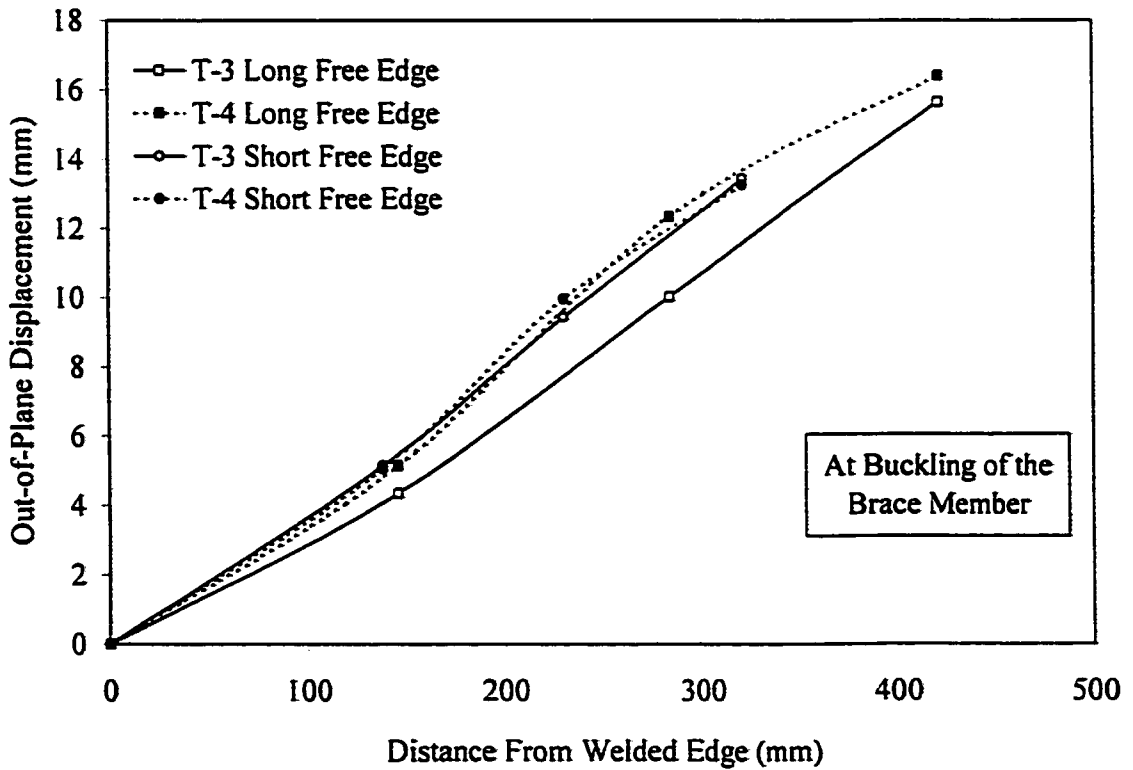


**Figure 6-4: Experimental Gusset Plate Free Edge Displacements at the Peak Compressive Load: Specimens T-3 and T-4**

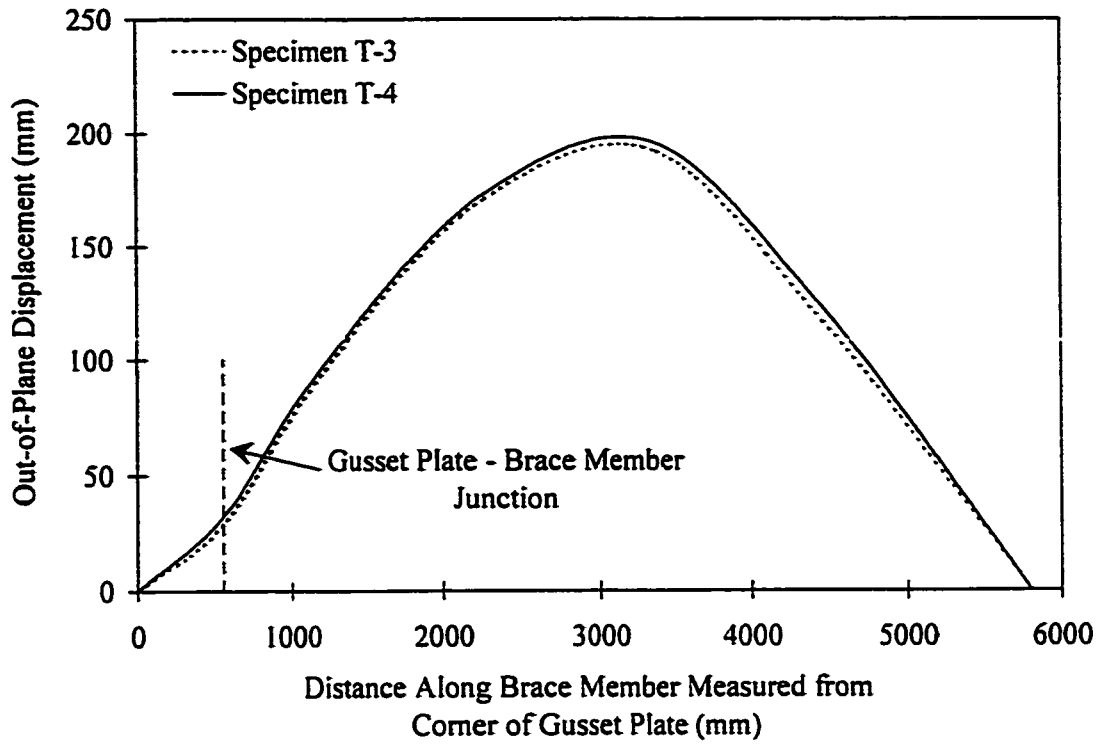


**Figure 6-5 : Out-of-Plane Deformation of Brace Member at the Peak Compressive Load of the Last Load Cycle: Specimens T-3 and T-4**

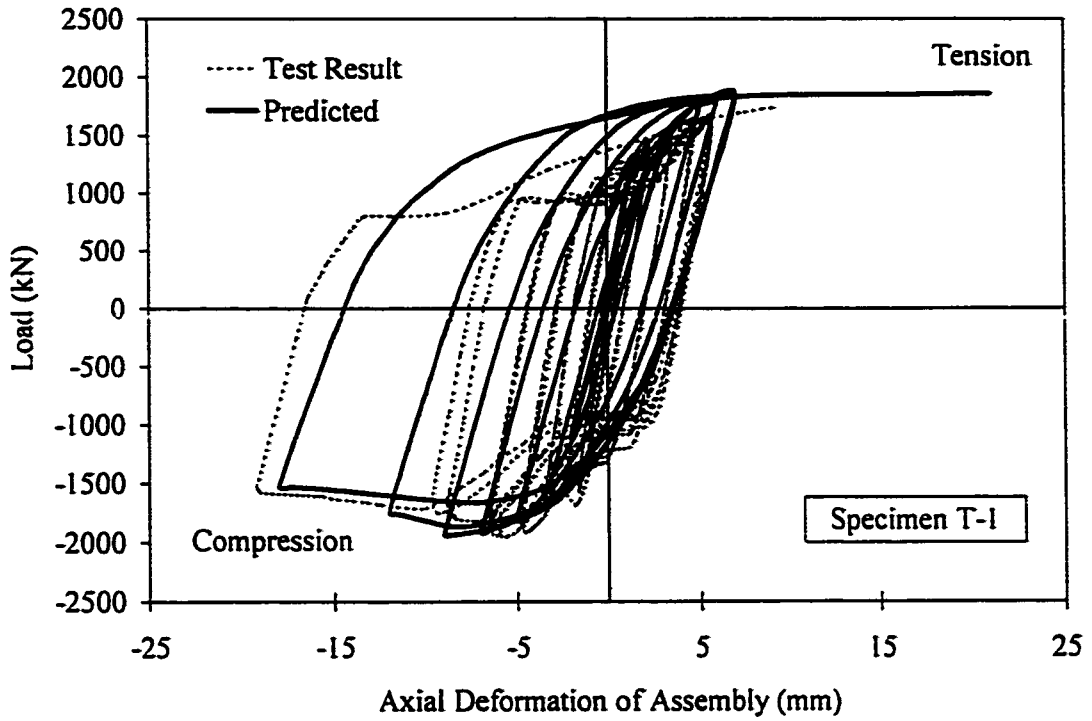


**Figure 6-6: Load versus Displacement Relationship for Assembly: Specimen T-1**

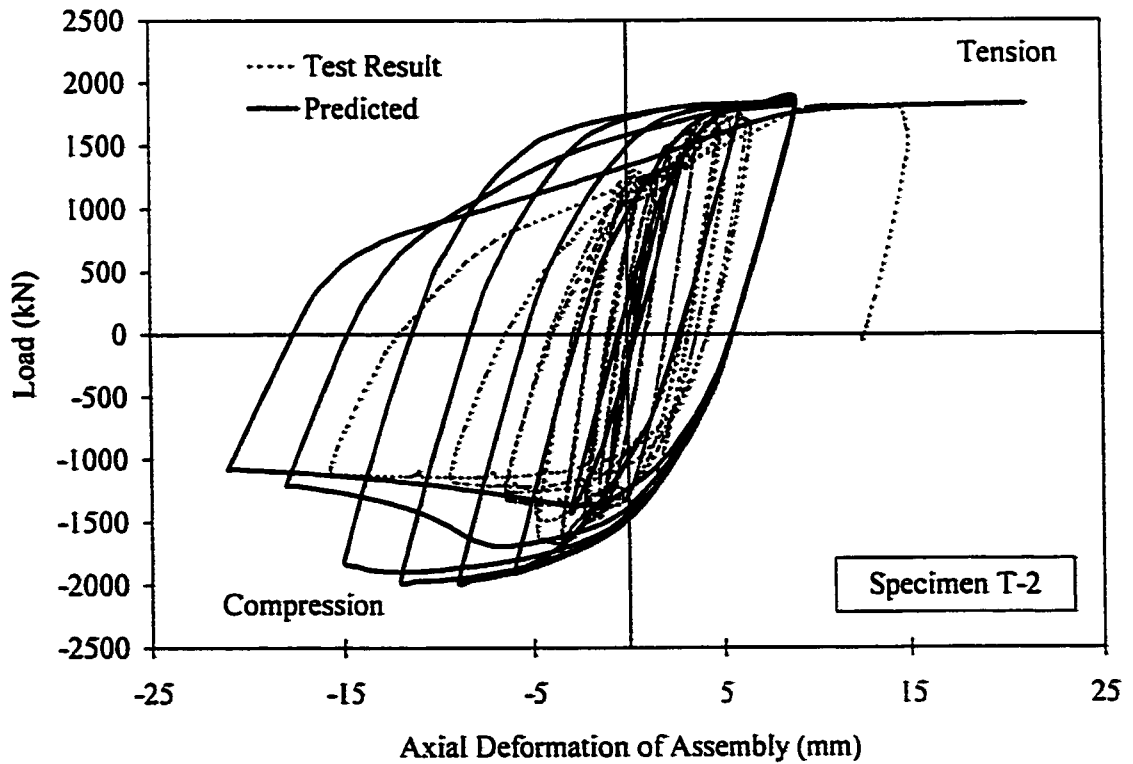


**Figure 6-7: Load versus Displacement Relationship for Assembly: Specimen T-2**



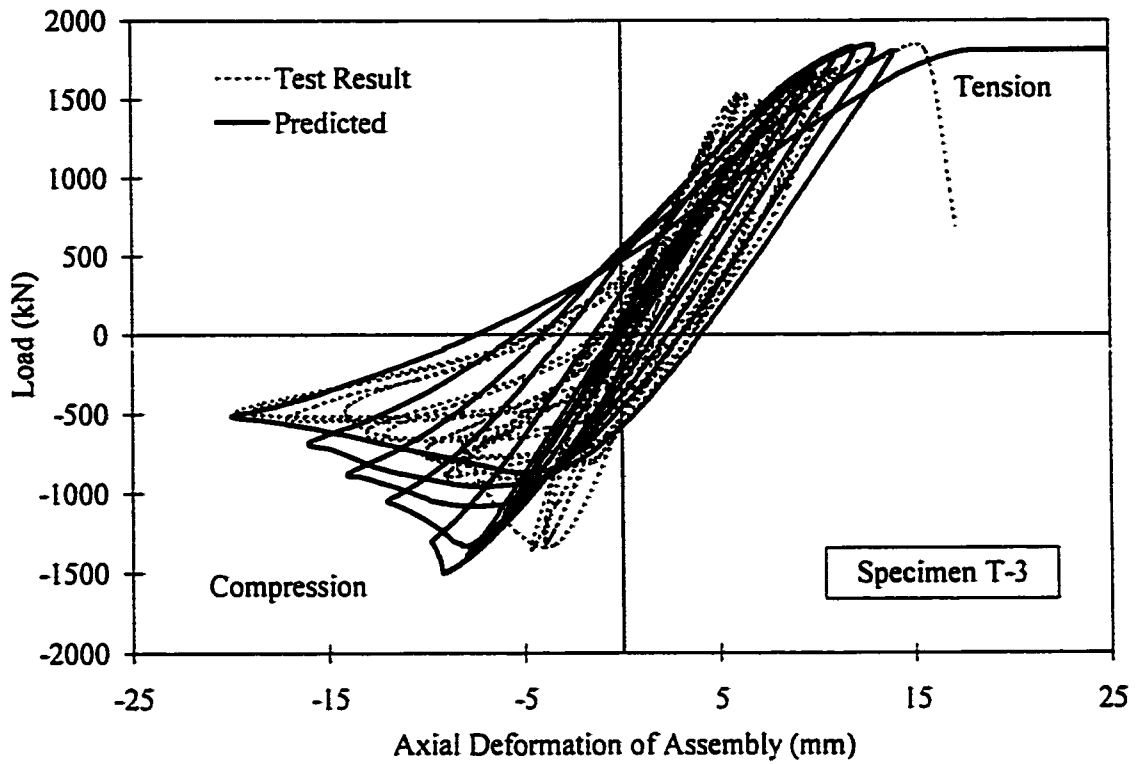


**Figure 6-8: Load versus Displacement Relationship for Assembly:  
Specimen T-3**

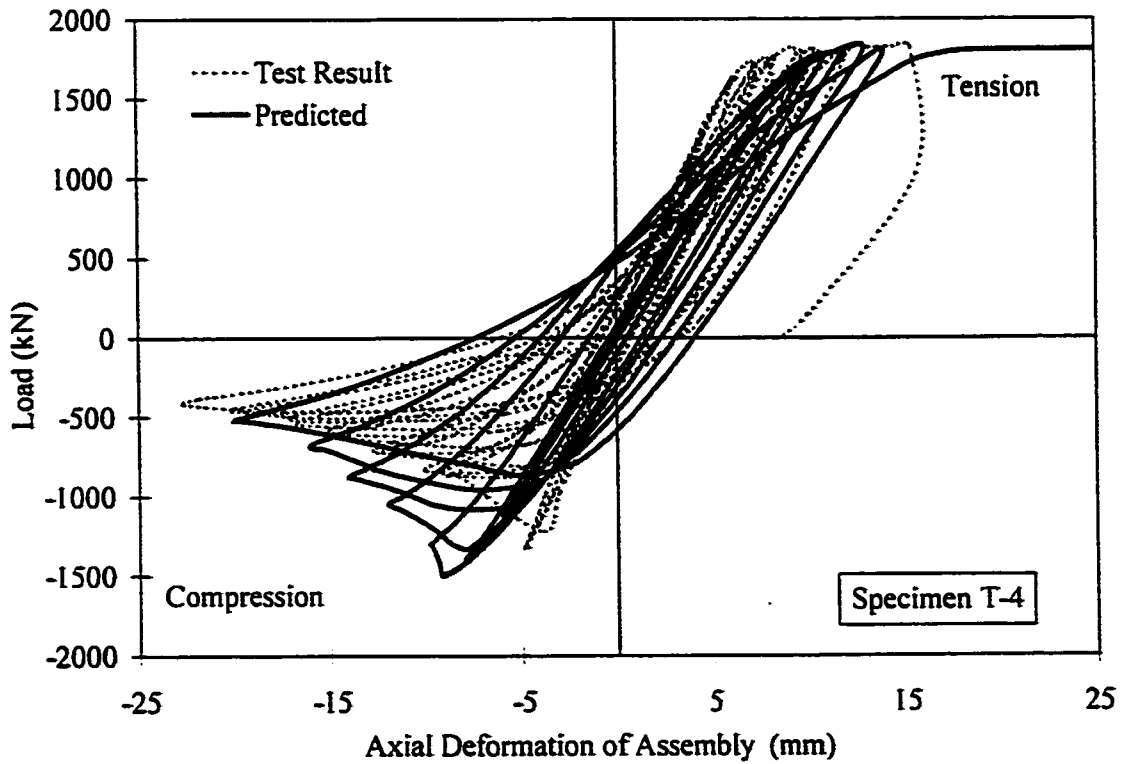


**Figure 6-9: Load versus Displacement Relationship for Assembly:  
Specimen T-4**

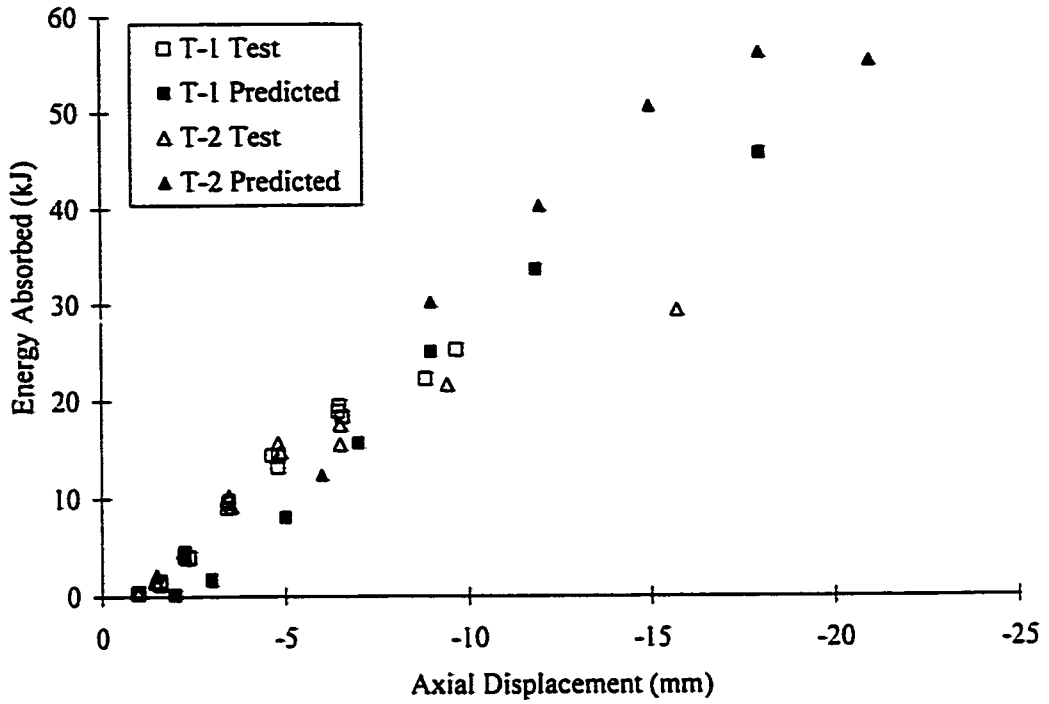


**Figure 6-10: Energy Dissipated by Specimen T-1 and T-2:  
Test Result versus Predicted**

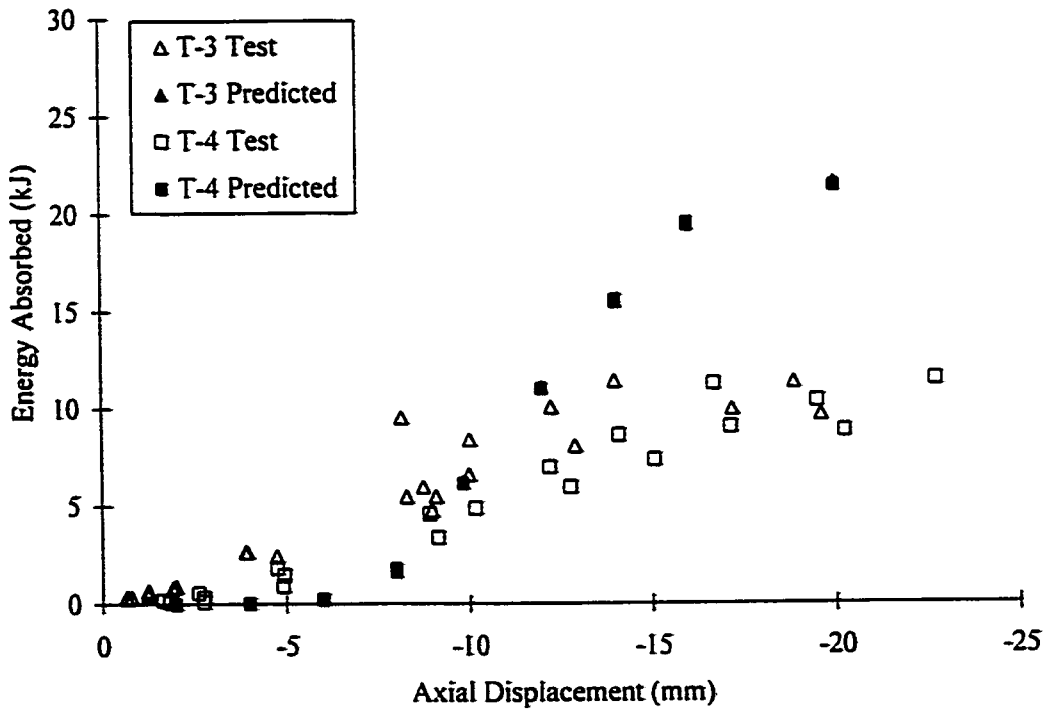


**Figure 6-11: Energy Dissipated by Specimen T-3 and T-4:  
Test Result versus Predicted**

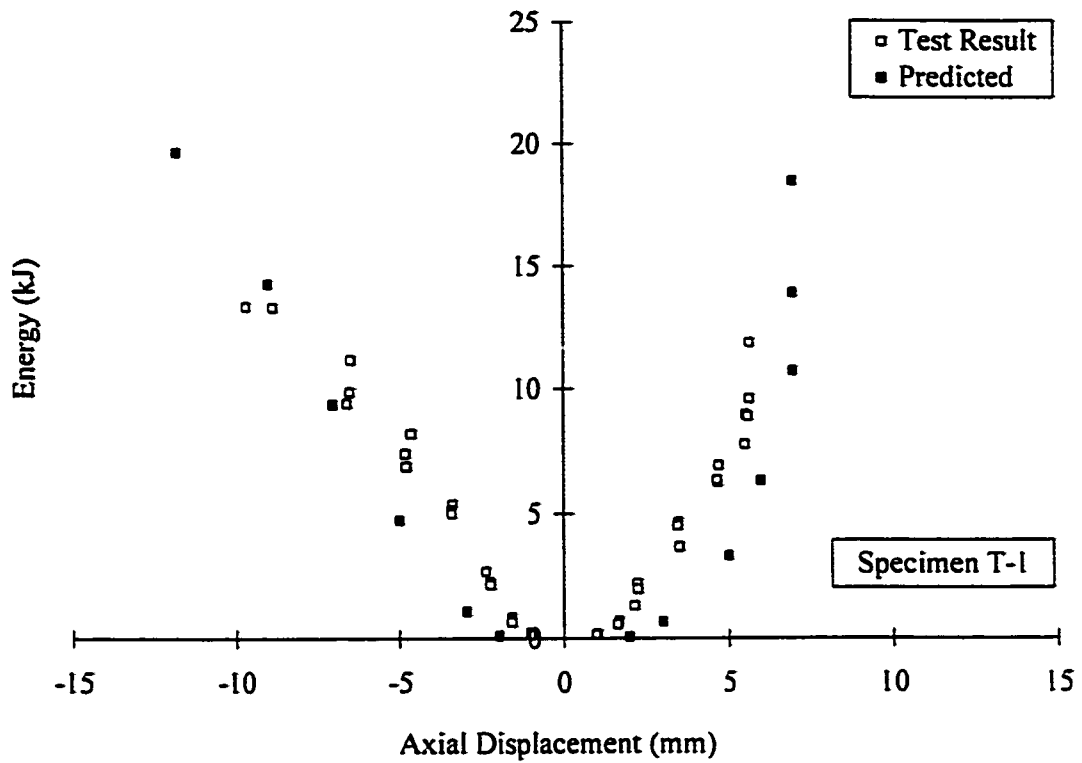


**Figure 6-12: Tensile and Compressive Energy Dissipated by Specimen T-1: Test Result versus Predicted**

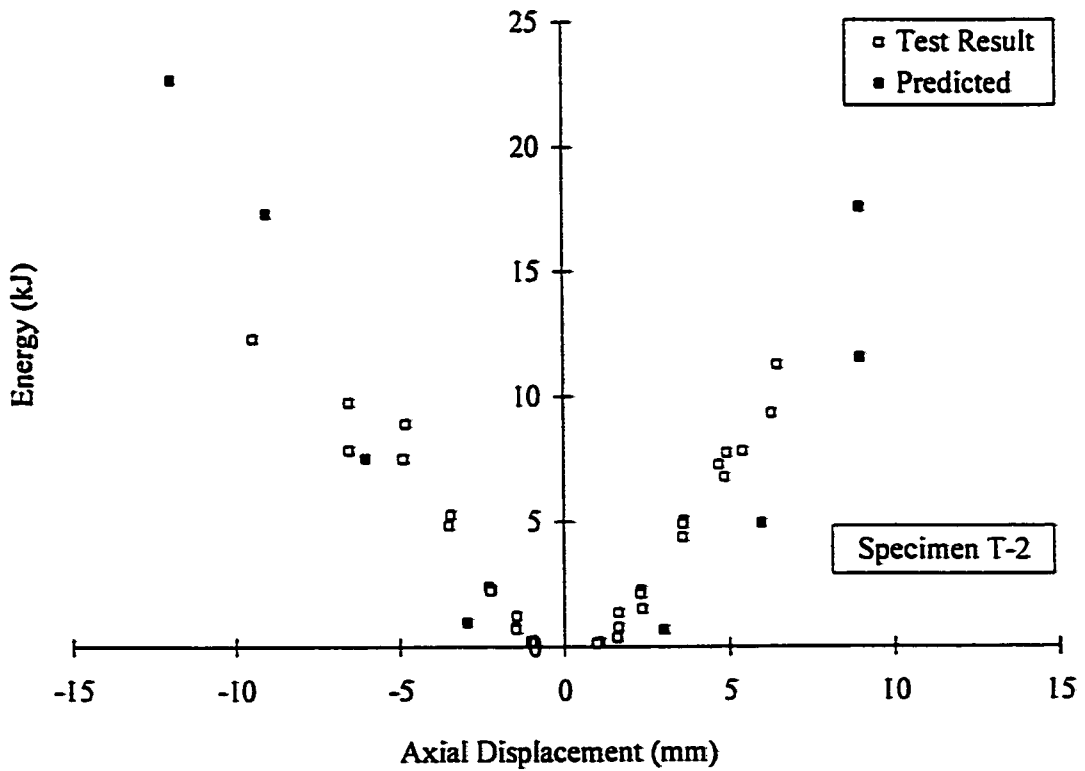


**Figure 6-13: Tensile and Compressive Energy Dissipated by Specimen T-2: Test Result versus Predicted**

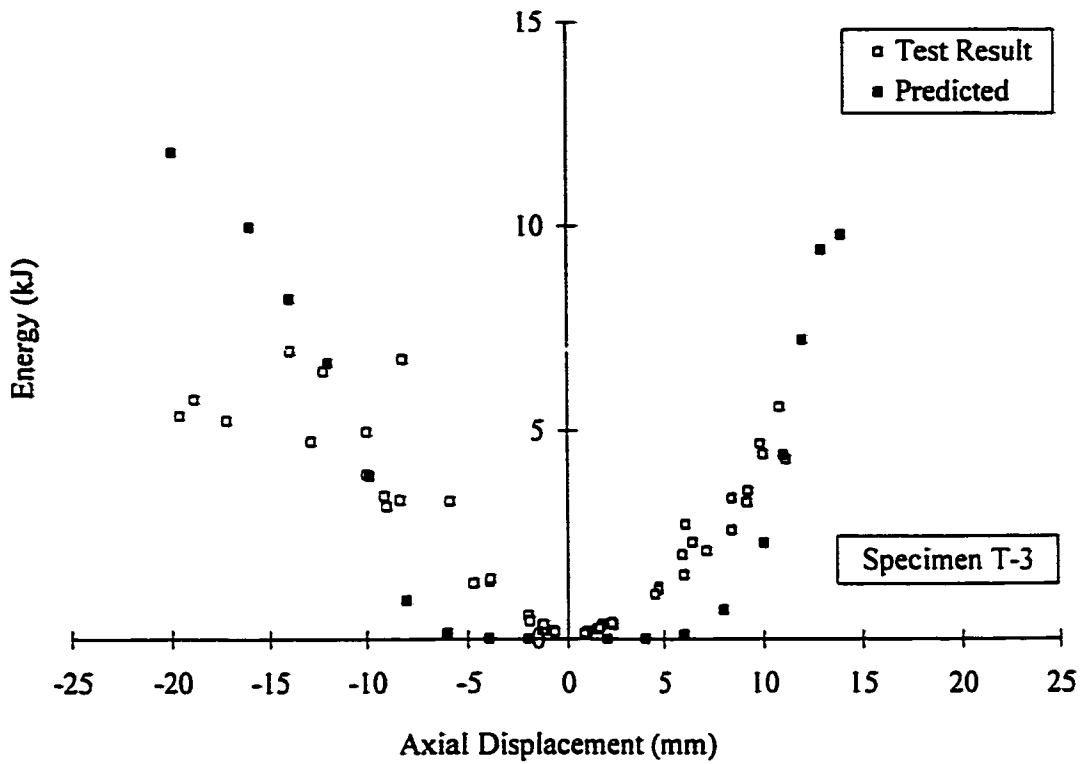


**Figure 6-14: Tensile and Compressive Energy Dissipated by Specimen T-3: Test Result versus Predicted**

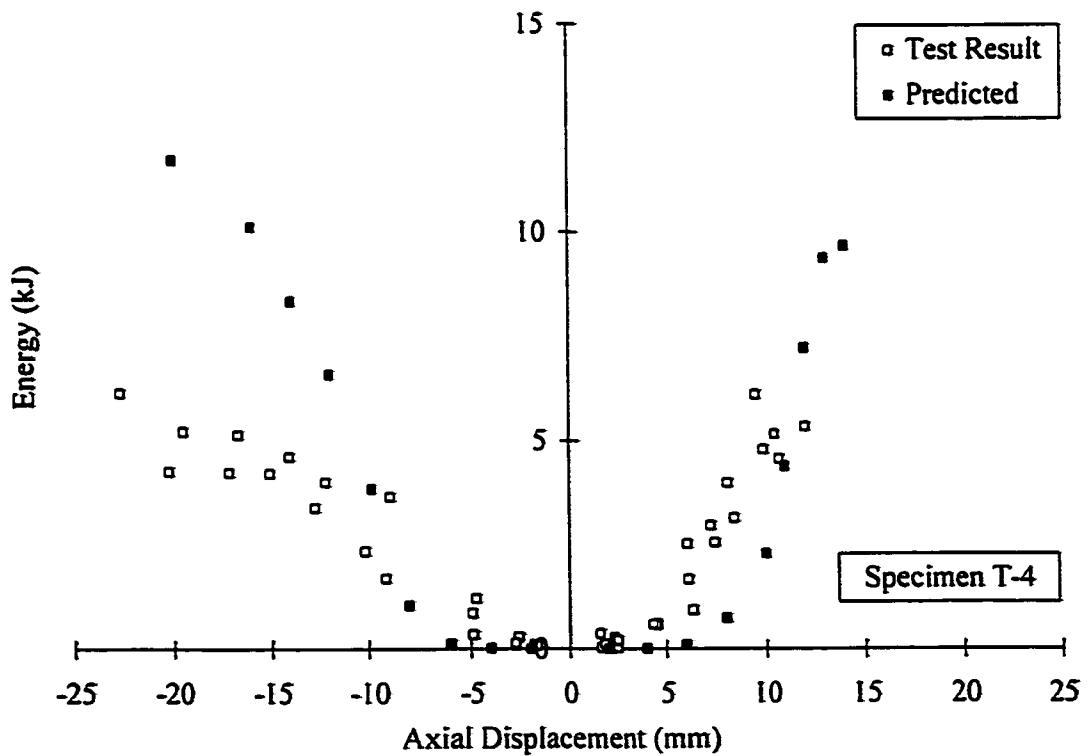


**Figure 6-15: Tensile and Compressive Energy Dissipated by Specimen T-4: Test Result versus Predicted**

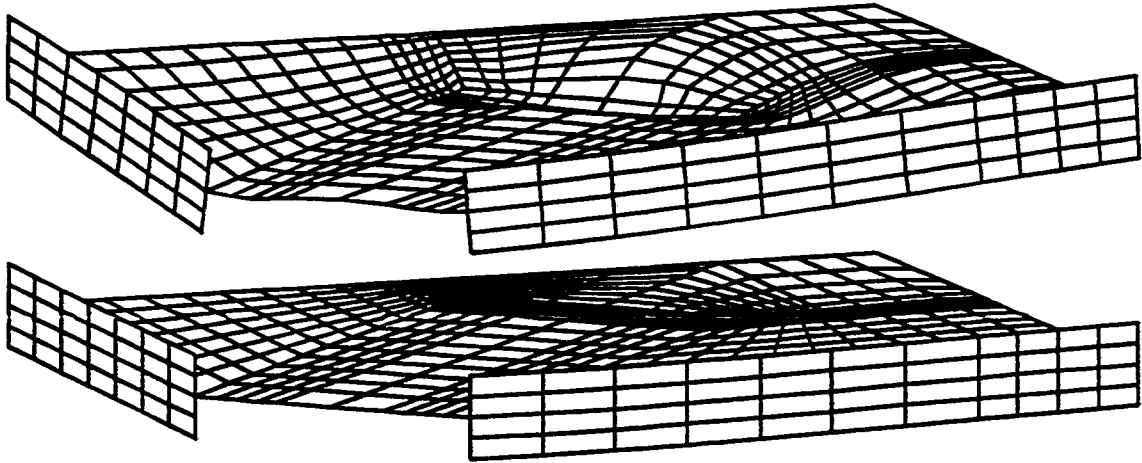


**Figure 6-16: Buckled Shape of Gusset Plate at Maximum Displacement of the Final Compression Cycle (Magnification Factor = 1.0): Specimen T-1**

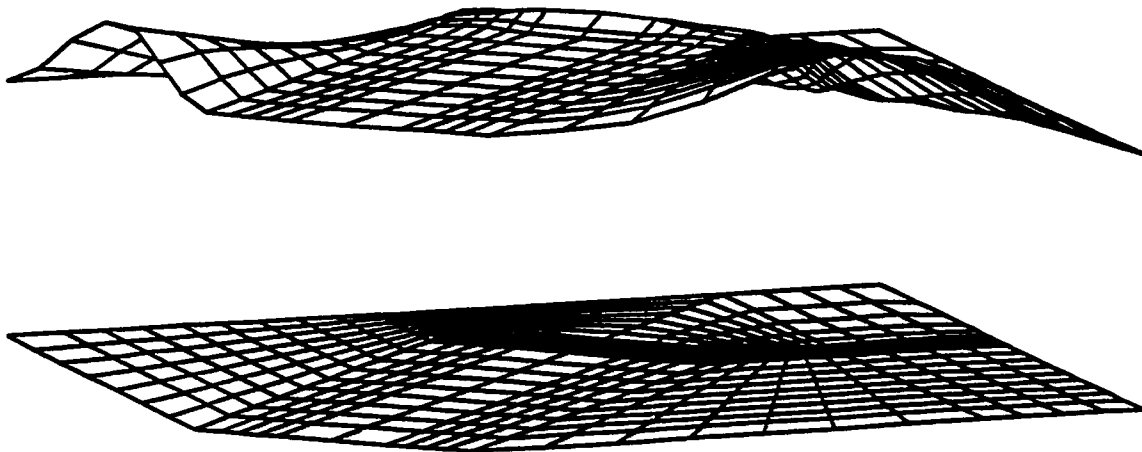


**Figure 6-17: Buckled Shape of Gusset Plate at Maximum Displacement of the Final Compression Cycle (Magnification Factor = 1.0): Specimen T-2**

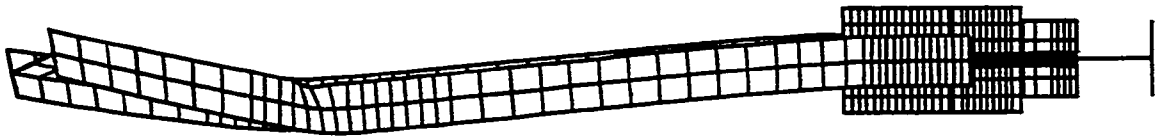


**Figure 6-18: Buckled Shape of Brace Member at Maximum Displacement of Final Compression Cycle (Magnification Factor = 1.0): Specimen T-3**

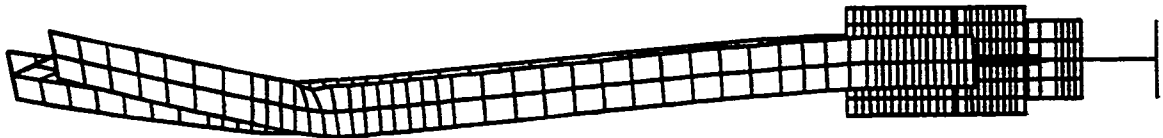


**Figure 6-19: Buckled Shape of Brace Member at Maximum Displacement of Final Compression Cycle (Magnification Factor = 1.0): Specimen T-4**

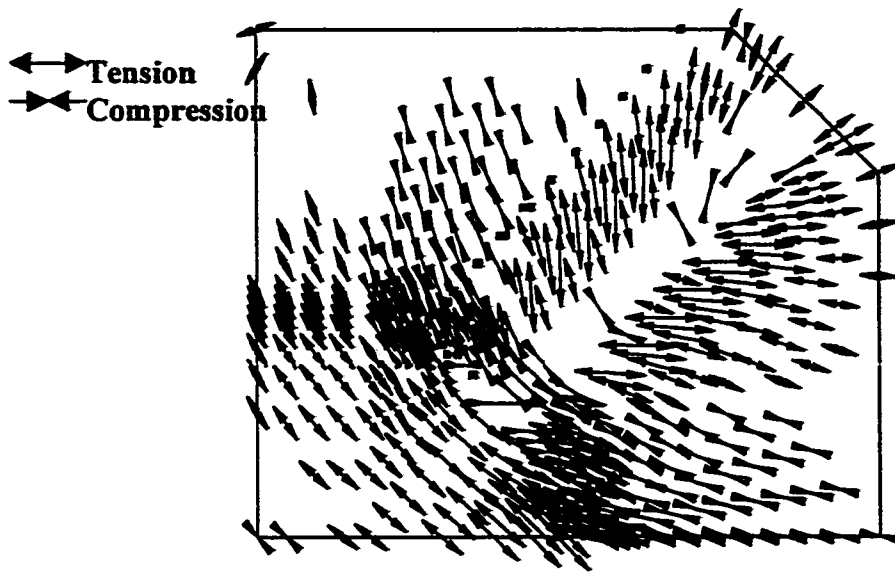


**Figure 6-20: Major Principal Strain Distribution just before First Yield in Compression in the Gusset Plate: Specimen T-1**

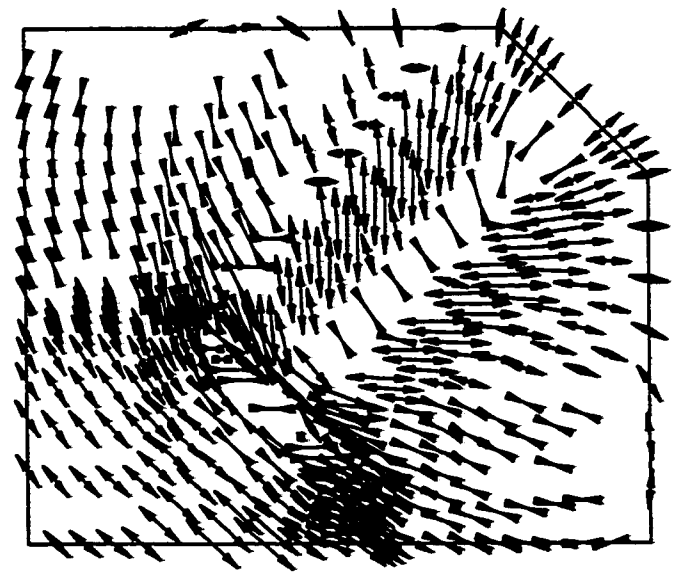


**Figure 6-21: Major Principal Strain Distribution just before First Yield in Compression in the Gusset Plate: Specimen T-2**

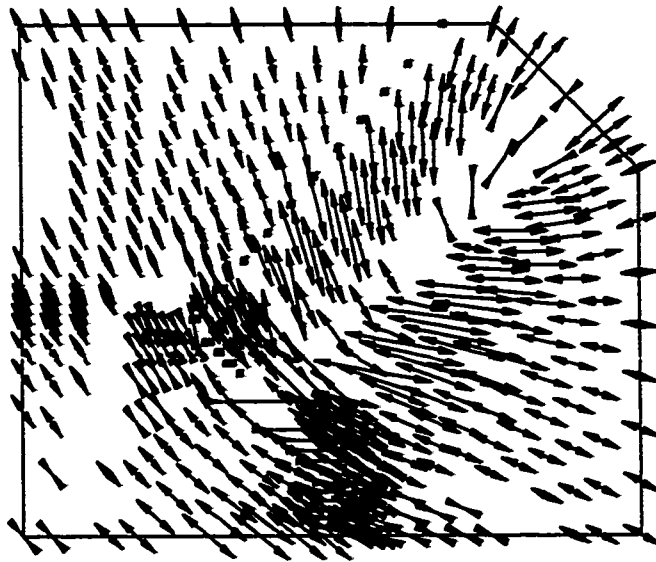


**Figure 6-22: Major Principal Strain Distribution just before First Yield in Compression in the Gusset Plate: Specimen T-3**

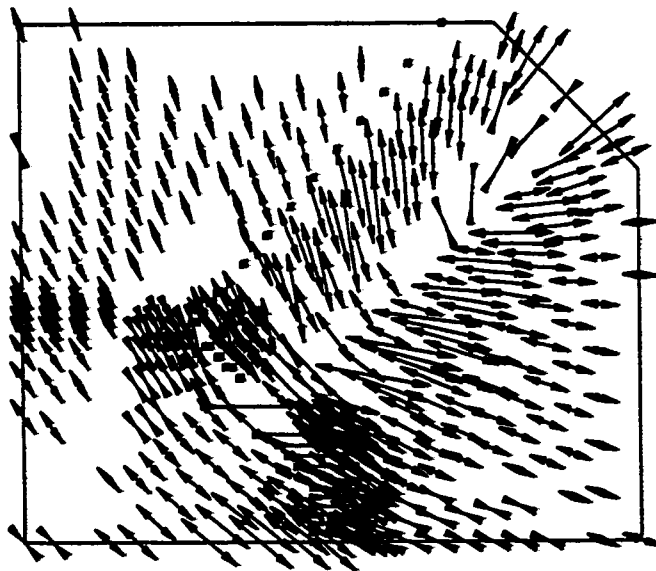


**Figure 6-23: Major Principal Strain Distribution just before First Yield in Compression in the Gusset Plate: Specimen T-4**



## CHAPTER 7

### SUMMARY, CONCLUSIONS, AND RECOMMENDATIONS

#### 7.1 Summary

The intent of the research presented in this thesis was to investigate the effect of free edge stiffeners on the behavior of gusset plate connections under cyclic loading, and to investigate the interaction between the gusset plate and brace member with either the brace member or gusset plate designed as the weak element in compression. Finite element models presented in earlier research by Walbridge and Cheng (1998) were also verified by comparing numerical analysis results with experimental results. These objectives were achieved through an experimental and numerical analysis program.

Four full-scale gusset plate connections, simulating gusset plates in a concentrically braced frame, were tested. All specimens included the same connection details, brace member cross-sections, a 45-degree brace member, gusset plate geometry, and were subjected to cyclic loading. Two test specimens were designed with the brace member as the load-limiting element in compression; one specimen included gusset plate free edge stiffeners, and the other did not. The tests on these two specimens indicated yielding of the gusset plate before buckling. The two other specimens were designed with the gusset plate as the weak element in compression; one with free edge stiffeners, and the other without. The test specimens were then modeled using the finite element models proposed by Walbridge *et al.* (1998) to verify the models for gusset plates with edge stiffeners and gusset plate – brace member assemblies designed with the brace member as the weak element in compression.

The following presents the conclusions drawn from the experimental and analytical investigations as well as recommendations for future research.

## **7.2 Conclusions**

A preliminary numerical analysis of gusset plate –brace member assemblies was conducted to determine an adequate size of free edge stiffener to include into the testing program. The following conclusions can be drawn from this preliminary analysis.

- Free edge stiffeners do not have a significant effect on the gusset plate buckling strength, but help stabilize the gusset plate in the post buckling range, resulting in a higher post-buckling strength. The effectiveness of the free edge stiffeners on the increase in post buckling strength seems to be dependent on the thickness of the gusset plate.

The test results indicated that:

- The addition of free edge stiffeners to the gusset plates designed as the weak element in compression increases the post-buckling and the peak compressive load carrying capacity. This effect is much less pronounced when the brace member is designed as the weak element in compression.
- The tensile strength and behavior of the gusset plate assemblies tested is relatively unaffected by the presence of free edge stiffeners.
- The presence of free edge stiffeners increases the energy absorbed by the gusset plate – brace member assembly in the compression cycle, but has little effect in the tension cycle.

- The out-of-plane deformation of the gusset plate free edges is greatly influenced by the presence of free edge stiffeners when the load limiting mechanism in compression is buckling of the gusset plate. This effect is negligible when the load limiting mechanism in compression is buckling of the brace member.

The specimens used in the experimental program were designed with the load limiting mechanism in compression to be either inelastic buckling of the gusset plate or elastic buckling of the brace member. In tension, the specimens were designed with yielding of the gusset plate followed by block shear failure of the gusset plate - splice member connection. The compressive yield and buckling strengths of the gusset plate were calculated with the measured material properties using the methods proposed by Whitmore (1952) and Thornton (1984), respectively, and the tensile strength was calculated using the block shear models proposed by Hardash and Bjorhovde (1985) and CAN/CSA S16.1 (1997). The following observations were made.

- The block shear model proposed by Hardash and Bjorhovde (1985) most accurately predicted the tensile strength of the connection.
- The compressive strength of the gusset plate was predicted accurately using either Whitmore's effective width concept or Thornton's method for unstiffened gusset plates and slightly less accurately for the stiffened gusset plates. Whitmore's effective width provides an upper bound estimate of the compression strength and must therefore be used with caution.
- The buckling strength of the brace members as calculated using the method outlined in CAN/CSA S16.1 (1997) with an effective length factor of 0.7 is conservative for the assembly tested.

In order to test the finite element models and the conclusions proposed by Walbridge *et al.* (1998) the models were modified to incorporate the measured initial imperfections, material properties, and geometry. The following conclusions can be drawn from the comparison of the finite element analysis results with the test results.

- The finite element models give good predictions of tensile strength but over estimated the peak compressive and post buckling capacities of the gusset plate-brace member assemblies.
- The finite element models displayed a more flexible assembly than observed in the test specimens in the elastic and inelastic ranges of both compressive and tensile loading, but was able to predict the rate at which the stiffness of the assemblies deteriorated in the post buckling range.
- The finite element models were able to predict the energy absorption characteristics of the assemblies.

### **7.3 Recommendations for Future Research**

Based on the experimental and numerical analysis investigations presented, the following recommendations are made for future research:

- bolt slip contribution to the energy absorption capacity of the assembly should be further investigated;
- further investigation is required to determine the cause of the significantly lower initial stiffness of the finite element models compared to the test specimens;

- the size of free edge stiffeners included in the test program was determined by modifying the validated models by Walbridge *et al.* (1998). This limited investigation indicated that the required stiffener size may be a function of the gusset plate thickness. Further investigation is required to determine the required size of stiffener for various sizes of gusset plates;
- a validated finite element model should be used to further investigate the effect of interaction between the bracing member and the gusset plate, and some additional tests should be conducted to verify some of these findings;
- further testing is required on test specimens of similar capacity but governed by different failure mechanisms to assess the difference in the energy absorption characteristics of weak gusset – strong brace assemblies compared to strong gusset – weak brace assemblies.

## REFERENCES

- Astaneh-Asl, A., 1998. "Seismic Behavior and Design of Gusset Plates". Steel Tips, Structural Steel Educational Council, December.
- Astaneh-Asl, A., and Goel, S.C., 1984. "Cyclic In-Plane Buckling of Double Angle Bracing." *Journal of Structural Engineering*, ASCE, Vol. 110, No. 9, pp. 2036-2055.
- Astaneh-Asl, A., Goel, S.C., Hanson, R.D., 1985. "Cyclic Out-of-Plane Buckling of Double Angle Bracing." *Journal of Structural Engineering*, ASCE, Vol. 111, No. 5, pp. 1135-1153.
- ASTM A370-96, 1996. Standard Test Methods and Definitions for Mechanical Testing of Steel Products. American Society for Testing and Materials, Philadelphia, PA.
- Applied Technology Council-24, 1992. Guidelines for Cyclic Seismic Testing of Components of Steel Structures. Report No. 24 Applied Technology Council, Redwood City, CA.
- Bjorhovde, R., 1988. "Limit States Design Considerations for Gusset Plates." *Journal of Construction*. Steel Research, Elsevier Applied Science Publishers Ltd., England.
- Bjorhovde, R., and Chakrabarti, S.K., 1985. "Tests of Full-Size Gusset Plate Connections." *Journal of Structural Engineering*, ASCE, Vol. 111, No. 3, pp. 667-684.
- CAN3-S6-M, 1983, Design of Highway Bridges. Canadian Standards Association, National Standard of Canada.
- CAN/CSA-G40.20-M92, 1992. General Requirements for Rolled or Welded Structural Quality Steel. Canadian Standards Association, Rexdale, Ontario.
- CAN/CSA-S16.1-M94. 1997. Limit States Design of Steel Structures. Canadian Standards Association, Rexdale, Ontario, 1997.
- Chakrabarti, S.K., and Richard, R.M., 1990. "Inelastic Buckling of Gusset Plates." *Structural Engineering Review*, Vol. 2, pp. 13-29.
- Davis, H.E., Troxell, G.E., Hauck, G.F.W., 1982. *The Testing of Engineering Materials*. 4<sup>th</sup> Edition, McGraw-Hill, New York.
- Hardash, S.G., and Bjorhovde, R., 1985. "New Design Criteria for Gusset Plate Connections." *Engineering Journal*, AISC, Vol. 22, No. 2, pp. 77-94.

Hardin, B.O., 1958. "Experimental Investigation of the Primary Stress Distribution in the Gusset Plates of a Double Plane Pratt Truss Joint with Chord Splice at the Joint." Bulletin No. 49, University of Kentucky Engineering Experiment Station.

Hibbitt, Karlsson & Sorenson Inc. 1996. "ABAQUS /Standard" User's Manual Volumes I, II, and III, Version 5.6, Pawtucket, RI.

Hu, S.Z., and Cheng, J.J.R., 1987. "Compressive Behavior of Gusset Plate Connections." Structural Engineering Report No. 153, Department of Civil Engineering, University of Alberta, Edmonton, Alberta.

Irvan, W.G., 1957. "Experimental Study of Primary Stresses in Gusset Plates of a Double Plane Pratt Truss." Bulletin No. 46, University of Kentucky Engineering Experiment Station.

Jain, A.K., Goel, S.C., and Hanson, R.D., 1978. "Inelastic Response of Restrained Steel Tubes." Journal of the Structural Division, ASCE, Vol. 104, ST6, pp. 897-910.

Jain, A.K., Goel, S.C., and Hanson, R.D., 1980. "Hysteretic Cyclics of Axially Loaded Steel Members." Journal of the Structural Division, ASCE, Vol. 106, ST8, pp. 1777-1795.

Ontario Highway Bridge Design Code, 2d ed. Highway Engineering Division, 1990.

Rabinovitch, J.S., and Cheng, J.J.R., 1993. "Cyclic Behavior of Gusset Plate Connections." Structural Engineering Report No. 191, Department of Civil Engineering, University of Alberta, Edmonton, Alberta.

Thornton, W.A., 1984. "Bracing Connections for Heavy Construction." Engineering Journal, AISC, Vol. 21, No. 3, pp. 139-148.

Walbridge, S.S., Grondin, G.Y., and Cheng, J.J.R., 1998. "An Analysis of the Cyclic Behavior of Steel Gusset Plate Connections." Structural Engineering Report No. 225, Department of Civil Engineering, University of Alberta, Edmonton, Alberta.

Whitmore, R.E., 1952. "Experimental Investigation of Stresses in Gusset Plates." Bulletin No. 16, Engineering Experiment Station, University of Tennessee.

Williams, G.C., and Richard, R.M., 1986. "Steel Connection Design Based on Inelastic Finite Element Analysis." Report of the Department of Civil Engineering and Engineering Mechanics, The University of Arizona.

Williams, G.C., and Richard, R.M., 1996. "Analysis and Design of Large Diagonal Bracing Connections." Structural Engineering Review, Vol. 8, No.1, pp. 1-27.

Yam, C.H.M., and Cheng, J.J.R., 1993. "Experimental Investigation of the Compressive Behavior of Gusset Plate Connections." Structural Engineering Report No. 194, Department of Civil Engineering, University of Alberta, Edmonton, Alberta.

Yam, C.H.M., and Cheng, J.J.R., 1994. "Analytical Investigation of the Compressive Behavior and Strength of Steel Gusset Plate Connections." Structural Engineering Report No. 207, Department of Civil Engineering, University of Alberta, Edmonton, Alberta.



## **APPENDIX A**

### **Preliminary Finite Element Analysis Results**

## APPENDIX A

The measured out-of-plane initial imperfections of the gusset plates and brace members for each test specimen are presented in this Appendix. The measurements were taken following the procedures presented in Chapter 3.

Tables A-1 through A-4 present the out-of-plane measurements of the gusset plates at the points located in Figure A-1. For each point, a minimum of two out-of-plane measurements were taken. Nodal point 563 was used as the reference point for each of the gusset plates. The out-of-plane measurements of the brace members for test specimens T-3 and T-4 are presented in Table A-5.

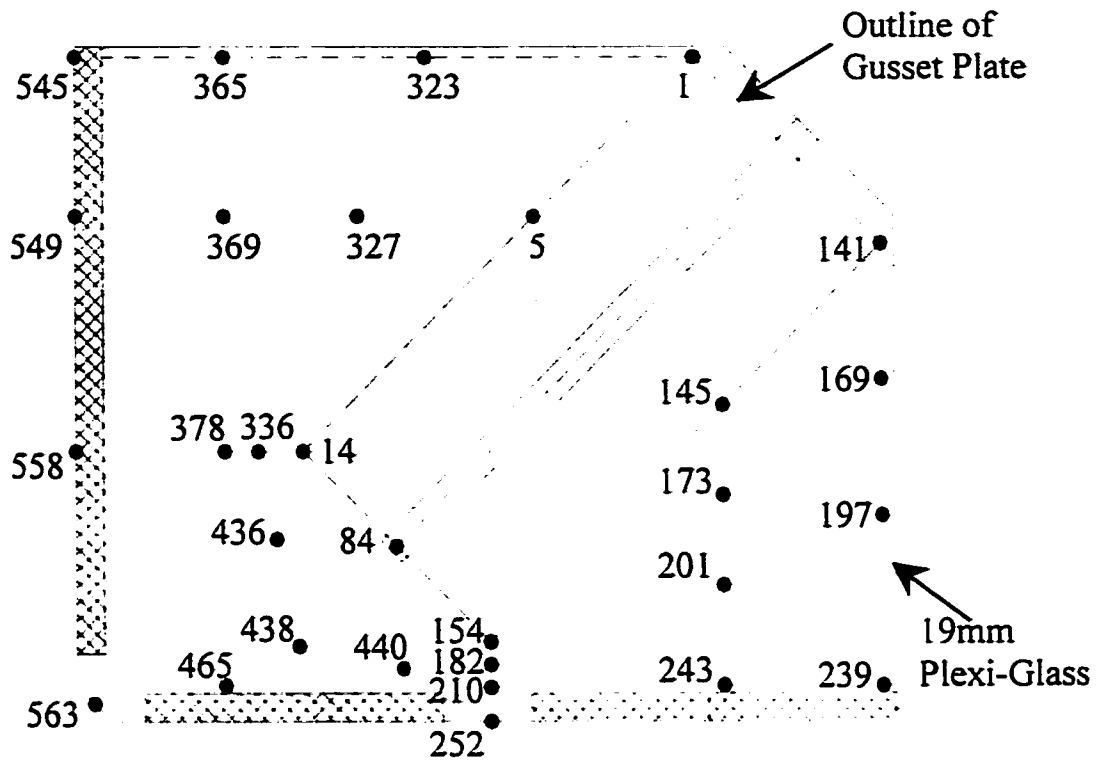


**Figure A-1: Nodes at Which Gusset Plate Out-of-Plane Initial Imperfections are Measured**

**Table A-1**  
**Gusset Plate Initial Imperfection Measurements (mm): Specimen T-1**

<b>Gusset Plate - Specimen T-1</b>					
<i>Node</i>	<i>1</i>	<i>2</i>	<i>3</i>	<i>Average</i>	<i>Avg. - Ref.</i>
<b>1</b>	88.02	88.04		88.03	-0.50
<b>5</b>	88.33	88.13		88.23	-0.31
<b>14</b>	88.81	88.68		88.75	0.21
<b>84</b>	87.5	87.51		87.51	-1.03
<b>141</b>	86.73	86.82		86.78	-1.76
<b>145</b>	86.73	86.79		86.76	-1.77
<b>154</b>	87.49	87.36		87.43	-1.11
<b>169</b>	87.12	87.08		87.10	-1.44
<b>173</b>	86.95	87.01		86.98	-1.55
<b>182</b>	87.71	87.73		87.72	-0.81
<b>197</b>	87.55	87.49		87.52	-1.02
<b>201</b>	87.44	87.25		87.35	-1.19
<b>210</b>	87.78	87.52		87.65	-0.88
<b>239</b>	88.12	88.18		88.15	-0.38
<b>243</b>	88.02	88.11		88.07	-0.47
<b>252</b>	87.8	87.79		87.80	-0.74
<b>323</b>	89.76	89.66		89.71	1.18
<b>327</b>	89.62	89.77	89.84	89.74	1.21
<b>336</b>	89.39	89.32		89.36	0.82
<b>365</b>	93.45	93.47		93.46	4.93
<b>369</b>	92.19	92.01	91.98	92.06	3.53
<b>378</b>	89.94	90.09		90.02	1.48
<b>436</b>	88.59	88.69		88.64	0.11
<b>438</b>	88.02	88		88.01	-0.53
<b>440</b>	87.86	87.63		87.75	-0.79
<b>465</b>	88.25	88.07		88.16	-0.38
<b>545</b>	95.96	95.9		95.93	7.40
<b>549</b>	94.4	94.31	94.25	94.32	5.79
<b>558</b>	91.53	91.59		91.56	3.03
<b>REF: 563</b>	88.52	88.55		88.54	0.00

**Table A-2**  
**Gusset Plate Initial Imperfection Measurements (mm): Specimen T-2**

<b>Gusset Plate - Specimen T-2</b>					
<i>Node</i>	<i>1</i>	<i>2</i>	<i>3</i>	<i>Average</i>	<i>Avg. - Ref.</i>
<b>1</b>	91.81	91.74		91.78	<b>1.30</b>
<b>5</b>	91.24	91.45	91.36	91.35	<b>0.88</b>
<b>14</b>	90.6	90.49	90.64	90.58	<b>0.10</b>
<b>84</b>	90.47	90.4		90.44	<b>-0.04</b>
<b>141</b>	90.86	90.64	90.71	90.74	<b>0.26</b>
<b>145</b>	90.63	90.59		90.61	<b>0.14</b>
<b>154</b>	90.62	90.64		90.63	<b>0.16</b>
<b>169</b>	91.03	91.14	90.97	91.05	<b>0.57</b>
<b>173</b>	90.76	90.75		90.76	<b>0.28</b>
<b>182</b>	90.84	90.81		90.83	<b>0.35</b>
<b>197</b>	91.36	91.25	91.3	91.30	<b>0.83</b>
<b>201</b>	91.12	90.97	90.98	91.02	<b>0.55</b>
<b>210</b>	90.81	90.8		90.81	<b>0.33</b>
<b>239</b>	92.24	92.24		92.24	<b>1.77</b>
<b>243</b>	92.06	92.04		92.05	<b>1.58</b>
<b>252</b>	90.83	90.87		90.85	<b>0.38</b>
<b>323</b>	91.76	91.66	91.71	91.71	<b>1.24</b>
<b>327</b>	91.29	91.32		91.31	<b>0.83</b>
<b>336</b>	90.75	90.62	90.65	90.67	<b>0.20</b>
<b>365</b>	91.93	91.92		91.93	<b>1.45</b>
<b>369</b>	91.33	91.31		91.32	<b>0.85</b>
<b>378</b>	90.74	90.78		90.76	<b>0.29</b>
<b>436</b>	90.64	90.48	90.42	90.51	<b>0.04</b>
<b>438</b>	90.48	90.48		90.48	<b>0.01</b>
<b>440</b>	90.48	90.56	90.55	90.53	<b>0.06</b>
<b>465</b>	90.54	90.58		90.56	<b>0.09</b>
<b>545</b>	91.84	91.8		91.82	<b>1.35</b>
<b>549</b>	91.06	90.87	90.86	90.93	<b>0.46</b>
<b>558</b>	90.23	90.41	90.23	90.29	<b>-0.18</b>
<b>REF: 563</b>	90.44	90.48	90.5	90.47	<b>0.00</b>

**Table A-3**  
**Gusset Plate Initial Imperfection Measurements (mm): Specimen T-3**

<b>Gusset Plate - Specimen T-3</b>					
<i>Node</i>	<i>1</i>	<i>2</i>	<i>3</i>	<i>Average</i>	<i>Avg. - Ref.</i>
1	90.19	90.28	90.23	90.23	-3.71
5	91.11	91.04		91.08	-2.87
14	91.93	91.92		91.93	-2.02
84	92.37	92.16	92.26	92.26	-1.68
141	93.78	93.69	93.79	93.75	-0.19
145	93.67	93.78	93.66	93.70	-0.24
154	93.14	92.96	93.11	93.07	-0.88
169	94.19	94.23		94.21	0.26
173	93.65	93.68		93.67	-0.28
182	93.22	93.13	93.09	93.15	-0.80
197	94.99	95.12	94.95	95.02	1.07
201	94.13	94.23	94.18	94.18	0.23
210	93.33	93.37		93.35	-0.60
239	96.28	96.21		96.25	2.30
243	94.64	94.48	94.52	94.55	0.60
252	93.32	93.29		93.31	-0.64
323	91.2	91.17		91.19	-2.76
327	91.27	91.24		91.26	-2.69
336	91.9	91.89		91.90	-2.05
365	92.22	92.19		92.21	-1.74
369	91.84	91.96	91.93	91.91	-2.04
378	91.99	92.13	91.95	92.02	-1.92
436	92.16	92.12		92.14	-1.81
438	92.55	92.57		92.56	-1.39
440	92.81	92.81		92.81	-1.14
465	93.16	92.99	93.23	93.13	-0.82
545	92.78	92.77		92.78	-1.17
549	92.17	91.99	92	92.05	-1.89
558	92.67	92.73		92.70	-1.25
<b>REF: 563</b>	93.95	93.92	93.97	93.95	0.00

**Table A-4**  
**Gusset Plate Initial Imperfection Measurements (mm): Specimen T-4**

<b>Gusset Plate - Specimen T-4</b>					
<i>Node</i>	<i>1</i>	<i>2</i>	<i>3</i>	<i>Average</i>	<i>Avg. - Ref.</i>
<b>1</b>	93.85	93.92	93.73	93.83	<b>-1.55</b>
<b>5</b>	94.57	94.65	94.62	94.61	<b>-0.77</b>
<b>14</b>	95.55	95.52		95.54	<b>0.15</b>
<b>84</b>	95.35	95.3	95.31	95.32	<b>-0.06</b>
<b>141</b>	94	93.92	93.94	93.95	<b>-1.43</b>
<b>145</b>	94.76	94.62	94.58	94.65	<b>-0.73</b>
<b>154</b>	95.16	95.13		95.15	<b>-0.24</b>
<b>169</b>	94.21	94.19		94.20	<b>-1.18</b>
<b>173</b>	94.69	94.68		94.69	<b>-0.70</b>
<b>182</b>	95.39	95.16	95.17	95.24	<b>-0.14</b>
<b>197</b>	94.73	94.7		94.72	<b>-0.67</b>
<b>201</b>	95.08	94.86	94.85	94.93	<b>-0.45</b>
<b>210</b>	95.15	95.17		95.16	<b>-0.22</b>
<b>239</b>	95.44	95.37	95.4	95.40	<b>0.02</b>
<b>243</b>	94.82	94.9	94.83	94.85	<b>-0.53</b>
<b>252</b>	95.02	95.19	95.13	95.11	<b>-0.27</b>
<b>323</b>	94.85	94.82		94.84	<b>-0.55</b>
<b>327</b>	95.19	95.2		95.20	<b>-0.19</b>
<b>336</b>	95.6	95.55	95.55	95.57	<b>0.18</b>
<b>365</b>	96.17	96.19		96.18	<b>0.80</b>
<b>369</b>	95.82	95.78	95.79	95.80	<b>0.41</b>
<b>378</b>	95.67	95.64		95.66	<b>0.27</b>
<b>436</b>	95.43	95.4		95.42	<b>0.03</b>
<b>438</b>	95.07	95.05		95.06	<b>-0.32</b>
<b>440</b>	95.05	95.09	95.06	95.07	<b>-0.32</b>
<b>465</b>	95.24	95.13	95.13	95.17	<b>-0.22</b>
<b>545</b>	96.89	96.92		96.91	<b>1.52</b>
<b>549</b>	96.22	96.24		96.23	<b>0.85</b>
<b>558</b>	95.53	95.61	95.69	95.61	<b>0.23</b>
<b>REF: 563</b>	95.37	95.4	95.38	95.38	<b>0.00</b>

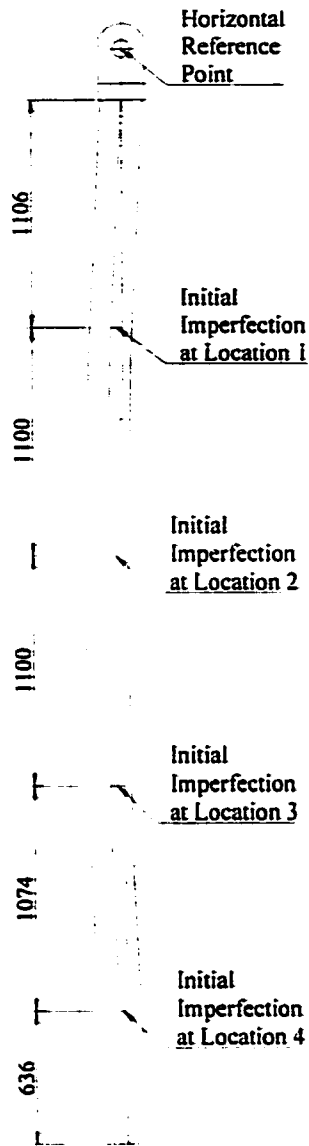


**Table A-5**  
**Brace Member Initial Imperfections Measurements (mm)**

	Specimen T-3	Specimen T-4
Location 1	1.59	0.79
Location 2	1.98	5.56
Location 3	1.98	8.73
Location 4	1.59	7.94



## **APPENDIX B**

### **Initial Imperfection Measurements**

## **APPENDIX B**

Included in this Appendix are the detailed results of the preliminary finite element analysis. These results were used to determine the stiffeners size to include into the testing program. Table B-1, B-2, and B-3 present the numerical results of Series I, II, and III, respectively. This numerical study is discussed in detail in Chapter 5.

**Table B-1**  
**Results of Preliminary Finite Element Analysis—Series I**  
**Without Bracing Member Under Monotonic Compressive Loading**

Model	2b	2b / t <sub>st</sub>	Buckling Load (kN)	Post Buckling Strength, P <sub>post</sub> (kN)	$\frac{P_{post}(MC9xx)}{P_{post}(MC9)}$
mc9	—	—	-1258	-887	1.0
mc9S1	25.0	2.78	-1289	-1127	1.3
mc9S3	25.0	2.08	-1294	-1182	1.3
mc9S2	37.5	4.17	-1293	-1206	1.4
mc9S4	37.5	3.13	-1298	-1258	1.4
mc12	—	—	-1834	-1401	1.0
mc12S1	25.0	2.78	-1896	-1634	1.2
mc12S3	25.0	2.08	-1905	-1690	1.2
mc12S2	37.5	4.17	-1904	-1723	1.2
mc12S4	37.5	3.13	-1915	-1770	1.2
mc12S5	51.0	5.67	-1906	-1748	1.2
mc12S6	51.0	4.25	-1915	-1794	1.3
mc15	—	—	-2458	-1787	1.0
mc15S1	25.0	2.78	-2556	-1846	1.0
mc15S3	25.0	2.08	-2569	-1887	1.0
mc15S2	37.5	4.17	-2572	-1946	1.1
mc15S4	37.5	3.13	-2581	-1975	1.1

**Table B-2**  
**Results of Preliminary Finite Element Analysis—Series II**  
**With Brace Member Under Monotonic Compressive Loading**

Model	2b	2b / t <sub>st</sub>	Buckling Load (kN)	Post Buckling Strength, P <sub>post</sub> (kN)	$\frac{P_{post}(MC12xx)}{P_{post}(MC12)}$
mc12B	—	—	-1800	-1359	1.0
mc12BS1	25.0	2.78	-1844	-1578	1.1
mc12BS2	37.5	4.17	-1851	-1662	1.2
mc12BS5	51.0	5.67	-1853	-1708	1.3

**Table B-3**  
**Results of Preliminary Finite Element Analysis—Series III**  
**With Brace Member Under Cyclic Loading**

Model	2b	2b / t <sub>st</sub>	Buckling Load (kN)	Post Buckling Strength, P <sub>post</sub> (kN)	$\frac{P_{post}(CY12xx)}{P_{post}(CY12)}$
cy12B	—	—	-1828	-952	1.0
cy12BS1	25.0	2.78	-1831	-1205	1.3
cy12BS2	37.5	4.17	-1835	-1304	1.4
cy12BS5	51.0	5.67	-1832	-1309	1.4